UNIVERSIDAD NACIONAL AUTÓNOMA DE MÉXICO

PROGRAMA DE MAESTRÍA Y DOCTORADO EN INGENIERÍA
INGENIERÍA ELÉCTRICA – INSTRUMENTACIÓN

DEVELOPMENT OF A STOKES POLARIMETER EMPLOYING THREE WAVELENGTHS SIMULTANEOUSLY

TESIS
QUE PARA OPTAR POR EL GRADO DE:
DOCTOR EN INGENIERÍA

PRESENTA:
EUSEBIO AGUILAR FERNÁNDEZ

TUTOR (ES) PRINCIPAL(ES)
DR. NEIL CHARLES BRUCE DAVIDSON, ICAT-UNAM

MIEMBROS DEL COMITÉ TUTOR
DR. OSCAR GABRIEL RODRIGUEZ HERRERA, ICAT-UNAM
DR. RAFAEL ESPINOSA LUNA, CENTRO DE INVESTIGACIONES EN ÓPTICA A.C.

CIUDAD UNIVERSITARIA, CD. MX. SEPTIEMBRE 2023

JURADO ASIGNADO:

Presidente: Dr. Avendaño Alejo Maximino

Secretario: Dr. Cuevas Cardona Salvador C.

Vocal: Dr. Bruce Davidson Neil Charles

1er Suplente: Dr. Espinosa Luna Rafael

2do Suplente: Dr. Rodríguez Herrera Oscar G.

Lugar donde se realizó la tesis: Instituto de Ciencias Aplicadas y Tecnología, UNAM.

TUTOR DE TESIS:

Dr. Neil Charles Bruce Davidson

NOMBRE

_____

FIRMA

Agradecimientos

En primer lugar dedico un agradecimiento muy especial a mi familia, mi esposa Naiceli, mi hija Geraldine y el más pequeño Gabrielito, ya que sin duda ellos han sido, son y seguirán siendo la base de cualquier logro en mi vida. También agradezco a mis padres, Eusebio y Micaela, ya que sin su apoyo incondicional no hubiera logrado llegar hasta este momento.
Agradezco también de manera muy especial a mi tutor el Dr. Neil, quién siempre logro sacar lo mejor de mí y tuvo total confianza en que lograría finalizar este proyecto, a pesar de las circunstancias. También quiero expresar mi total agradecimiento al Dr. Oscar porque con cada una de sus críticas bien fundamentadas logró sembrar en mí esa duda que finalizo en un aprendizaje nuevo. Así mismo al resto de los integrantes del comité tutor los doctores Maximino, Rafael y Salvador.
Me gustaría agradecer al Consejo Nacional de Ciencia y Tecnología (CONACYT) por la beca de doctorado otorgada para el desarrollo de este proyecto, y a la Dirección General de Asuntos del Personal Académico de la UNAM (DGAPA-UNAM) por el apoyo de este trabajo a través del proyecto IG100121, y por la beca adicional para finalizar este escrito.

Porque el día que creí no poder más, tú hallaste la mejor manera de hacerme saber que debo seguir adelante a pesar de las circunstancias. Una dedicatoria muy especial a ese pequeño ser que con un suave golpecito me confortó para seguir adelante.

Eusebio Aguilar.

Abstract

Polarimetry has received a great deal of interest recently, mainly because of advances in technology, particularly with advances in variable retarders, and polarized detectors. Also, many new applications have been developed, for example in remote sensing, microscopy, medical applications, astronomy, and metrology, among others. With this interest in new techniques and applications, there has been a great deal of work on data-extraction and calibration methods, required to correct the effects of experimental or measurement errors in polarimeters. In this thesis, we present a method for calibration and data-extraction for a Stokes polarimeter working with three different wavelengths simultaneously. This type of system has applications in the measurement of glucose in blood, or in remote sensing to measure in multiple wavelengths to have a better characterization of a scene. In the Stokes polarimeter considered in this work, we use two liquid crystal variable retarders (LCVR's) combined with a Glan-Thompson linear polarizer. A recently developed fitting calibration procedure is used. We use the same calibration samples and LCVR voltages for all three wavelengths, giving simultaneous measurement and calibration. We compare the performance of the polarimeter, after calibration, using four or six calibration samples in our experiment. Experimental results show good agreement with the expected results, with the fitting calibration procedure giving an approximately 50% reduction in total RMS error with four calibration samples, and a small increased reduction in the error, as compared to the four samples case, when six calibration samples are used.

Resumen

El interés en la polarimetría recientemente ha tenido un aumento significativo, esto en gran parte debido al avance tecnológico, particularmente por los avances de los retardadores variables y los detectores polarizados. También, el desarrollo de nuevas aplicaciones, por ejemplo, en percepción remota, microscopía, aplicaciones médicas, astronomía y metrología, entre otras. Dado el interés en estas nuevas técnicas y aplicaciones, hay mucho trabajo sobre los métodos de calibración y extracción de datos, que son requeridos para corregir los efectos de los errores experimentales y de medición en los polarímetros. En esta tesis, se presenta un método para la calibración y extracción de datos para un polarímetro de Stokes trabajando con tres diferentes longitudes de onda simultáneamente. Este tipo de sistemas tienen aplicaciones en la medición de glucosa en la sangre, o en percepción remota para medir en múltiples longitudes de onda lo cual permite una mejor caracterización para una imagen que se esté analizando. Para el polarímetro de Stokes considerado en este trabajo, empleamos un par de retardadores variables de cristal líquido (LCVR´s por sus siglas en inglés) combinado con un polarizador lineal Glan-Thompson. Además, un método reciente de ajuste es empleado en el proceso de calibración. Usamos las mismas muestras de calibración y los mismos valores de voltaje aplicados a las LCVR's para las tres longitudes de onda, permitiendo obtener las mediciones y la calibración de datos de manera simultánea. Se comparó el rendimiento del polarímetro, después de la calibración, usando cuatro y seis muestras de calibración en nuestro experimento. Los resultados experimentales muestran una adecuada concordancia con los resultados esperados, con el procedimiento de ajuste del método de calibración dando una reducción de aproximadamente el 50% en el error total RMS con cuatro muestras de calibración, y un pequeño incremento en la reducción del error, en comparación con el caso de cuatro muestras de calibración, cuando usamos seis muestras.

Contents

1. Introduction

Polarimetry has attracted a great deal of interest recently, particularly for applications in medicine [1-5], remote sensing [1,6,7] and astronomy [1,8-16], among others. Many applications require the polarization characterization of a light beam, through the measurement of the Stokes vector of the light. The Stokes vector is a four-element vector:

$$S = \begin{pmatrix} S_0 \\ S_1 \\ S_2 \\ S_3 \end{pmatrix}$$

where, as will be shown in Chapter 2 of this thesis, S_0 is related to the total intensity in the beam, S_1 is related to the difference between horizontal and vertical linear polarized light, $S_2$is the difference between linear polarized light at +45° and at -45°, and S_3 is the difference between right and left circular polarized light. This vector completely describes the polarization state of a light beam. In this thesis we present analysis of systems to measure the Stokes vector. There are also polarimeters to measure the Mueller matrix of a sample, that is the changes a sample makes on an input Stokes vector, but this type of polarimeter will not be discussed in this work.

New calibration and data-extraction techniques, combined with electro-optic retarders, have permitted the development of polarimeters which are faster and more precise [17-28]. There have also been developments in large bandwidth polarimeters, particularly in channeled spectropolarimeters. However, there are still many applications which require measurement of polarization at only a few wavelengths, particularly in medicine, microscopy and remote sensing for which dual-wavelength or RGB (Red, Green, Blue) polarization images provide useful information [2,3,29]. There are methods that can reconstruct full Stokes spectra, for example channeled polarimetry. However, this method requires the measurement of the complete spectrum to be able to reconstruct the variation of the Stokes parameters, so it will not work if only a few wavelengths are available. Also, for other methods, the calibration process becomes complicated to correct for all the wavelengths [2], and the experimental setups are more complicated [29].

The main problem with all of these systems is the calibration and data extraction for the different wavelengths, since the retardances of the polarimeter components vary with these wavelengths [2, 3]. In this work, we propose a calibration and data-extraction method for the measurement of three wavelengths simultaneously, which uses only one configuration of retardances and one set of calibration samples. The method is shown to be fast, robust and precise. It uses a simple calibration process, a standard Stokes polarimeter experimental setup, and can be extended easily to more wavelengths if required. These advantages reduce the measurement time required and the cost of the polarimeter, compared to similar setups. The proposed method is applied to a Stokes polarimeter using two liquid-crystal variable retarders (LCVR's). It is clear that the polarimeter cannot be optimized for the three wavelengths simultaneously, and because of this we use a recently developed fitting procedure to reduce the errors in the measured Stokes vectors [25].

The proposed experimental setup employs beam splitters similar to the division of amplitude polarimeters in order to introduce the beams for different wavelengths into the optical system and to separate the three wavelengths to three different detectors. Although, in this case it is not relevant to know the proportions of the total intensity for the different segmented beams, we know this information for each arm in the system. Also, the results are normalized with respect to the total intensity and therefore variations of the source intensities do not affect the final results. A time-sequential polarimeter with phase modulation elements was instrumented in this project. The phase modulation was induced by applying a set of retardance configurations to analyze four or six polarization states and register the intensity values associated with them. A Mueller matrix analysis was performed to be able to reconstruct the Stokes vectors of the three wavelengths used.

There are different types of polarimeters which have been developed and used for different applications and purposes. It is possible to distinguish the following classification: time-sequential polarimeters which can employ rotating, or phase modulation, elements (polarization modulation), division of aperture and division of amplitude polarimeters. In this section a brief summary of the main types of polarimeters is presented. A detailed discussion of the polarimeter used in this work is given in chapter 2.

In time-sequential polarimeters the measurements are taken sequentially in time and variables such as angle positions or retardance values are changed between measurements with the polarimeter. Usually, this class of polarimeters employ a single source and a detector. Rotating element polarimeters employ rotating polarization elements such as linear retarders and polarizers. One advantage of this class of polarimeters is that in general the optical system design is very simple and one disadvantage is that they employ rotating mounts to rotate the polarizing elements. Phase modulation or polarization modulation polarimeters also take measurements sequentially in time, but these employ polarization modulators which are polarizing devices that induce a retardance between the orthogonal

components of the electric field of the light as a function of an applied voltage. Some advantages of this class of polarimeters are the simplicity of the optical system and the absence of moving elements. On the other hand, one disadvantage is that to describe the modulation of the retardance induced by the polarization modulators on the light beam as a function of the applied voltage, it is necessary obtain the characterization curve of each of the polarizing devices used in the polarimeter [17,18]. A time-sequential polarimeter with two polarization modulators followed by a linear polarizer is used in this work given the advantages listed above.

Generally, rotating element polarimeters work by modulating the intensity signal at the output of the polarimeter as a function of the rotation angle of the elements. This modulation signal can be described by a Fourier series and the polarization information can be obtained from the coefficients of this series, specifically, the four Stokes parameters can be reconstructed by using these coefficient values. Some optical systems for this class of polarimeters are described below.

- A rotating linear polarizer: for this optical system only a polarizer is used to modulate the intensity signal while it rotates.

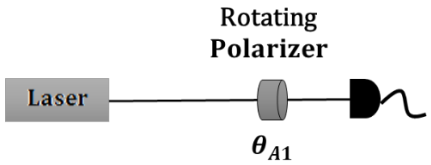

Figure 1 Rotating polarimeter employing only one rotating linear polarizer as analyzer.

The intensity signal modulation is given by the Fourier series [18]:

$$I(\theta_{A1}) = \frac{a_0}{2} + \frac{a_1}{2}\cos 2\theta_{A1} + \frac{b_2}{2}\sin 2\theta_{A1} \quad (1)$$

This expression is given as a function of the rotation angle of the polarizer. Carrying out a Fourier analysis only the three linear Stokes parameters can be obtained:

$$S_0 = a_0, \quad S_1 = a_1 \quad and \quad S_2 = b_2 \quad (2)$$

- Rotating and fixed linear polarizers: in this optical system a pair of linear polarizers are used, one of them fixed in front of the detector after the other which rotates to modulate the intensity signal. The fixed polarizer guarantees that the detector detects only one polarization to avoid errors from the variation of the detector signal with polarization [18].

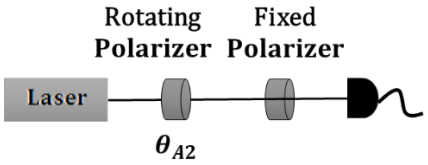

Figure 2 Rotating polarimeter employing a pair of linear polarizers, one of them fixed and the other rotating.

The modulated signal is composed of two frequencies, and it is described by the Fourier series [18]:

$$I(\theta_{A2}) = \frac{a_0}{4} + \frac{1}{4}\sum_{n=1}^{2}(a_{2n}\cos 2n\theta_{A2} + b_{2n}\sin 2n\theta_{A2}) \tag{3}$$

Similarly to the previous case, only the first three linear Stokes parameters can be obtained [18]:

$$S_0 = a_0 - a_4, \quad S_1 = \frac{2}{3}(a_2 - a_0 + 2a_4) \quad and \quad S_2 = 0.4(2b_2 + b_4) \tag{4}$$

- A rotating retarder and a fixed polarizer: in this system a fixed linear polarizer is employed in front of the detector followed by a retarder which rotates, generating a modulation signal at the output of the system. For this case, the generated signal is also composed of two frequencies [18].

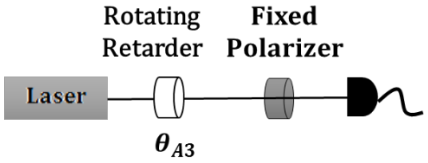

Figure 3 Rotating polarimeter employing a linear fixed polarizer and a rotating retarder.

For this configuration the Fourier series that describes de modulation signal is [18]:

$$I(\theta_{A3}) = \frac{a_0}{2} + \frac{1}{2}\sum_{n=1}^{2}(a_{2n}\cos 2n\theta_{A3} + b_{2n}\sin 2n\theta_{A3}) \tag{5}$$

Given this, the four Stokes parameters are given by [18]:

$$S_0 = a_0 - a_4, \quad S_1 = 2a_4 \quad S_2 = 2b_4 \quad and \quad S_3 = b_2 \tag{6}$$

Another class of time-sequential polarimeter is the phase modulation polarimeter, this type of polarimeter employs polarization modulators which induce a retardance between the orthogonal components of the electric field of the light beam as a response to an electrical signal. In general, the modulation of the intensity signal for the phase modulation

polarimeters is given by changing the retardance values induced by the polarization modulators on the light beam. In this sense, to calculate the Stokes parameters, it is necessary to analyze the optical system employed by performing a matrix analysis through the Mueller matrix calculus, as described in chapter 2 of this thesis. Below are described some optical systems for this class of polarimeter.

- A fixed linear polarizer and a fixed polarization modulator (PM): this polarimeter employs a linear polarizer and a polarization modulator, with fixed axes angles, with their principal axes at 45° to each other [18].

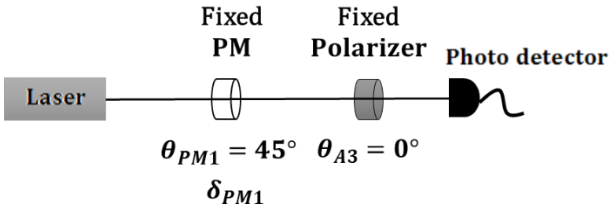

Figure 4 Phase modulation polarimeter employing a linear fixed polarizer and a fixed polarization modulator (PM).

By analyzing this optical system through the individual Mueller matrices of its optical elements it is possible obtain the expression for the modulated intensity as a function of the retardance values induced by the polarization modulator, δ_{PM1}:

$$I(\delta_{PM1}) = \frac{S_0}{2} + \frac{S_1}{2}\cos\delta_{PM1} - \frac{S_3}{2}\sin\delta_{PM1} \tag{7}$$

If the Bickel and Bailey [19] method is used to reconstruct the Stokes parameters, only simple algebraic operations have to be performed with the intensity measurement values. For this system, only three Stokes parameters can be calculated, S_0, S_1 and S_3, and at least four intensity measurements are needed to do that [18] through the following equation:

$$\begin{pmatrix} S_0 \\ S_1 \\ S_2 \\ S_3 \end{pmatrix} = \begin{pmatrix} I_H + I_V \\ I_H - I_V \\ I_- - I_+ \\ I_R - I_L \end{pmatrix} \tag{8}$$

where I_H, I_V, I_-, I_+, I_R and I_L are the intensity values associated with the six polarization states analyzed in the beam under study (Horizontal, Vertical, -45°, +45, Left-handed and Right-handed polarization states). To analyze for these polarization states, it is necessary to apply electrical signals to the polarization modulator (shown in figure 4) to modulate the retardance induced on the beam. In this case only four retardance values are applied, as shown in Table 1.

Table 1 Retardance values induced by the polarization modulator in order to analyze a specific polarization state which is associated with an intensity value.

δ_{PM1} (degrees)	Intensity
0	I_H
180	I_V
90	I_L
270	I_R

When these retardance values are configured in the Stokes polarimeter then the corresponding intensity values are measured and the three Stokes parameters can be calculated through equation (8).

To calculate the S_2 Stokes parameter an alternative configuration can be used.

- A fixed linear polarizer and a fixed polarization modulator (PM): this configuration employs a linear polarizer and a fixed polarization modulator, with their principal axes at 45° to each other and rotated 45° with respect to the previous configuration (see figure 4) [18].

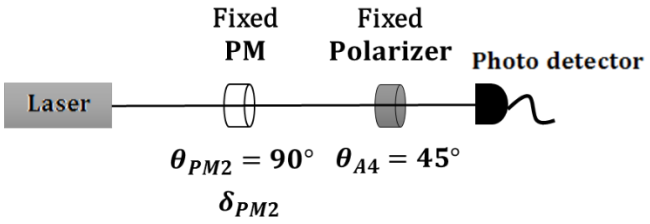

Figure 5 Alternative phase modulation polarimeter employing a linear fixed polarizer and a fixed polarization modulator (PM).

In this case, the intensity signal modulation is given by:

$$I(\delta_{PM2}) = \frac{S_0}{2} + \frac{S_2}{2}\cos\delta_{PM2} + \frac{S_3}{2}\sin\delta_{PM2} \tag{9}$$

By a similar analysis, it is possible to show that the retardance values necessary to measure intensities associated with specific polarization states are given in Table 2.

Table 2 Retardance values induced by the polarization modulator to analyze a specific polarization state associated with an intensity value for the alternative optical system.

$\delta_{PM2}\,(degrees)$	Intensity
0	I_+
180	I_-
90	I_R
270	I_L

In this sense, equation (8) is used to reconstruct the Stokes parameters S_0, S_2 and S_3, considering that $S_0 = I_+ + I_-$. At least four intensity measurements are needed to do that.

- A fixed linear polarizer and a pair of fixed polarization modulators: in this polarimeter a pair of PM´s with their fast axes at 45° to each other are employed followed by a linear polarizer with its transmission axis parallel to the fast axis of the first PM.

The configuration and analysis for this polarimeter is presented in detail in chapter two in points 2.4 and 2.5 as this type of polarimeter was used in this work.

A division of amplitude polarimeter consists of an optical setup which employs a beam splitter (BS) to divide an incident beam into a reflected and a transmitted beam. The beam splitter introduces known amounts of retardance and diattenuation into the transmitted and reflected beams. Each beam is analyzed by a pair of Wollastone prisms (WP1 and WP2) which are followed by four photodetectors (D1, D2, D3 and D4), see figure 7 [36,37].

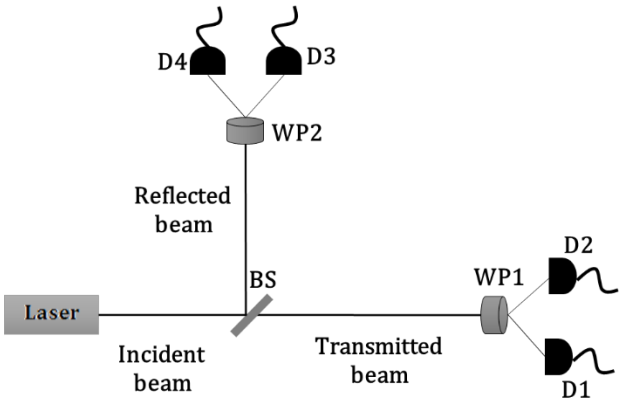

Figure 6 Division of amplitude polarimeter experimental setup. A beam splitter (BS) splits an incident beam into a reflected and a transmitted beam. Then each beam is analyzed by a Wollaston prism (WP1 and WP2) followed by four photodetectors (D1, D2, D3 and D4).

Two advantages of this type of polarimeter are that they do not employ moving elements and they allow us to obtain the four Stokes parameters of the incident beam which describe the polarization state of this beam. Three points to consider for this type of polarimeter are: they require that the cross section of the incident beam be uniformly polarized, it is necessary to know the proportions of the total light flux for the different segmented beams and, we need to assume that ideally all photodetectors have the same absolute response, or we have to calibrate them [36,37].

The response ξ of the polarimeter as a function of the Stokes vector of the incident beam S_{DAi} and the characteristic matrix $\boldsymbol{F}$ for the system which depends on the wavelength used is:

$$\xi = \boldsymbol{F} S_{DAi} \tag{10}$$

where the response of each photodetector can be described in terms of its sensitivity C_k, and the light flux arriving on each detector, I_{fluxk}.

$$\xi = C_k I_{fluxk} \tag{11}$$

Four signals are detected, so $k = 1,2,3,4$.

Given this, the Stokes vector of the incident beam can be calculated as:

$$S_{DAi} = \boldsymbol{F}^{-1}\xi \tag{12}$$

$\boldsymbol{F}$ is a 4x4 matrix where each element (f_{ij}, $i = 1,2,3,4$ and $j = 1,2,3,4$) is given as a function of the elements of the reflection and transmission matrices of the beam splitters (r_{ij} and t_{ij}, $i = 1,2,3,4$ and $j = 1,2,3,4$), the azimuth angles of the Wollastone prisms ($A_1\ and\ A_2$), and the detector sensitives ($C_1, C_2, C_3\ and\ C_4$) [36, 37].

$$f_{1j} = C_1\left(r_{1j} + r_{2j}\cos 2A_1 + r_{3j}\sin 2A_1\right) \tag{13}$$

$$f_{2j} = C_2\left(r_{1j} - r_{2j}\cos 2A_1 - r_{3j}\sin 2A_1\right) \tag{14}$$

$$f_{3j} = C_3\left(t_{1j} + t_{2j}\cos 2A_2 + t_{3j}\sin 2A_2\right) \tag{15}$$

$$f_{4j} = C_4\left(t_{1j} - t_{2j}\cos 2A_2 - t_{3j}\sin 2A_2\right) \tag{16}$$

where $j = 1,2,3,4$.

A division of aperture polarimeter works by subdividing its aperture into a specific number of sub-apertures. Polarization information of the beam is analyzed by independent polarization analyzers for each subdivision [17, 38]. Different configurations have been proposed for this type of polarimeter [39]. Given the well-known matrix analysis through Mueller matrices and Stokes vectors, an optimal configuration for this type of polarimeter has four sub-apertures. A commercial setup for a polarized CMOS camera is shown in Figure 7, using a 2x2 block of miniature polarizers in front of the CMOS pixels. This system measures only the linear components of the Stokes vector

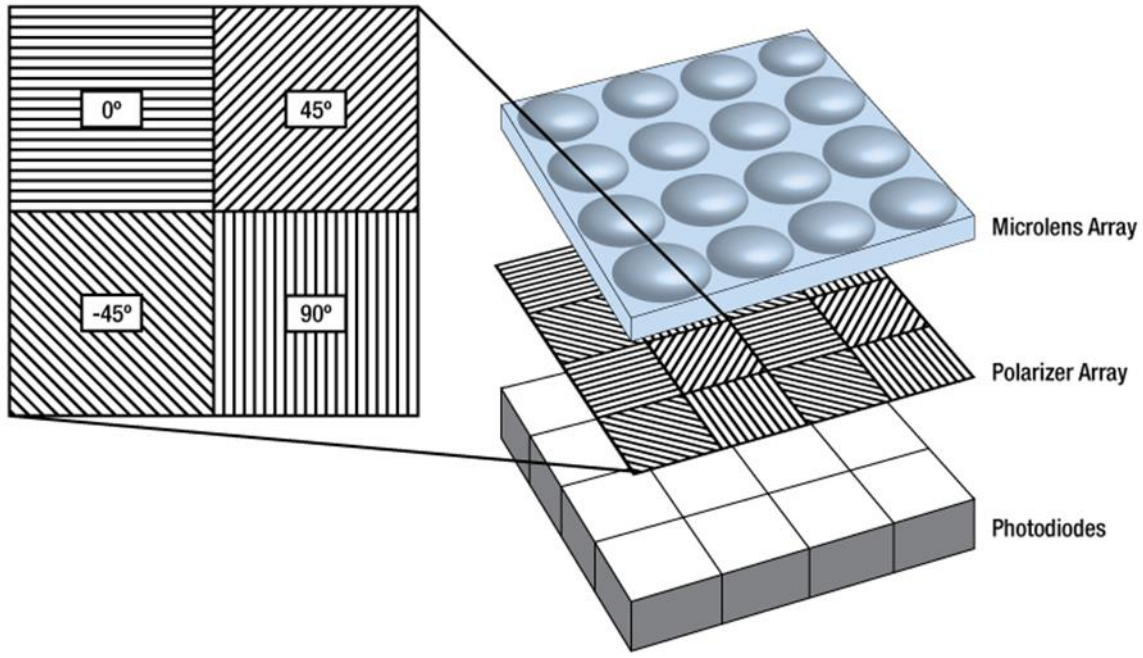

Figure 7 Construction of a CMOS camera with a 2x2 array of polarizers in front of the pixels. Taken from the ThorLabs catalog https://www.thorlabs.com/newgrouppage9.cfm?objectgroup_id=13033

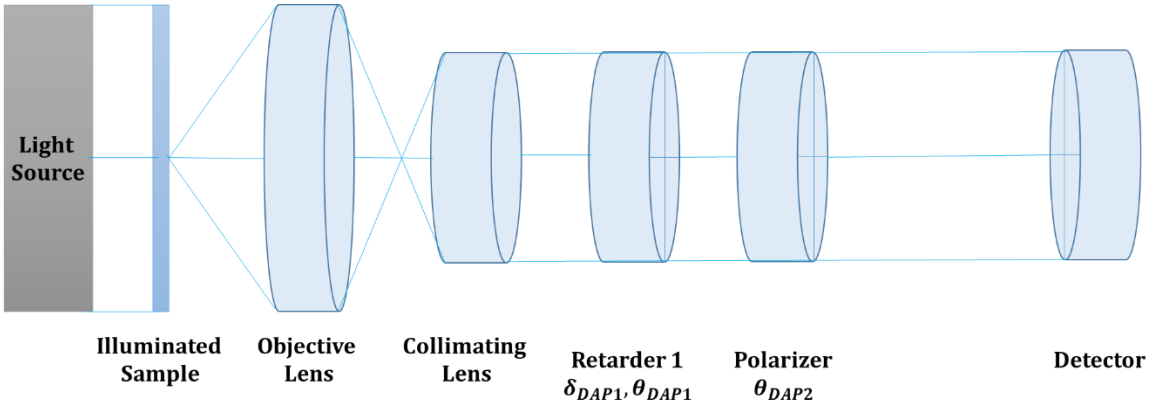

Figure 8 Division of aperture polarimeter experimental setup. The sample is illuminated by a source, the light travels through this sample and is collected by an objective lens which is followed by a collimating lens. Then, the light travels to the polarization analyzer which consists of a linear retarder and a polarizer subdivided in four quadrants.

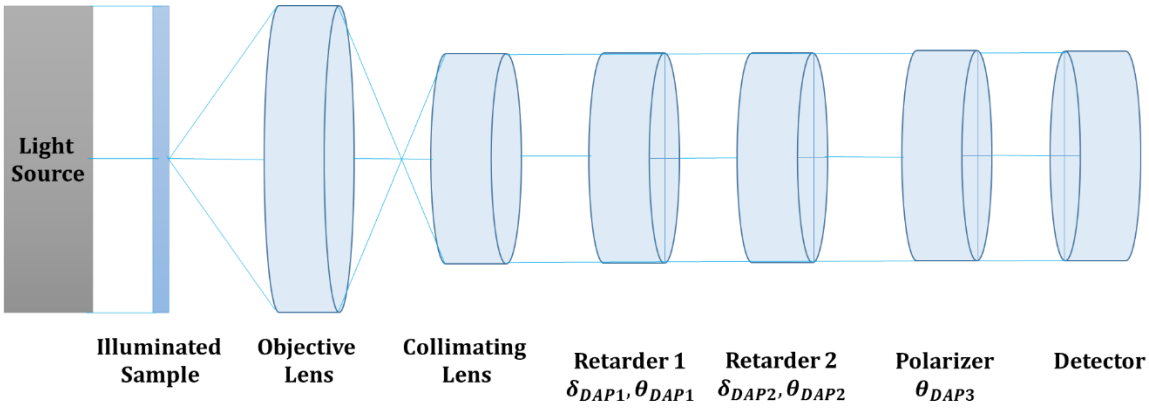

Figure 9 Similar to the above setup but in this division of aperture polarimeter a second retarder has been added.

Figure 8 shows a laboratory system used to measure the full Stokes vector. In this case the retarder, polarizer and detector are subdivided in 4 quadrants and in which the retardance and/or the polarization can vary.

For each quadrant or sub-aperture, the relationship between the Stokes vectors for the incident and output beams of light is given by:

$$S_{DAPOUT} = \boldsymbol{M}_{DAPSYS} S_{DAPIN} \tag{17}$$

To calculate the four Stokes parameters of the Stokes vector for the incident beam, S_{DAPIN}, at least four intensity measurements are required. These intensity measurements are taken simultaneously by the four subdivisions of the aperture Stokes polarimeter. From equation (17), the first parameter of the Stokes vector for the output beam represents the total intensity measured by the detector. In this sense, the Mueller matrices of the optical systems shown in figures 8 and 9, are very important and can be calculated through the individual Mueller matrices of their polarization elements. Equations (18) and (19) represent these matrices for each setup [39].

$$\boldsymbol{M}_{DAPSYS8} = \boldsymbol{M}_{POL}(\theta_{DAP2}) \boldsymbol{M}_{RET1}(\theta_{DAP1}, \delta_{DAP1}) \tag{18}$$

$$\boldsymbol{M}_{DAPSYS9} = \boldsymbol{M}_{POL}(\theta_{DAP3}) \boldsymbol{M}_{RET2}(\theta_{DAP2}, \delta_{DAP2}) \boldsymbol{M}_{RET1}(\theta_{DAP1}, \delta_{DAP1}) \tag{19}$$

Given that the first Stokes parameter of the output beam is the total intensity and a total of four intensity measurements can be taken with the Stokes polarimeter and the matrix of the optical system is also known, the relationship for the two setups shown in figures 8 and 9 is [39]:

$$I_{DAP} = \boldsymbol{A}_{DAP} S_{DAPIN} \tag{20}$$

where $\boldsymbol{A}_{DAP}$ is a 4x4 characteristic matrix of the system, and it is expressed as a function of the retardance values and the position of the principal axes of the retarders and polarizers in the polarimeter [39].

From equation (20), the full Stokes vector and therefore the polarization state of the incident beam can be calculated as [39]:

$$S_{DAPIN} = \boldsymbol{A}_{DAP}^{-1} I \tag{21}$$

where $\boldsymbol{A}_{DAP}^{-1}$ is the inverse of the 4x4 characteristic matrix $\boldsymbol{A}_{DAP}$ [39].

In this thesis we present the principal results of the experimental and simulated work performed using a two LCVR and one linear polarizer to form a full-Stokes polarimeter. In chapter 2, the general polarimetry theory used is presented, in chapter 3 we describe the results obtained, and in chapter 4 the principal conclusions are discussed.

2. Polarization of light.

2.1 Introduction.

Polarization is a fundamental property of light which is directly related to its vector nature, more specifically, to the behavior of its electric field vector. In nature, light is non-polarized or partially polarized and therefore the electric field amplitude and the phase can vary randomly, spatially and temporarily. A polarized light beam is one that has preference either as to transverse direction or it maintains a constant phase relation between its component fields. The polarization of light is directly related to amplitude, direction and phase values of the electric field vector components. If we consider that a beam is traveling along the positive z axis the electric field vector will be contained within the $x - y$ plane and it is described by [18]:

$$\boldsymbol{E}_0 = E_x\hat{x} + E_y\hat{y} \tag{22}$$

where the orthogonal electric field components are given by [18]:

$$E_x = E_{0x}\cos(\Omega t - kz) \tag{23}$$

$$E_y = E_{0y}\cos(\Omega t - kz + \delta) \tag{24}$$

In these equations Ω is the angular frequency of the light beam, k is the wave number in the propagation medium $k = 2\pi/\lambda$ and $\delta = \delta_y - \delta_x$ is the phase difference between the oscillations of the orthogonal components, E_x and E_y [18].

The electric field vector can describe a geometric figure when it moves on the $x - y$ plane, and generally, the movement can be described by an ellipse. Figure 9 represents this ellipse [18].

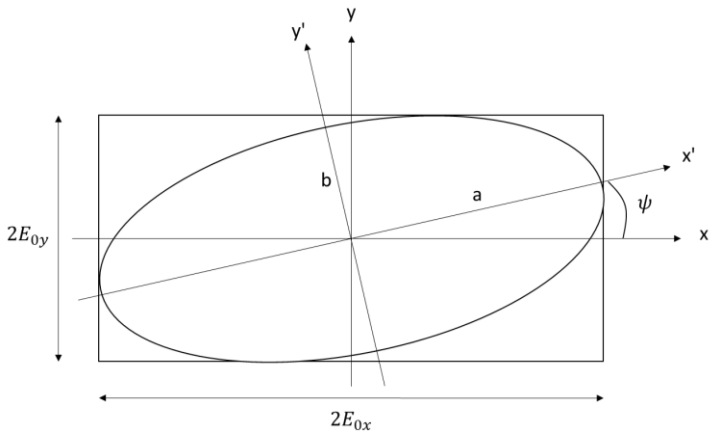

Figure 9 Polarization ellipse [18].

The orthogonal components of the electric field can also be written as:

$$E_x = E_{0x}\cos(\tau + \delta_x) \tag{25}$$

$$E_y = E_{0y}\cos(\tau + \delta_y) \tag{26}$$

where the propagator term is $\tau = \Omega t - kz$.

If we apply the trigonometric identity for the cosine of the sum of two angles, we can rewrite equations (25) and (26) as [18]:

$$\frac{E_x}{E_{0x}} = \cos\tau\cos\delta_x - \sin\tau\sin\delta_x \tag{27}$$

$$\frac{E_y}{E_{0y}} = \cos\tau\cos\delta_y - \sin\tau\sin\delta_y \tag{28}$$

Multiplying equations (27) and (28) by $\sin\delta_y$ and $\sin\delta_x$, respectively [18]:

$$\frac{E_x}{E_{0x}}\sin\delta_y = \cos\tau\cos\delta_x\sin\delta_y - \sin\tau\sin\delta_x\sin\delta_y \tag{29}$$

$$\frac{E_y}{E_{0y}}\sin\delta_x = \cos\tau\cos\delta_y\sin\delta_x - \sin\tau\sin\delta_y\sin\delta_x \tag{30}$$

and subtracting equation (30) from equation (29), squaring and applying the trigonometric identity $\sin(\delta_y - \delta_x) = \sin\delta_y\cos\delta_x - \cos\delta_y\sin\delta_x$ [18]:

$$\frac{E_x^2}{E_{0x}^2}\sin^2\delta_y + \frac{E_y^2}{E_{0y}^2}\sin^2\delta_x - 2\frac{E_x}{E_{0x}}\frac{E_y}{E_{0y}}\sin\delta_x\sin\delta_y = \cos^2\tau\sin^2(\delta_y - \delta_x) \tag{31}$$

In a similar way, equations (27) and (28) can be multiplied by $\cos\delta_y$ and $\cos\delta_x$, respectively [18]:

$$\frac{E_x}{E_{0x}}\sin\delta_y = \cos\tau\cos\delta_x\cos\delta_y - \sin\tau\sin\delta_x\cos\delta_y \tag{32}$$

$$\frac{E_y}{E_{0y}}\sin\delta_x = \cos\tau\cos\delta_y\cos\delta_x - \sin\tau\sin\delta_y\cos\delta_x \tag{33}$$

The difference between equations (33) and (32) is calculated, the result is squared and the same trigonometric identity for $\sin(\delta_y - \delta_x)$ is applied to obtain [18]:

$$\frac{E_x^2}{E_{0x}^2}\cos^2\delta_y + \frac{E_y^2}{E_{0y}^2}\cos^2\delta_x - 2\frac{E_x}{E_{0x}}\frac{E_y}{E_{0y}}\cos\delta_x\cos\delta_y = \sin^2\tau\sin^2(\delta_y - \delta_x) \qquad (34)$$

By adding equations (31) and (34) and applying the trigonometric identity $\cos(\delta_y - \delta_x) = \cos\delta_y\cos\delta_x + \sin\delta_y\sin\delta_x$ [18]:

$$\frac{E_x^2}{E_{0x}^2} + \frac{E_y^2}{E_{0y}^2} - 2\frac{E_x^2}{E_{0x}^2}\frac{E_y^2}{E_{0y}^2}\cos\delta = \sin^2\delta \qquad (35)$$

where $\delta = \delta_y - \delta_x$ as before.

This is the general equation of the ellipse of figure 9. Two possible degenerate cases of the ellipse can be a circle and a line, which correspond to circularly and linearly polarized states, respectively [18]. For circularly polarized light $\delta = 90°$ (or $-90°$) and the amplitudes $E_{0x} = E_{0y}$, and for linearly polarized light $E_{0y} = 0$ for horizontal polarized light, $E_{0x} = 0$ for vertical polarized light, $\delta = 0°$ and $\delta = 180°$ with $E_{0x} = E_{0y}$, for +45° and -45° polarized light, respectively. In general, for linear polarized light $\delta = 0°$ and the polarization direction is given by $\tan^{-1}\left(\frac{E_{0y}}{E_{0x}}\right)$.

Considering a monochromatic wave, only the orthogonal components of the electric field E_x and E_y in equation (35) are dependent on time. The amplitudes and relative phases are constant. To represent equation (35) in terms of observables we can take the time average for these components which are denoted as [18]:

$$\langle E_x^2\rangle = \frac{1}{2}E_{0x}^2 \qquad (36)$$

$$\langle E_y^2\rangle = \frac{1}{2}E_{0y}^2 \qquad (37)$$

$$\langle E_x E_y\rangle = \tfrac{1}{2}E_{0x}E_{0y}\cos\delta \qquad (38)$$

where the factor ½ comes from the average over an integer number of periods of the cosine time variation. Multiplying equation (35) by $4E_{0x}^2E_{0y}^2$ and substituting equations (36), (37) and (38), we have [18]:

$$2E_{0x}^2E_{0y}^2 + 2E_{0x}^2E_{0y}^2 - (2E_{0x}E_{0y}\cos\delta)^2 = \left(2E_{0x}E_{0y}\sin\delta\right)^2 \qquad (39)$$

If we add and subtract the quantity $E_{0x}^4 + E_{0y}^4$ to the left side of equation (39) and regroup terms, we get [18]:

$$(E_{0x}^2 + E_{0y}^2)^2 - \left(E_{0x}^2 - E_{0y}^2\right)^2 - (2E_{0x}E_{0y}\cos\delta)^2 = \left(2E_{0x}E_{0y}\sin\delta\right)^2 \quad (40)$$

Each term inside parentheses is renamed as a Stokes parameter [18]:

$$S_0 = E_{0x}^2 + E_{0y}^2 \quad (41)$$

$$S_1 = E_{0x}^2 - E_{0y}^2 \quad (42)$$

$$S_2 = 2E_{0x}E_{0y}\cos\delta \quad (43)$$

$$S_3 = 2E_{0x}E_{0y}\sin\delta \quad (44)$$

Then equation (40) can be written as:

$$S_0^2 = S_1^2 + S_2^2 + S_3^2 \quad (45)$$

where S_0, S_1, S_2 and S_3 are known as the Stokes parameters of the light wave. Equation (45) is valid for a completely polarized light beam. If the beam is partially polarized or unpolarized, it can be shown [18] that:

$$S_0^2 \geq S_1^2 + S_2^2 + S_3^2 \quad (46)$$

It is also important to point out that the parameter S_0 is the total energy in the beam and corresponds to the direct measurement of the beam by a detector.

2.2 Stokes vectors and Mueller matrices.

A very useful mathematical tool for representing the polarization state of light was described by Sir George Gabriel Stokes (1819-1903). The polarization state of light is represented by the four measurable quantities described in the previous section called the Stokes polarization parameters. One characteristic which is very important is that unpolarized or partially polarized (and completely polarized) light can be described by the Stokes parameters. The four Stokes parameters are defined as S_0, S_1, S_2 and S_3. The first parameter represents the total intensity of the optical field; the remaining parameters describe the predominance of a determined polarization state in the beam. S_1 describes the predominance of linear horizontal or vertical polarization states, S_2 describes the tendency of linear +45° or -45° polarization states and S_3 describes the predominance of circular right- or left-handed polarization states. All Stokes parameters represent observables; this means that they are real quantities [18]. The four parameters can be represented as a vector which is called the Stokes vector and describes the polarization state of a light beam.

$$S = \begin{pmatrix} S_0 \\ S_1 \\ S_2 \\ S_3 \end{pmatrix} \tag{47}$$

In figure 10, we can see a geometrical representation of six polarization states and their polarization Stokes vectors.

In general, the polarization state of a beam of light changes when the beam interacts with matter due to different effects such as scattering or diffraction, diattenuation or birefringence, within the matter. Matter changes the initial polarization state of an incident beam by changing the amplitudes of the constituent electric fields, the direction of propagation or the relative phase between the electric field components, as well as by transferring energy from polarized states to the un-polarized state, called depolarization [18].

Polarizers and retarders are the two most common optical devices used to change the polarization state of light and are the basis of polarimeters. A linear polarizer produces a linearly polarized beam of light for any polarization of light passing through it. There are also circular and elliptical polarizers, which also require the use of a retarder, as described below, as well as a linear polarizer. The orientation of the polarization state transmitted by a linear polarizer is defined by the properties of the polarizer, this direction is called the transmission axis of the linear polarizer (the extinction axis is perpendicular to it). An important parameter of the linear polarizer is the extinction coefficient, which is the attenuation capability to extinguish a component along the extinction axis; it is expressed as the ratio between the transmittance of an incident linear polarization parallel to the transmission axis and an incident linear polarization perpendicular to the transmission axis. So, an extinction coefficient of 100,000:1 means that the polarizer transmits 100,000 times more light when the incident polarization is parallel to the transmission axis than when the incident polarization is perpendicular to the extinction axis.

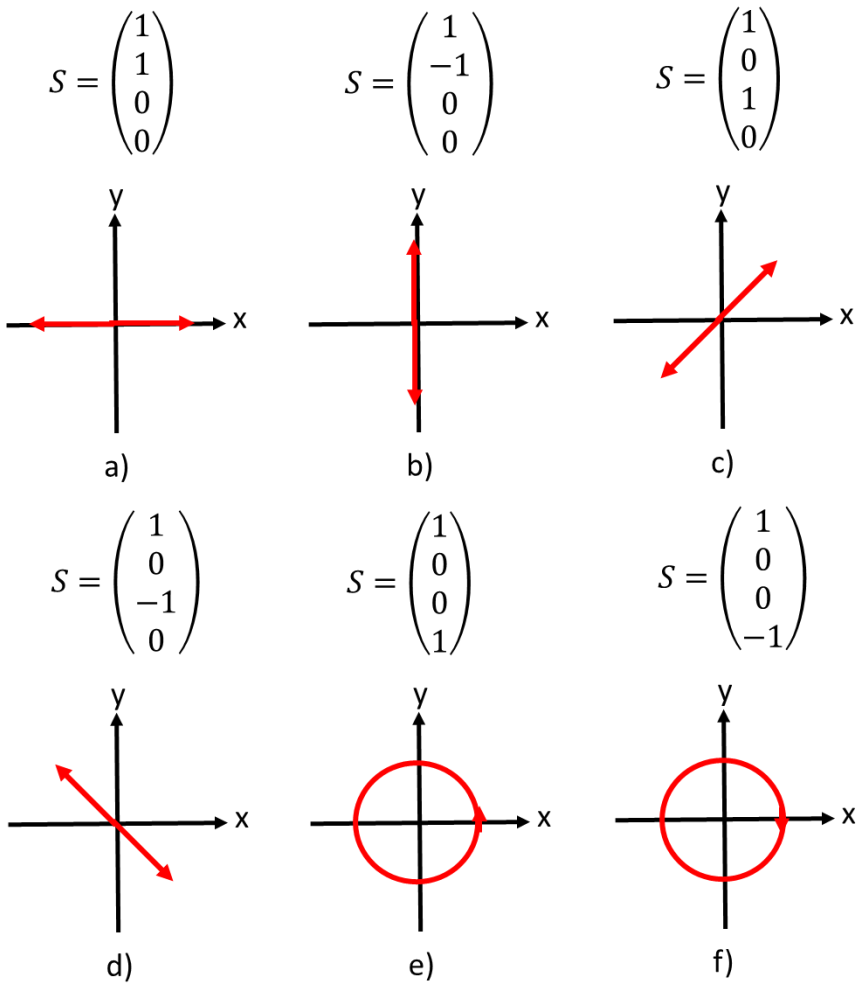

Figure 10 Geometrical representations for a) horizontal, b) vertical, c) +45, d) -45, e) circular left-handed and f) circular right-handed polarization states. These geometrical figures are registered at a fixed point, and the red lines indicate the trajectory of the end point of the electric field vector in time.

A retarder is an optical element which changes the phase between the orthogonal components of the electric field of the incident beam. A retarder is a plate cut from a birefringent material so that it has two orthogonal axes, one of them with a smaller refractive index than the other. The direction on the plate with the smaller refractive index is called the fast axis and the direction with the high refractive index is the slow axis. The materials used for retarders can be plastics for low-quality devices, and quartz or calcite for higher quality retarders. The delay between the orthogonal electric field components is the retardance [18]. For normal incidence on a retarder, the phase difference or retardance is given by the product of the wave number, $k = 2\pi/\lambda$, the refractive index difference between the fast and slow axes, Δn, and the thickness of the retarder plate, t:

$$\Delta\phi = k\,\Delta n\,t \tag{48}$$

A phase difference of 2π between the two electric field components will give no change in the polarization since this phase change gives the same relative positions in the wave cycle for the two components. This means that the thickness, t, of the retarder plate can be such that the retardance is an integer times 2π plus the retardance required, or the thickness can give a phase equal to the retardance. The first type of retarder is called a multiple-order retarder, and the second is a zero-order retarder. Zero-order retarders are more expensive and more difficult to manufacture, because they are very thin, although they are more stable than the multiple-order retarders. Therefore, the retardances reported for retarders are $\Delta\phi \ mod \ 2\pi$. The most common commercial retarders are half-wave plates, with a retardance of 180°, generally used to rotate linear polarization, and quarter-wave plates, with a retardance of 90°, used to produce circular or elliptical polarized light. Clearly, since the retardance, $\Delta\phi$, depends on the wavelength through the wavenumber, retarders are wavelength dependent.

These polarizing elements, or any sample, can change the initial polarization state of light beams, that is they can change the incident Stokes vector of a light beam into a different output Stokes vector. In general, this interaction can be represented by matrix algebra:

$$\begin{pmatrix} S_0' \\ S_1' \\ S_2' \\ S_3' \end{pmatrix} = \begin{pmatrix} m_{00} & m_{01} & m_{02} & m_{03} \\ m_{10} & m_{11} & m_{11} & m_{13} \\ m_{20} & m_{21} & m_{22} & m_{23} \\ m_{30} & m_{31} & m_{32} & m_{33} \end{pmatrix} \begin{pmatrix} S_0 \\ S_1 \\ S_2 \\ S_3 \end{pmatrix} \tag{49}$$

Where the first vector on the left is the Stokes vector of the output beam of light after the interaction with the optical element and the vector on the right-hand side of the equation is the Stokes vector of the incident beam. The 4x4 matrix is known as the Mueller matrix of the optical element and represents the effect of this optical element or sample on the polarization state of the light. Mueller matrices were used by Hans Mueller to describe polarizing properties such as diattenuation, retardance, depolarization, and their form, either linear, circular, or elliptical. As was mentioned before, two important elements for this work are the polarizer and retarder. The Mueller matrices for these cases are described by the following equations [17]: for a polarizer with its transmission axis at an angle θ to the horizontal:

$$\boldsymbol{M}_{pol}(\theta) = \frac{1}{2}\begin{pmatrix} 1 & \cos 2\theta & \text{sen } 2\theta & 0 \\ \cos 2\theta & \cos^2 2\theta & \text{sen } 2\theta \cos 2\theta & 0 \\ \text{sen } 2\theta & \text{sen } 2\theta \cos 2\theta & \text{sen}^2 2\theta & 0 \\ 0 & 0 & 0 & 0 \end{pmatrix} \tag{50}$$

and for a retarder:

$$\boldsymbol{M}_{ret}(\phi,\theta) = \begin{pmatrix} 1 & 0 & 0 & 0 \\ 0 & \cos^2 2\theta + \cos\phi \operatorname{sen}^2 2\theta & (1-\cos\phi)\operatorname{sen} 2\theta \cos 2\theta & -\operatorname{sen}\phi \operatorname{sen} 2\theta \\ 0 & (1-\cos\phi)\operatorname{sen} 2\theta \cos 2\theta & \operatorname{sen}^2 2\theta + \cos\phi \cos^2 2\theta & \operatorname{sen}\phi \cos 2\theta \\ 0 & \operatorname{sen}\phi \operatorname{sen} 2\theta & -\operatorname{sen}\phi \cos 2\theta & \cos\phi \end{pmatrix} \quad (51)$$

where θ is the rotation angle of the transmission axis for the polarizer and the fast axis for the retarder, and ϕ is the retardance of the retarder. Examples of these elements for commonly used values of the parameters in the polarimeters developed in this thesis are:

Horizontal linear polarizer:

$$\boldsymbol{M}_{pol}(0) = \frac{1}{2}\begin{pmatrix} 1 & 1 & 0 & 0 \\ 1 & 1 & 0 & 0 \\ 0 & 0 & 0 & 0 \\ 0 & 0 & 0 & 0 \end{pmatrix} \quad (52)$$

Linear polarizer at 45°:

$$\boldsymbol{M}_{pol}(45) = \frac{1}{2}\begin{pmatrix} 1 & 0 & 1 & 0 \\ 0 & 0 & 0 & 0 \\ 1 & 0 & 1 & 0 \\ 0 & 0 & 0 & 0 \end{pmatrix} \quad (53)$$

Vertical linear polarizer:

$$\boldsymbol{M}_{pol}(90) = \frac{1}{2}\begin{pmatrix} 1 & -1 & 0 & 0 \\ -1 & 1 & 0 & 0 \\ 0 & 0 & 0 & 0 \\ 0 & 0 & 0 & 0 \end{pmatrix} \quad (54)$$

Half-wave retarder with its fast axis horizontal:

$$\boldsymbol{M}_{ret}(180,0) = \begin{pmatrix} 1 & 0 & 0 & 0 \\ 0 & 1 & 0 & 0 \\ 0 & 0 & -1 & 0 \\ 0 & 0 & 0 & -1 \end{pmatrix} \quad (55)$$

Half-wave retarder with its fast axis at 45°:

$$\boldsymbol{M}_{ret}(180,45) = \begin{pmatrix} 1 & 0 & 0 & 0 \\ 0 & -1 & 0 & 0 \\ 0 & 0 & 1 & 0 \\ 0 & 0 & 0 & -1 \end{pmatrix} \quad (56)$$

Half-wave retarder with its fast axis vertical:

$$\boldsymbol{M}_{ret}(180,90) = \begin{pmatrix} 1 & 0 & 0 & 0 \\ 0 & 1 & 0 & 0 \\ 0 & 0 & -1 & 0 \\ 0 & 0 & 0 & -1 \end{pmatrix} \tag{57}$$

Quarter-wave retarder with its fast axis horizontal:

$$\boldsymbol{M}_{ret}(90,0) = \begin{pmatrix} 1 & 0 & 0 & 0 \\ 0 & 1 & 0 & 0 \\ 0 & 0 & 0 & 1 \\ 0 & 0 & -1 & 0 \end{pmatrix} \tag{58}$$

Quarter-wave retarder with its fast axis at 45°:

$$\boldsymbol{M}_{ret}(90,45) = \begin{pmatrix} 1 & 0 & 0 & 0 \\ 0 & 0 & 0 & -1 \\ 0 & 0 & 1 & 0 \\ 0 & 1 & 0 & 0 \end{pmatrix} \tag{59}$$

Quarter-wave retarder with its fast axis vertical:

$$\boldsymbol{M}_{ret}(90,90) = \begin{pmatrix} 1 & 0 & 0 & 0 \\ 0 & 1 & 0 & 0 \\ 0 & 0 & 0 & -1 \\ 0 & 0 & 1 & 0 \end{pmatrix} \tag{60}$$

2.3 Stokes polarimeter.

Polarimetry is the science that allows the measurement of polarization properties of light. Stokes polarimeters are optical devices used to determine the polarization state of light in a beam, and can be used to extract, for example, oscillation direction and helicity of the electric field, or degree of polarization. Mueller polarimeters determine the change in polarization caused by the interaction of a controlled beam with a sample. A light beam can be transmitted, reflected, diffracted or scattered beam by a sample. Generally, the term sample describes some type of light-matter interaction, or the sequence of such interactions.

A polarization State Analyzer (PSA) is a combination of retarders and polarizer to permit the measurement of different polarization states of a light beam. The elements of a PSA can change through rotation, or, in the case of electrooptic elements, change in retardance through changes in applied voltage. This allows various polarization states to be measured to permit the reconstruction of the Stokes vector of the incident beam. To measure the Mueller matrix of a sample, the changes between controlled polarization states incident on the sample, and the output polarization states after the sample must be measured. This means that a Mueller

polarimeter is composed of a Polarization State Generator (PSG) to control the incident polarization, and a PSA is used to analyze the output polarization states [17].

To measure the Stokes vector a minimum of 4 measurements are needed, since the Stokes vector has 4 unknown parameters. If we consider a classical method to measure the four parameters of the Stokes vector for a light beam when the experimental setup is configured by a wave plate with its fast axis at 0°, $\boldsymbol{M}_{ret}(\phi, 0°)$ and, a polarizer, $\boldsymbol{M}_{pol}(\theta)$, that is a variable retarder and a rotating linear polarizer, the Mueller matrix for the Stokes polarimeter can be obtained from equations (50) and (51) [18]:

$$\boldsymbol{M}_{SP}(\phi, \theta) = \boldsymbol{M}_{pol}(\theta)\boldsymbol{M}_{ret}(\phi, 0°)$$

$$\boldsymbol{M}_{SP}(\phi, \theta) = \begin{pmatrix} 1 & \cos 2\theta & \cos\phi \sin 2\theta & \sin\phi \sin 2\theta \\ \cos 2\theta & \cos^2 2\theta & \cos\phi \sin 2\theta \cos 2\theta & \sin\phi \sin 2\theta \cos 2\theta \\ \sin 2\theta & \sin 2\theta \cos 2\theta & \cos\phi \sin^2 2\theta & \sin\phi \sin^2 2\theta \\ 0 & 0 & 0 & 0 \end{pmatrix} \quad (61)$$

The Stokes vector after the polarizer is given by $S' = \boldsymbol{M}_{SP}(\phi, \theta)S$ and from equation (49) we can obtain the expression for the first parameter of the output beam, S_0', which represents the total intensity at the output of the Stokes polarimeter. By substituting equation (61) into equation (49) the expression for S_0' is given by:

$$S_0' = \frac{1}{2}(S_0 + S_1 \cos 2\theta + S_2 \cos\phi \sin 2\theta + S_3 \sin\phi \sin 2\theta) = I_T(\phi, \theta) \quad (62)$$

From equation (62), and using the values of the cosine and sine, it is possible to calculate the Stokes parameters of the incident beam, S_0, S_1, S_2 and S_3 [18].

$$S_0 = I_T(0°, 0°) + I_T(0°, 90°) \quad (63)$$

$$S_1 = I_T(0°, 0°) - I_T(0°, 90°) \quad (64)$$

$$S_2 = 2I_T(0°, 45°) - S_0 \quad (65)$$

$$S_3 = 2I_T(90°, 45°) - S_0 \quad (66)$$

where $I_T(0°, 0°), I_T(0°, 90°), I_T(0°, 45°)$ and $I_T(90°, 45°)$ are the intensities associated with horizontal, vertical, +45 and circular right-handed polarization states, respectively. To calibrate the Stokes polarimeter, note that the total error value obtained with these equations can be large given that the parameters S_2 and S_3 depend on the value of S_0, so any error in S_0 due to the experimental errors or measurement noise, is repropagated in the values of S_2 and S_3. This represents a problem for the calibration of Stokes polarimeters with this configuration.

In order to eliminate this problem, it is possible to add two intensity measurements, $I_T(0°,-45°)$ and $I_T(90°,-45°)$ which are associated with -45° and circular left-handed polarization states, respectively. For this case, six measurements are made to determine the four Stokes parameters for the incident beam. Equations (65) and (66) are valid for this case but the parameters S_2 and S_3 can also be calculated independently from S_0, as:

$$S_2 = I_T(0°,45°) - I_T(0°,-45°) \tag{67}$$

$$S_3 = I_T(90°,45°) - I_T(90°,-45°) \tag{68}$$

For this case, as will be seen below, the method to determine the Stokes vector of the incident beam is optimized in terms of the propagation of experimental errors to the final calculated Stokes parameters.

Now, the above analysis can be performed by using an equation system represented by a matrix equation. If we use only four intensity measurements, associated with horizontal, vertical, +45 and circular right-handed polarization states, to calculate the Stokes parameters for the incident beam, from equation (62) we have the following equation system:

$$\frac{1}{2}(S_0 + S_1\cos 2\theta_h + S_2\cos\phi_h \sin 2\theta_h + S_3 \sin\phi_h \sin 2\theta_h) = I_{T_h} \tag{69}$$

$$\frac{1}{2}(S_0 + S_1\cos 2\theta_v + S_2\cos\phi_v \sin 2\theta_v + S_3 \sin\phi_v \sin 2\theta_v) = I_{T_v} \tag{70}$$

$$\frac{1}{2}(S_0 + S_1\cos 2\theta_+ + S_2\cos\phi_+ \sin 2\theta_+ + S_3 \sin\phi_+ \sin 2\theta_+) = I_{T_+} \tag{71}$$

$$\frac{1}{2}(S_0 + S_1\cos 2\theta_R + S_2\cos\phi_R \sin 2\theta_R + S_3 \sin\phi_R \sin 2\theta_R) = I_{T_R} \tag{72}$$

where sub-indexes h, v, + and R denote the four polarization states analyzed. This system of equations can be rewritten as follows:

$$\frac{1}{2}\begin{pmatrix} 1 & \cos 2\theta_h & \cos\phi_h \sin 2\theta_h & \sin\phi_h \sin 2\theta_h \\ 1 & \cos 2\theta_v & \cos\phi_v \sin 2\theta_v & \sin\phi_v \sin 2\theta_v \\ 1 & \cos 2\theta_+ & \cos\phi_+ \sin 2\theta_+ & \sin\phi_+ \sin 2\theta_+ \\ 1 & \cos 2\theta_R & \cos\phi_R \sin 2\theta_R & \sin\phi_R \sin 2\theta_R \end{pmatrix}\begin{pmatrix} S_0 \\ S_1 \\ S_2 \\ S_3 \end{pmatrix} = \begin{pmatrix} I_{T_h} \\ I_{T_v} \\ I_{T_+} \\ I_{T_R} \end{pmatrix} \tag{73}$$

which can be written as:

$$\boldsymbol{M}_4 S = I_4 \tag{74}$$

where

$$\boldsymbol{M}_4 = \frac{1}{2}\begin{pmatrix} 1 & \cos 2\theta_h & \cos\phi_h \sin 2\theta_h & \sin\phi_h \sin 2\theta_h \\ 1 & \cos 2\theta_v & \cos\phi_v \sin 2\theta_v & \sin\phi_v \sin 2\theta_v \\ 1 & \cos 2\theta_+ & \cos\phi_+ \sin 2\theta_+ & \sin\phi_+ \sin 2\theta_+ \\ 1 & \cos 2\theta_R & \cos\phi_R \sin 2\theta_R & \sin\phi_R \sin 2\theta_R \end{pmatrix} \quad (75)$$

So that, the Stokes vector of the incident beam, S_{inc} can be calculated as:

$$S_{inc} = (\boldsymbol{M}_4)^{-1} I_4 \quad (76)$$

where $(\boldsymbol{M}_4)^{-1}$ is the inverse matrix of $\boldsymbol{M}_4$.

$\boldsymbol{M}_4$ is called the characteristic matrix of the polarimeter. Tyo demonstrated that the experimental error propagation of the intensity measurement can be determined by the condition number of the characteristic matrix [20]. The condition number is defined as the quotient between the largest and the smallest singular value of the characteristic matrix. To ensure an optimized intensity measurement, the condition number of the Stokes polarimeter characteristic matrix must be optimized to the minimum value. The minimum value found by Tyo for the condition number is $\sqrt{3}$ for a Stokes polarimeter measuring all 4 Stokes parameters [20].

Given the matrix representation, it is clear that to optimize the Stokes parameter measurement when we work with only four intensity measurements, we need to minimize the condition number associated with the matrix $\boldsymbol{M}_4$. Experimentally, we can optimize the condition number of the PSA by adjusting the individual retardance values for the LCVR's, and the position of the principal axes for them and for the polarizer. For the matrix $\boldsymbol{M}_4$, with the configuration given by equation (48), the matrix has the values:

$$\boldsymbol{M}_4 = \frac{1}{2}\begin{pmatrix} 1 & 1 & 0 & 0 \\ 1 & -1 & 0 & 0 \\ 1 & 0 & 1 & 0 \\ 1 & 0 & 0 & 1 \end{pmatrix} \quad (77)$$

and the condition number of this matrix is 3.2255, which is larger than the optimized value $\sqrt{3} = 1.7321$.

For the other case, in which six intensity measurements are taken, the equation system is represented by the following matrix equation:

$$\frac{1}{2}\begin{pmatrix} 1 & \cos 2\theta_h & \cos\phi_h \sin 2\theta_h & \sin\phi_h \sin 2\theta_h \\ 1 & \cos 2\theta_v & \cos\phi_v \sin 2\theta_v & \sin\phi_v \sin 2\theta_v \\ 1 & \cos 2\theta_+ & \cos\phi_+ \sin 2\theta_+ & \sin\phi_+ \sin 2\theta_+ \\ 1 & \cos 2\theta_- & \cos\phi_- \sin 2\theta_- & \sin\phi_- \sin 2\theta_- \\ 1 & \cos 2\theta_R & \cos\phi_R \sin 2\theta_R & \sin\phi_R \sin 2\theta_R \\ 1 & \cos 2\theta_L & \cos\phi_L \sin 2\theta_L & \sin\phi_L \sin 2\theta_L \end{pmatrix}\begin{pmatrix} S_0 \\ S_1 \\ S_2 \\ S_3 \end{pmatrix} = \begin{pmatrix} I_{T_h} \\ I_{T_v} \\ I_{T_+} \\ I_{T_-} \\ I_{T_R} \\ I_{T_L} \end{pmatrix} \tag{78}$$

For this case, two intensity measurements are added, which are associated with -45 and left-handed polarization states. Sub-indexes – and L in equation (78) refer to these polarization states. Equation (78) can be written as:

$$\boldsymbol{M}_6 S = I_6 \tag{79}$$

where

$$\boldsymbol{M}_6 = \frac{1}{2}\begin{pmatrix} 1 & \cos 2\theta_h & \cos\phi_h \sin 2\theta_h & \sin\phi_h \sin 2\theta_h \\ 1 & \cos 2\theta_v & \cos\phi_v \sin 2\theta_v & \sin\phi_v \sin 2\theta_v \\ 1 & \cos 2\theta_+ & \cos\phi_+ \sin 2\theta_+ & \sin\phi_+ \sin 2\theta_+ \\ 1 & \cos 2\theta_- & \cos\phi_- \sin 2\theta_- & \sin\phi_- \sin 2\theta_- \\ 1 & \cos 2\theta_R & \cos\phi_R \sin 2\theta_R & \sin\phi_R \sin 2\theta_R \\ 1 & \cos 2\theta_L & \cos\phi_L \sin 2\theta_L & \sin\phi_L \sin 2\theta_L \end{pmatrix} \tag{80}$$

The Stokes vector of the incident beam, S can be calculated as:

$$S = (\boldsymbol{M}_6)^{\uparrow} I_6 \tag{81}$$

where, in this case, $(\boldsymbol{M}_6)^{\uparrow}$ is the pseudoinverse matrix of $\boldsymbol{M}_6$. For this case the Moore-Penrose pseudoinverse is employed given that $\boldsymbol{M}_6$ is a non-square matrix [33].

Similarly to the four intensity measurements case, the minimum condition number value for the pseudoinverse matrix of $\boldsymbol{M}_6$ allows us to obtain the optimized Stokes vector for the incident beam.

For the configuration of equation (78),

$$\boldsymbol{M}_6 = \frac{1}{2}\begin{pmatrix} 1 & 1 & 0 & 0 \\ 1 & -1 & 0 & 0 \\ 1 & 0 & 1 & 0 \\ 1 & 0 & -1 & 0 \\ 1 & 0 & 0 & 1 \\ 1 & 0 & 0 & -1 \end{pmatrix} \tag{82}$$

and the condition number of this matrix is $\sqrt{3} = 1.7321$, equal to the optimized value, with the least propagation of experimental errors to the final Stokes vector.

2.4 Stokes polarimeter with two LCVR´s.

By measuring the intensities obtained with different configurations of retardance in the PSA, it is possible to determine the polarization state of a beam. As shown above, to measure the four unknown Stokes parameters we require six configurations of retardance on the LCVR´s to obtain six independent measurements of intensity according to the work of Bickel and Bailey [19]. Then, one characteristic matrix is obtained from the retardance values on the LCVR´s. Given that the retardance induced by the LCVR´s depends on the wavelength of the incident beam then the configurations of retardance of the polarimeter will also be different for each wavelength for a chosen configuration of voltages. To choose the voltages to be used for the LCVR's in our polarimeter, we take the Bickel and Bailey configuration [19] for a specific wavelength called the 'central wavelength' or the 'reference wavelength' and calculate the retardances obtained for the other wavelengths using their respective calibration curves.

To avoid rotation of polarization elements, in our polarimeter we use one LCVR with its fast axis horizontal, followed by a second LCVR with its fast axis at 45° to the horizontal, and followed by a linear polarizer with its transmission axis horizontal.

Equation (83) is the Mueller matrix of the Stokes polarimeter and it can be calculated as the product of the individual matrices of the optical elements (see equations (50) and (51)). In this case, see Figure 4, for LCVR 1, $\theta_{L1} = 0°$ and δ_1, are the angle of the fast axis and the retardance, respectively. Similarly, for LCVR 2, $\theta_{L2} = 45°$ and δ_2, are the angles of the fast axis and the retardance, respectively.

$$\boldsymbol{M}_S = \boldsymbol{M}_{pol}(0)\boldsymbol{M}_{ret}(\delta_2, 45)\boldsymbol{M}_{ret}(\delta_1, 0)$$
$$= \frac{1}{2}\begin{pmatrix} 1 & \cos\delta_2 & \sin\delta_1 \sin\delta_2 & -\cos\delta_1 \sin\delta_2 \\ 1 & \cos\delta_2 & \sin\delta_1 \sin\delta_2 & -\cos\delta_1 \sin\delta_2 \\ 0 & 0 & 0 & 0 \\ 0 & 0 & 0 & 0 \end{pmatrix} \qquad (83)$$

The Stokes vector of the incident beam (light beam coming from the laser) is given as $S = (S_0 \quad S_1 \quad S_2 \quad S_3)^T$ where T is the transpose, and the total intensity, I, of the light beam at the photo detector is given by the first parameter of, S', the Stokes vector at the output of the experimental system. By multiplying the Stokes vector S by the Mueller matrix $\boldsymbol{M}_S$, it can be seen that the first parameter of the Stokes vector S', denoted as ${S_0}'$, is given by

$${S_0}' = I(\delta_1, \delta_2) = \frac{1}{2}(S_0 + S_1 \cos\delta_2 + S_2 \sin\delta_1 \sin\delta_2 - S_3 \cos\delta_1 \sin\delta_2) \qquad (84)$$

Using the Bickel and Bailey [19] configuration, we obtain the Stokes vector from:

$$S = \begin{pmatrix} S_0 \\ S_1 \\ S_2 \\ S_3 \end{pmatrix} = \begin{pmatrix} I_H + I_V \\ I_H - I_V \\ I_{+45} - I_{-45} \\ I_R - I_L \end{pmatrix} \tag{85}$$

We require the detection of the linearly polarized components I_H, I_V, I_+ and I_-, (horizontal, vertical, +45 and -45 polarization, respectively), and circularly polarized components, I_R and I_L, (circular right- and left-handed polarization, respectively). From equations (84) and (85), it can be seen that to detect the horizontal polarization component of the incident Stokes vector there are two necessary conditions: $\cos\delta_2 = 1$ and $\sin\delta_2 = 0$, that is, $\delta_2 = 0, 2\pi, 4\pi, ...$ For those conditions the intensity at the detector is described as:

$$S_0 = I = \frac{1}{2}(S_{0i} + S_{1i}) = \frac{1}{2}((I_H + I_V) + (I_H - I_V)) = I_H \tag{86}$$

To analyze for the intensity associated with the vertical polarization state, the conditions are $\cos\delta_2 = -1$ and $\sin\delta_2 = 0$, that is, $\delta_2 = \pi, 3\pi, 5\pi, ...$, and, therefore S_0 is given as:

$$S_0 = I = \frac{1}{2}(S_{0i} - S_{1i}) = \frac{1}{2}\big((I_H + I_V) - (I_H - I_V)\big) = I_V \tag{87}$$

For the +45 polarization state the conditions are $\sin\delta_1 = 1$ and $\sin\delta_2 = 1$, that is, $\delta_1 = \frac{\pi}{2}, \frac{5\pi}{2}, \frac{9\pi}{2}, ...$, and $\delta_2 = \frac{\pi}{2}, \frac{5\pi}{2}, \frac{9\pi}{2}, ...$, and therefore the total intensity is:

$$S_0 = I = \frac{1}{2}(S_{0i} + S_{2i}) = \frac{1}{2}\big((I_{+45} + I_{-45}) + (I_{+45} - I_{-45})\big) = I_{+45} \tag{88}$$

Similarly, forthe -45 polarization state we have the conditions are $\sin\delta_1 = -1$ and $\sin\delta_2 = 1$, that is, $\delta_1 = \frac{3\pi}{2}, \frac{7\pi}{2}, \frac{11\pi}{2}, ...$, and $\delta_2 = \frac{\pi}{2}, \frac{5\pi}{2}, \frac{9\pi}{2}, ...$, so that:

$$S_0 = I = \frac{1}{2}(S_{0i} - S_{2i}) = \frac{1}{2}\big((I_{+45} + I_{-45}) - (I_{+45} - I_{-45})\big) = I_{-45} \tag{89}$$

In the same way, to detect only the intensity associated with the circular right-handed polarization state, the conditions are $\cos\delta_1 = -1$ and $\sin\delta_2 = 1$, that is, $\delta_1 = \pi, 3\pi, 5\pi, ...$, and $\delta_2 = \frac{\pi}{2}, \frac{5\pi}{2}, \frac{9\pi}{2}, ...$, given this we have:

$$S_0 = I = \frac{1}{2}(S_{0i} + S_{3i}) = \frac{1}{2}\big((I_R + I_L) + (I_R - I_L)\big) = I_R \tag{90}$$

Finally, the total intensity associated with the left-handed polarization state is given by equation (91) under the conditions $\cos\delta_1 = 1$ and $\sin\delta_2 = 1$, that is, $\delta_1 = 0, 2\pi, 4\pi, ...$, and $\delta_2 = \frac{\pi}{2}, \frac{5\pi}{2}, \frac{9\pi}{2}, ...$:

$$S_0 = I = \frac{1}{2}(S_{0i} - S_{3i}) = \frac{1}{2}\big((I_R + I_L) - (I_R - I_L)\big) = I_L \qquad (91)$$

A summary of the required retardances is shown in Table 3.

Table 3: Set of configurations of retardance used to detect the six polarization states in a light beam with the Bickel and Bailey method [19].

Polarization state	LCVR 1	LCVR 2
Horizontal	0	0
Vertical	0	180
45	90	90
-45	270	90
Right-handed	180	90
Left-handed	0	90

In table 3, the retardances for LCVR1 required to detect horizontal and vertical linear polarization are undetermined, and in practice we use the same retardance as required for detection of the left-handed polarized light to reduce the number of voltage changes on this LCVR. The applied voltages are then found from the measured calibration curve for the central wavelength. It is important to emphasize that this set of configurations can only be employed for the central wavelength.

For the other wavelengths we use equation (84) which represents the total intensity at the detector, where δ_1 and δ_2, are the retardances induced on the LCVR's at the other wavelengths. Now, the six measurements required for the Bickel and Bailey case for the central wavelength give six measurements of intensity for the other wavelengths, which we shall denote as cases I, II, III,…VI. Using equation (84) for each of the six intensity measurements, we can write a matrix equation relating the detected intensities and the retardances of the LCVR's [10]

$$\frac{1}{2}\begin{pmatrix} 1 & cos\,\delta_{2I} & sin\,\delta_{1I}\,sin\,\delta_{2I} & cos\,\delta_{1I}\,sin\,\delta_{2I} \\ 1 & cos\,\delta_{2II} & sin\,\delta_{1II}\,sin\,\delta_{2II} & cos\,\delta_{1II}\,sin\,\delta_{2II} \\ 1 & cos\,\delta_{2III} & sin\,\delta_{1III}\,sin\,\delta_{2III} & cos\,\delta_{1III}\,sin\,\delta_{2III} \\ 1 & cos\,\delta_{2IV} & sin\,\delta_{1IV}\,sin\,\delta_{2IV} & cos\,\delta_{1IV}\,sin\,\delta_{2IV} \\ 1 & cos\,\delta_{2V} & sin\,\delta_{1V}\,sin\,\delta_{2V} & cos\,\delta_{1V}\,sin\,\delta_{2V} \\ 1 & cos\,\delta_{2VI} & sin\,\delta_{1VI}\,sin\,\delta_{2VI} & cos\,\delta_{1VI}\,sin\,\delta_{2VI} \end{pmatrix}\begin{pmatrix} S_0 \\ S_1 \\ S_2 \\ S_3 \end{pmatrix} = \begin{pmatrix} I_I \\ I_{II} \\ I_{III} \\ I_{IV} \\ I_V \\ I_{VI} \end{pmatrix} \qquad (92)$$

Which can be written as

$$\boldsymbol{M}_C S = I \tag{93}$$

Where $\boldsymbol{M}_C$ is the characteristic matrix of the polarimeter for the configuration of retardances for the given wavelength; S, is the Stokes vector of the incident beam; and I, is the vector of the intensity measurements. From equation (85), it is possible to calculate the Stokes parameters of the incident beam by using the pseudo-inverse of the matrix $\boldsymbol{M}_C$, denoted as $\boldsymbol{M}_C^{\uparrow}$ [22].

$$\boldsymbol{M}_C^{\uparrow} = (\boldsymbol{M}_C^T \boldsymbol{M}_C)^{-1} \boldsymbol{M}_C^T \tag{94}$$

and the solution of equation (94) is given by:

$$S = \boldsymbol{M}_C^{\uparrow} I \tag{95}$$

Equation (95) allows us to reconstruct the Stokes vector of the incident beam for the three wavelengths employed in the system.

3. Liquid crystal variable retarder characterization.

3.1 Liquid crystal variable retarders.

The characterization of an LCVR is very important to determine the relationship between the observed retardance and the applied voltage. It is important to verify the manufacturer's characterization, particularly given that we have measured variations in the performance of our LCVRs over time on the scale of weeks and months. It is also important to be able to produce a set of polarization states with high precision [2].

A nematic liquid-crystal variable retarder, LCVR, (nematic: is a state of a liquid crystal in which the molecules are oriented in parallel but are not arranged in well-defined planes [3]), is constructed by a pair of parallel, closely-spaced optically-flat fused silica windows coated with transparent conductive indium tin oxide (ITO). The space between the two windows is filled with birefringent nematic liquid-crystal material. Then, electrical contacts are attached, and the device is environmentally sealed. Uniaxial birefringent layers are formed by anisotropic nematic liquid crystal molecules which, on average, are aligned with their long axes parallel, but with their centers randomly distributed. With no voltage applied, the liquid crystal molecules lie parallel to the glass substrates and the maximum retardation is achieved. When voltage is applied, the molecules begin to tip perpendicularly to the fused silica windows. As the voltage increases, the molecules tip further causing a reduction in the effective birefringence and hence the retardance [4] (see figure 11).

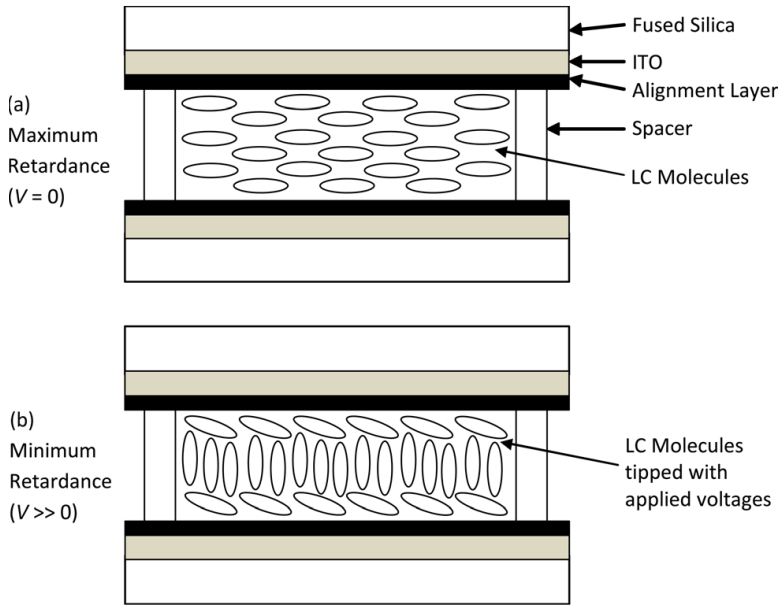

Figure 11 Schematic diagram of a LCVR showing molecular alignment with-out (a) and with (b) applied voltage [4].

3.2 Characterization method

The characterization of an LCVR involves an experimental setup such as that shown in figure 12.

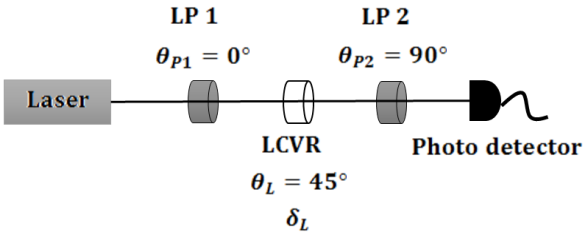

Figure 12 Experimental setup required to characterize a LCVR [4].

As is shown in figure 12, the nematic liquid-crystal variable retarder is placed between two crossed linear polarizers. A light source generates a beam which travels through the first linear polarizer, and then it travels through the variable retarder which has its optical axis oriented at 45° with respect to the first linear polarizer optical axis. Finally, the light beam travels through a second linear polarizer with its optical axis oriented perpendicularly to the first linear polarizer optical axis. A detector measures the transmitted light intensity through the optical system. The measured intensity depends on the retardance of the LCVR, which depends directly on the liquid crystal birefringence and on the applied voltage.

Through an analytical procedure, it is possible to determine the light intensity detected by the sensor at the output of the optical system shown in figure 12. In this sense, it is important to remember that the total intensity of a light beam is represented by the first parameter of its Stokes vector. Also, a sample can be represented by a Mueller matrix. The Mueller matrix of the optical system (sample) shown in figure 12 can be analyzed by using the Mueller matrices of each optical component in the system. So, to know the total intensity detected by the sensor, it is necessary to obtain the first element of the Stokes vector for the light beam which arrives at the sensor, in other words, the light beam at the output of the second linear polarizer. The Mueller matrix of the system is denoted by equation (96), which is the product of the Mueller matrix for the first polarizer at 0°, the LCVR with its axis at 45° and an unknown retardance δ, and the second polarizer with its axis at 90°. The Mueller matrices for each of these components are given in equations (97), (98) and (99).

$$\boldsymbol{M}_S = M_P(90°)M_R(\delta, 45°)M_P(0°) \tag{96}$$

$$\boldsymbol{M}_P(90°) = \frac{1}{2}\begin{pmatrix} 1 & -1 & 0 & 0 \\ -1 & 1 & 0 & 0 \\ 0 & 0 & 0 & 0 \\ 0 & 0 & 0 & 0 \end{pmatrix} \tag{97}$$

$$\boldsymbol{M}_R(\delta, 45°) = \begin{pmatrix} 1 & 0 & 0 & 0 \\ 0 & \cos\delta & 0 & -\text{sen}\,\delta \\ 0 & 0 & 1 & 0 \\ 0 & \text{sen}\,\delta & 0 & \cos\delta \end{pmatrix} \tag{98}$$

$$\boldsymbol{M}_P(0°) = \frac{1}{2}\begin{pmatrix} 1 & 1 & 0 & 0 \\ 1 & 1 & 0 & 0 \\ 0 & 0 & 0 & 0 \\ 0 & 0 & 0 & 0 \end{pmatrix} \tag{99}$$

Performing the matrix multiplications, the Mueller matrix of the full system is given by equation (100):

$$\boldsymbol{M}_S = \frac{1}{4}\begin{pmatrix} 1-\cos\delta & 1-\cos\delta & 0 & 0 \\ -1+\cos\delta & -1+\cos\delta & 0 & 0 \\ 0 & 0 & 0 & 0 \\ 0 & 0 & 0 & 0 \end{pmatrix} \tag{100}$$

From equation (17), it is clear that to obtain the Stokes vector for the output beam; we must multiply the Mueller matrix of the optical system by the Stokes vector of the incident beam. However, it is also clear that the polarization of the light beam generated by the source will make no difference because the first linear polarizer fixes it as linearly polarized light at 0°. The only difference for different incident polarizations is an intensity term depending on the incident polarization, which does not affect the relative intensity measurements. So, for simplicity we consider that the light beam generated by the source is unpolarized. The Stokes vector of the output light beam is, therefore, denoted by:

$$S = A\begin{pmatrix} 1-\cos\delta & 1-\cos\delta & 0 & 0 \\ -1+\cos\delta & -1+\cos\delta & 0 & 0 \\ 0 & 0 & 0 & 0 \\ 0 & 0 & 0 & 0 \end{pmatrix}\begin{pmatrix} 1 \\ 0 \\ 0 \\ 0 \end{pmatrix} = A\begin{pmatrix} 1-\cos\delta \\ -1+\cos\delta \\ 0 \\ 0 \end{pmatrix} \tag{101}$$

where A denotes all the constant terms which depend on the Stokes vector normalization and the experimental parameters such as the polarizer absorption and the polarization efficiency. The first component of the Stokes vector of the output light beam, and therefore the total light intensity detected by the sensor (I) is denoted by the expression $S_0 = I = A(1-\cos\delta)$, where δ denotes the retardance of the LCVR. By analyzing this expression, the maximum intensity detected by the sensor (I_{max}) occurs when $\cos\delta = -1$, which is when $\delta = 180°$:

$$I_{max} = A(1-\cos(180°)) = 2A \tag{102}$$

so that the value of the constant A is

$$A = \frac{I_{max}}{2} \tag{103}$$

Finally, the expression for the light intensity detected by the sensor can be written as [30, 31]:

$$I = \frac{I_{max}}{2}(1 - \cos\delta) \tag{104}$$

and the retardance is given by [30]:

$$\delta = \cos^{-1}\left(1 - \frac{2I}{I_{max}}\right) \tag{105}$$

Equation (105) allows us to determine the retardance of a nematic liquid-crystal variable retarder by measuring the intensity as the applied voltage is varied. Experimentally, the applied voltage on the LCVR can be varied and the intensity for each applied voltage must be registered. By using the experimental information, applied voltage versus intensity can be plotted. However, one problem with equation (105) is that it involves the $\cos^{-1}$ function. Numerical calculation of the $\cos^{-1}$ function gives results in the range $[0, \pi]$ so, when this equation is employed to determine the retardance of the LCVR, it is necessary to unwrap the retardance in order to obtain correct results outside this range [30, 31].

Another problem with this method is related to the error distribution for the calculation of the retardance. Equation (105) can be written as:

$$cos(\delta) = 1 - \frac{2I}{I_{max}} \tag{106}$$

and calculating the derivatives,

$$\frac{d\delta}{dI} = \frac{1}{sin(\delta)}\left(-\frac{2}{I_{max}}\right) \tag{107}$$

$$\frac{d\delta}{dI_{max}} = \frac{1}{sin(\delta)}\frac{2I}{(I_{max})^2} \tag{108}$$

and the total error is:

$$\sigma_\delta^2 = \left(\frac{1}{sin(\delta)}\right)^2 \left\{\left(\frac{2}{I_{max}}\right)^2 \sigma_I^2 + \left(\frac{2I}{(I_{max})^2}\right)^2 \sigma_{I_{max}}^2\right\} \tag{109}$$

where σ_δ is the error in the retardance value, σ_I is the error in the measured intensity value and $\sigma_{I_{max}}$ is the error in the maximum intensity value. In what follows we assume that $\sigma_I = \sigma_{I_{max}}$. The value of I goes from 0 to I_{max}, so the value of the error in the retardance has a minimum value, when $I = 0$, of

$$\sigma_\delta^2 = \left(\frac{1}{sin(\delta)}\right)^2 \left\{\left(\frac{2}{I_{max}}\right)^2 \sigma_I^2\right\} \tag{110}$$

and a maximum value, when $I = I_{max}$, of

$$\sigma_\delta^2 = \left(\frac{1}{sin(\delta)}\right)^2 \left\{2\left(\frac{2}{I_{max}}\right)^2 \sigma_I^2\right\} \tag{111}$$

When $\delta = 180°$ or $360°$, $sin(\delta) = 0$, and $\frac{1}{sin(\delta)} = \infty$, which means that the error in the retardance should be very high at the values of retardance of 180° or π (half a wavelength of retardance), or 360° or 2π (a full wave of retardance). However, in practice, we have found that the results for these values of the retardance are reasonably stable, with only a small increase in the error. This may be due to the measurement errors associated with the stability of the voltages applied to the LCVRs. There is a variability of the voltage meaning that it is not possible to have the case of a retardance of exactly π or 2π, meaning that the error in these values is reduced.

3.3 Results

In this section, the principal results of the process to obtain the characteristic curves for the two LCVR's used in the developed polarimeter are presented. First, the normalized intensity values are plotted as a function of the applied voltage. The retardance values are calculated through equation (105) and these normalized intensity values, and the retardance, are presented as a function of the applied voltage. Then, the unwrapping process is graphically represented. Finally, the characteristic curves are obtained and plotted for the three wavelengths used in the experiment.

Figure 13 shows the applied voltage versus the normalized intensity values for the two LCVR´s.

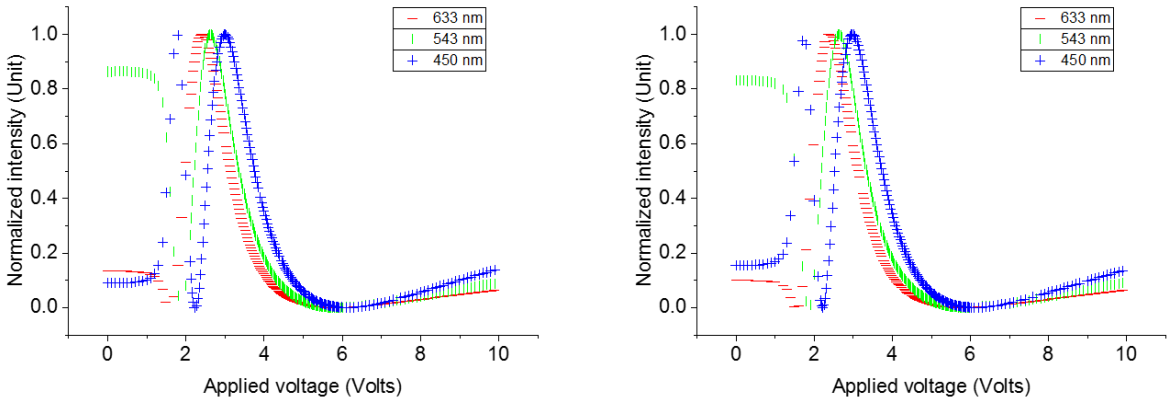

Figure 13 LCVR 1 (left) and LCVR 2 (right) normalized intensity curves for 450 nm, 543 nm and 633 nm.

Then equation (105) is used to calculate the retardance for each value of the applied voltage and in figure 14 the applied voltage versus retardance values are plotted.

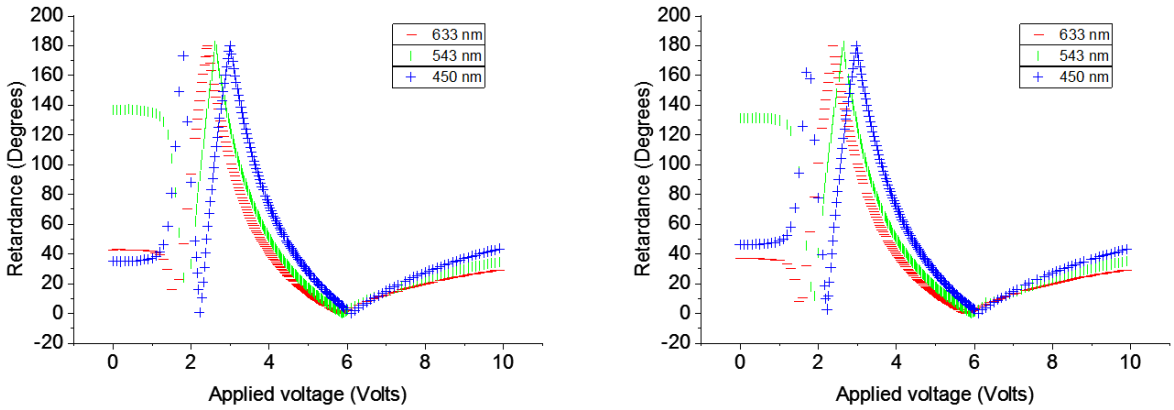

Figure 14 LCVR 1 (left) and LCVR 2 (right) retardance curves for 450 nm, 543 nm and 633 nm.

From figure 14 it can be seen that the retardance values are "locked" between the values of 0 and 180° because of the permitted values in the numerical calculation of the cos^{-1} function. These curves must be extended at the points where the gradient changes abruptly to give smooth curves. This is the unwrapping process which involves changing the sign of the gradient of the curves from the abrupt gradient change and to the left of this point, in our case, for each segment of the curves. This unwrapping process is shown graphically in figures 15,16 and 17.

From these characterization curves, the voltages required to produce the necessary retardances for the reference wavelength were found, and from these values the retardance values for the other wavelengths were calculated. Table 4 presents the voltages used in the experimental configuration of the polarimeter. The central wavelength, the green laser with

a wavelength of 543 nm, was used as the reference wavelength, with the retardances for this colour giving the Bickel and Bailey configuration [19].

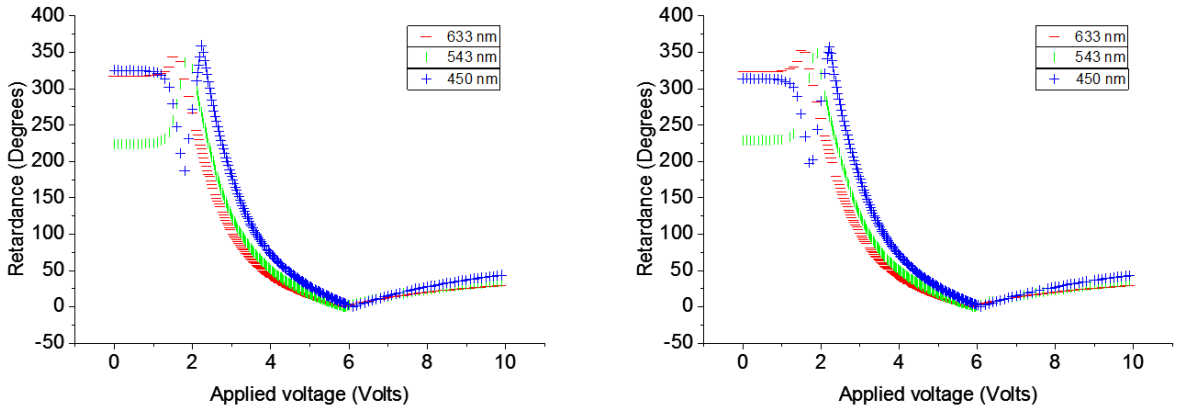

Figure 15 LCVR 1 (left) and LCVR 2 (right) first unwraping step for 450 nm, 543 nm and 633 nm, at the first abrupt gradient change on the left-hand side of the graphs.

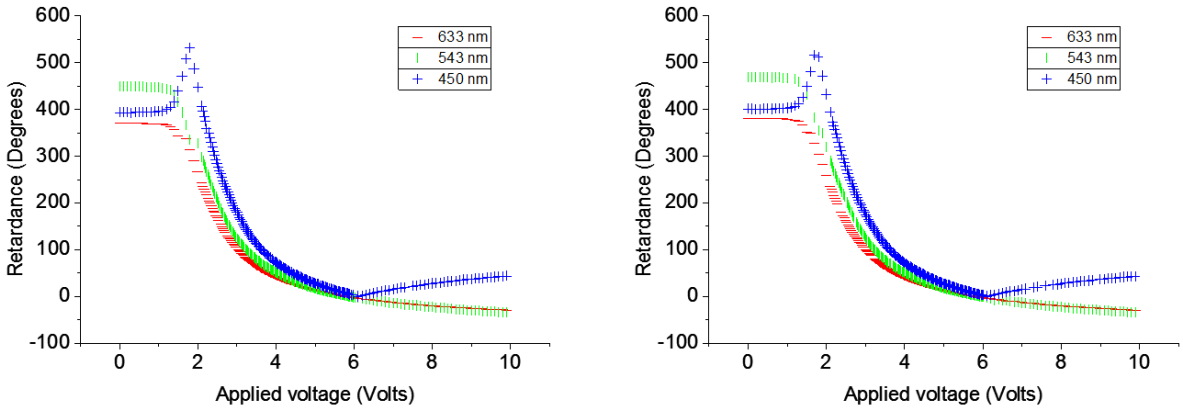

Figure 16 LCVR 1 (left) and LCVR 2 (right) second unwarping step for 450 nm, 543 nm and 633 nm, for the second abrupt gradient change from the left in the original curves.

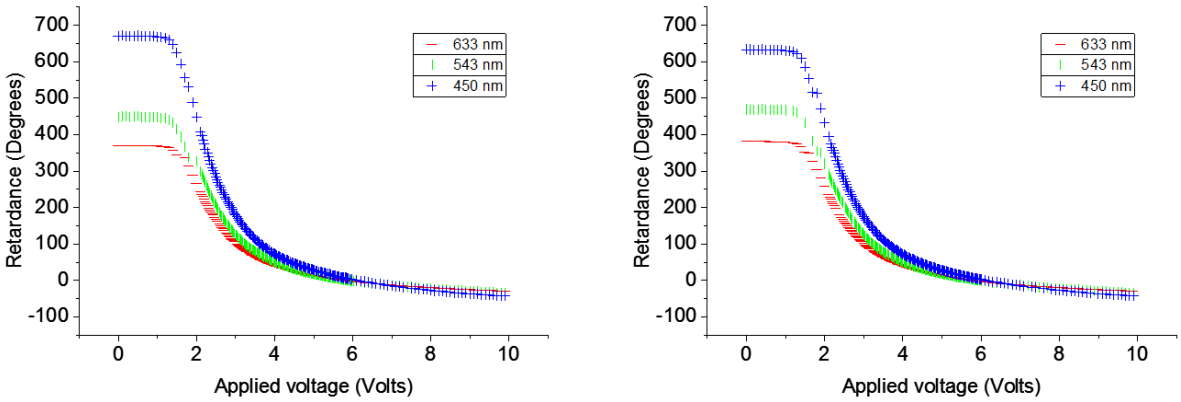

Figure 17 Completely unwrapped LCVR 1 (left) and LCVR 2 (right) characterization curves for 450 nm, 543 nm and 633 nm, by performing the unwrapping process on the final abrupt gradient change in the curves of Figure 16.

Table 4 shows the retardances calculated from the characterization curves of Figure 17, for the other two wavelengths using the same voltage values as for the central wavelength.

Polarization at 543 nm	Wavelength	LCVR 1		LCVR 2	
		Applied voltage (Volts)	Retardance (Degrees)	Applied voltage (Volts)	Retardance (Degrees)
Horizontal	633 nm	5.697	-0.389	5.797	2.203
	543 nm		0		0
	450 nm		4.751		5.038
Vertical	633 nm	5.697	-0.389	2.585	147.915
	543 nm		0		180
	450 nm		4.751		254.17
45	633 nm	3.286	73.057	3.325	72.71
	543 nm		90		90
	450 nm		126.823		127.305
-45	633 nm	2.142	218.471	3.325	72.71
	543 nm		270		90
	450 nm		364.595		127.305
Right-handed	633 nm	2.555	146.517	3.325	72.71
	543 nm		180		90
	450 nm		250.217		127.305
Left-handed	633 nm	5.697	-0.389	3.325	72.71
	543 nm		0		90
	450 nm		4.751		127.305

By using the retardance values shown in table 4, we can obtain the three characteristic matrices for the wavelengths employed in this work and which are calculated in the following Chapter.

4. Stokes polarimeter with three simultaneous wavelengths

4.1 Experimental setup

Figure 18 shows the experimental setup used in this work. Only one polarimeter is used to analyze the three wavelengths simultaneously.

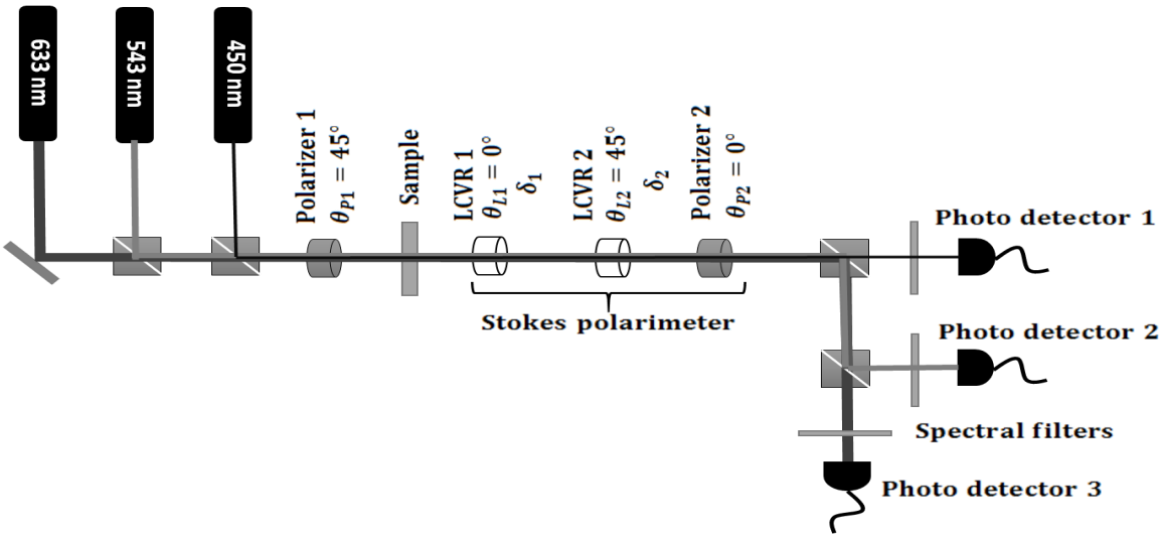

Figure 18 Scheme of the Stokes polarimeter setup employed in this work. The angles associated with each component refer to the relative angle of the optical axis of that component with respect to the horizontal plane. Measurements are taken simultaneously. The wavelengths employed are 633 nm, 543 nm y 450 nm.

The laser sources used are two He-Ne polarized lasers (Melles Griot, model 25-LGP-193-249, 543 nm and, JDS Uniphase, model 1137P 633 nm) and a polarized laser diode module (Thorlabs, model CPS450, 450 nm). One mirror and two beamsplitters (Thorlabs, model CM1-BP133 and CM1-BP150) are used to ensure co-propagating beams. At the input of the system there is a Glan-Thompson linear polarizer (Thorlabs, model GTH5M) to ensure that all three input beams are linearly polarized in the same plane. Then the sample is placed in the beam path, just before the components of the Stokes polarimeter, which are two Meadowlark compensated LCVR's and a Glan-Taylor linear polarizer (Thorlabs, model GT10-A), as described above. Finally, the light beam is split onto three photo sensors (Thorlabs, model S120C) by using beam splitters (Thorlabs, model CM1-BP150), and in front of each photo sensor there is a laser-line filter (bandwidth 10 nm) which selects only one of the three wavelengths to be analyzed (Thorlabs, models FL632.8-10, FL543.5-10 and FB450-10). Note that the effect of the beam splitters on the polarization of the beams is also compensated by the calibration procedure. The experiment is controlled from the computer

via LabView. For the results presented below, the sample can be rotated from 0° to 180° in steps of 10°. Software LabVIEW is used to configure the position of the rotation mount and the voltage values applied to the LCVR´s.

4.2 Fixed retarder retardance measurements: Chenault Chipman method.

To calibrate the polarimeter shown in figure 18, two wave plates were used to generate known calibration beams. Two configurations which have been published in the literature were tested: a system with four known calibration beams, and a system with six known calibration beams. Given that these optical elements induce a retardance on the orthogonal components of an incident beam, and that this retardance depends on the wavelength of the incident beam, we measured the retardance induced by the quarter-wave plate and the half-wave plate, which were designed for 633 nm, at the other two wavelengths used, with the technique described by Chenault and Chipman [30]. This technique also can be used to measure the linear diattenuation of a polarizer. In figure 19 a scheme of the experimental setup is shown.

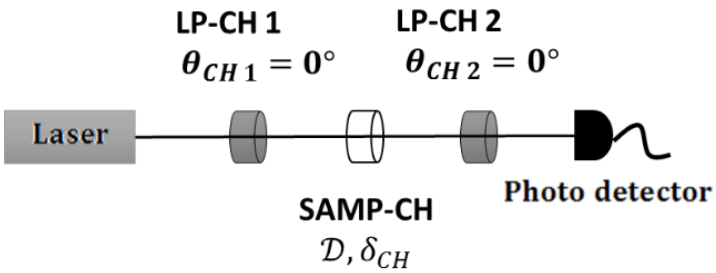

Figure 19 Scheme of the experimental setup used for the Chenault Chipman method.

This scheme uses a pair of linear polarizers with parallel transmission axes. The analyzed sample is placed between the polarizers with its principal axis parallel to the transmission axis of the polarizers and then is rotated, measuring the transmitted intensity at the detector for each rotation angle. The principal parameters of the sample are shown in figure 19, the linear diattenuation, $\mathcal{D}$; and the retardance δ_{CH}; which are given by [35]:

$$\mathcal{D} = \frac{q_1 - q_2}{q_1 + q_2} \tag{112}$$

$$\delta_{CH} = |\delta_{CH1} - \delta_{CH2}| \tag{113}$$

where q_1 and q_2 are the principal intensity transmittances and, δ_{CH1}, δ_{CH2} are the orthogonal retardance components. Given this, the Mueller matrix for a sample with linear diattenuation $\mathcal{D}$, and retardance δ_{CH}, is given by [35]:

$$\boldsymbol{M}_{SAMP-CH}(\mathcal{D},\delta_{CH}) = \mathcal{T}_{CH}\begin{pmatrix} 1 & \mathcal{D} & 0 & 0 \\ \mathcal{D} & 1 & 0 & 0 \\ 0 & 0 & \sqrt{1-\mathcal{D}^2}\cos\delta_{CH} & \sqrt{1-\mathcal{D}^2}\sin\delta_{CH} \\ 0 & 0 & -\sqrt{1-\mathcal{D}^2}\sin\delta_{CH} & \sqrt{1-\mathcal{D}^2}\cos\delta_{CH} \end{pmatrix} \quad (114)$$

where $\mathcal{T}_{CH} = \frac{1}{2}(q_1 + q_2)$ is the average transmission of the sample.

The Mueller matrix for the entire system shown in figure 19 is given by [35]:

$$\boldsymbol{M}_{Sys-CH} = \boldsymbol{M}_{LP-CH\,2}(\mathcal{D}_2)\boldsymbol{R}_{CH}(-\theta_{CH})\boldsymbol{M}_{SAMP-CH}(\mathcal{D},\delta_{CH})\boldsymbol{R}_{CH}(\theta_{CH})\boldsymbol{M}_{LP-CH\,1}(\mathcal{D}_1) \quad (115)$$

where $\boldsymbol{M}_{LP-CH\,i}(\mathcal{D}_i)$ $(i = 1,2)$ are the Mueller matrices of the fixed linear polarizers, LP-CH 1 and LP-CH 2[35]:

$$\boldsymbol{M}_{LP-CH\,i}(\mathcal{D}_i) = \mathcal{T}_{CH\,i}\begin{pmatrix} 1 & \mathcal{D}_i & 0 & 0 \\ \mathcal{D}_i & 1 & 0 & 0 \\ 0 & 0 & \sqrt{1-\mathcal{D}_i{}^2} & \sqrt{1-\mathcal{D}_i{}^2} \\ 0 & 0 & -\sqrt{1-\mathcal{D}_i{}^2} & \sqrt{1-\mathcal{D}_i{}^2} \end{pmatrix} \quad (116)$$

where $\mathcal{T}_{CH\,i}$ is the average transmission defined in the equation (114).

Also, $\boldsymbol{R}_{CH}(\theta_{CH})$ is the Mueller matrix of a rotator which is a very useful tool when it is necessary describe a rotatory movement of a polarizing element (our sample in this case) [18, 35]:

$$\boldsymbol{R}_{CH}(\theta_{CH}) = \begin{pmatrix} 1 & 0 & 0 & 0 \\ 0 & \cos 2\theta_{CH} & \sin 2\theta_{CH} & 0 \\ 0 & -\sin 2\theta_{CH} & \cos 2\theta_{CH} & 0 \\ 0 & 0 & 0 & 1 \end{pmatrix} \quad (117)$$

If the Mueller matrix of the optical system shown in figure 19 is known, see equation (115), then the relationship between the Stokes vectors of the incident and output beams is described by:

$$S_{CHo} = \boldsymbol{M}_{Sys-CH}S_{CHi} \quad (118)$$

Therefore, for a specific wavelength the total intensity in the system is modulated by the rotation angle of the sample, θ_{CH}; the linear diattenuation and retardance of the sample, $\mathcal{D}$ and δ_{CH}, respectively; the linear diattenuation of the fixed polarizers, $\mathcal{D}_i$; the average transmission of the polarizers; the radiance of the source and the responsivity of the detector. Given that the first parameter of the Stokes vector of the output beam, S_{CHo}, represents the

total measured intensity, it is possible to obtain the expression that describes this total intensity, $I(\theta_{CH})$, by solving equation (115) and employing equations (114), (116) and (117) [35]:

$$I(\theta_{CH}) = \rho_{CH}\left(1 + \frac{1}{2}\mathcal{D}_1\mathcal{D}_2\left(1 + \sqrt{1-\mathcal{D}^2}\cos\delta_{CH}\right) + \mathcal{D}(\mathcal{D}_1 + \mathcal{D}_2)\cos 2\theta_{CH} + \frac{1}{2}\mathcal{D}_1\mathcal{D}_2\left(1 - \sqrt{1-\mathcal{D}^2}\cos\delta_{CH}\right)\cos 4\theta_{CH}\right) \quad (119)$$

where ρ_{CH} is a normalization factor which carries information about the average transmission of the optical elements employed, the radiance of the source and the responsivity of the detector.

In equation (119) the principal parameter is the rotation angle of the sample, this is because experimentally, the sample is rotated from 0° to 360° to modulate the total intensity signal. This equation can be rewritten as a Fourier series by replacing the parameters, except the rotation angle of the sample, by the coefficients a_{CH0}, a_{CH2} and a_{CH4} [35]:

$$I(\theta_{CH}) = \rho_{CH}(a_{CH0} + a_{CH2}\cos 2\theta_{CH} + a_{CH4}\cos 4\theta_{CH}) \quad (120)$$

Hence, the linear diattenuation and retardance of the sample can be derived from equation (120) through a Fourier analysis of the detected intensity signal [35]:

$$\mathcal{D} = \frac{a_{CH2}}{a_{CH0} + a_{CH4}}\left(\frac{1 + \mathcal{D}_1\mathcal{D}_2}{\mathcal{D}_1 + \mathcal{D}_2}\right) \quad (121)$$

$$\delta_{CH} = \cos^{-1}\left(\frac{a_{CH0} + a_{CH4}\left(1 + \frac{2}{\mathcal{D}_1\mathcal{D}_2}\right)}{\left[(a_{CH0} + a_{CH4})^2 - a_{CH2}^2\left(\frac{1 + \mathcal{D}_1\mathcal{D}_2}{\mathcal{D}_1 + \mathcal{D}_2}\right)^2\right]^{\frac{1}{2}}}\right) \quad (122)$$

where $\mathcal{D}_1$ and $\mathcal{D}_2$ are the linear diattenuation of the fixed polarizers.

The values of $\mathcal{D}_1$ and $\mathcal{D}_2$ used were calculated experimentally by using a separate, simple method, to use Eq. (122) to give a more precise value of the retardances. Three polarizers were used in this case, one of them as the sample with diattenuation, $\mathcal{D}_s$. First, $\mathcal{D}_1$ and $\mathcal{D}_2$ are taken as the ideal diattenuation values. Then $\mathcal{D}_s$ is calculated experimentally through equation (121). Subsequently, $\mathcal{D}_1$ is calculated in a similar way but in this case the value for $\mathcal{D}_s$ calculated before is used and the diattenuation of the second polarizer is taken as the ideal value, $\mathcal{D}_2$. Finally, $\mathcal{D}_2$ is calculated experimentally by using equation (121) and taking the diattenuation values $\mathcal{D}_1$ and $\mathcal{D}_s$ calculated previously. This is an iterative methodology that can be repeated until the diattenuation values converge to constant values [35].

Experimentally diattenuation values were calculated, $\mathcal{D}_1 = 0.99 \pm 1.20x10^{-7}$ and $\mathcal{D}_2 = 0.99 \pm 1.87x10^{-6}$, for the two fixed polarizers shown in figure 19.

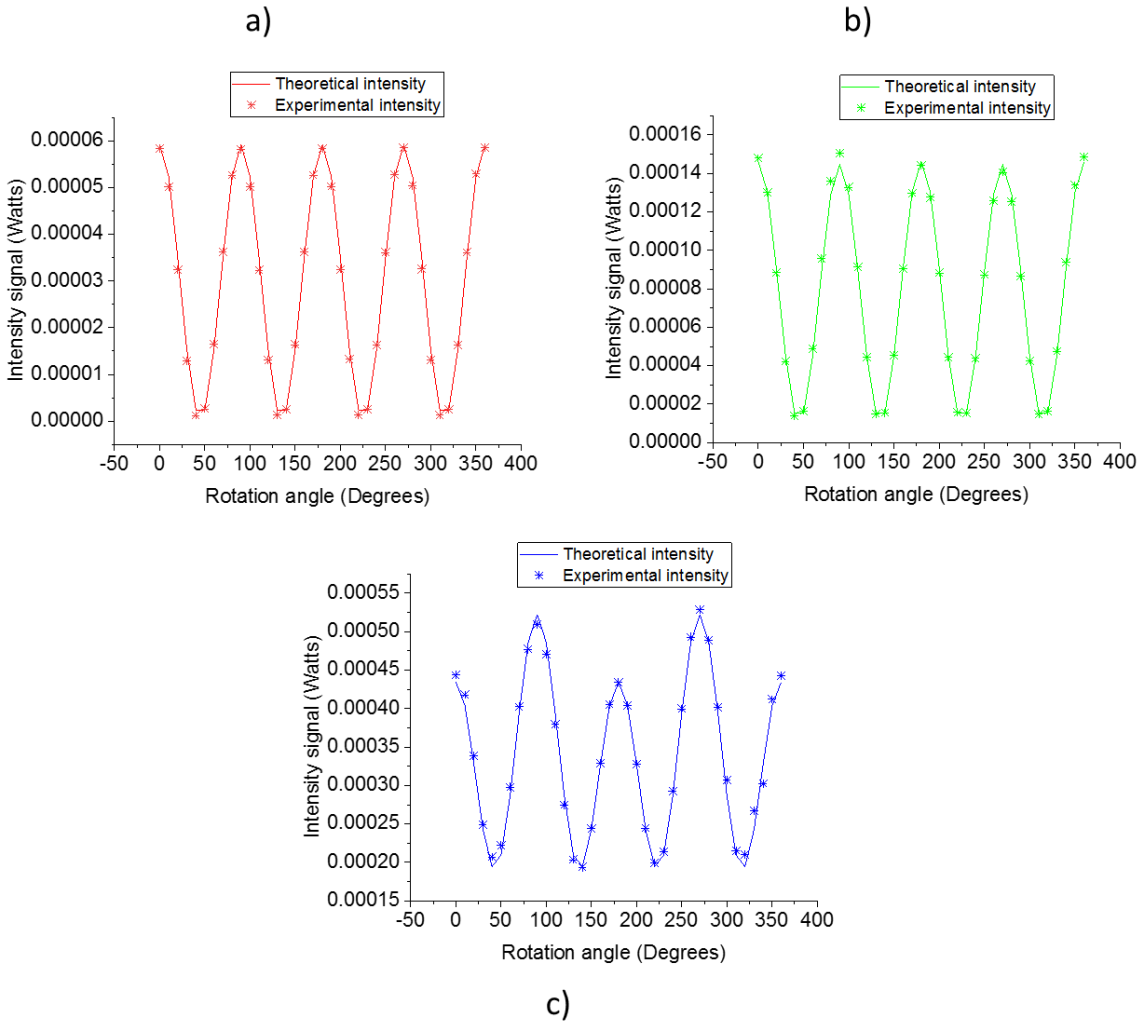

Figure 20 Theoretical (line) and experimental (asterisks) curves for the half-wave plate for a) 633 nm, b) 543 nm and c) 450 nm.

Once the linear diattenuation of the fixed polarizers shown in figure 19 are known, it is possible to calculate the retardance of the half- and a quarter-wave plates for a specific wavelength through equation (122). The total intensity signal is modulated experimentally as a function of the rotation angle of the sample by rotating it from 0° to 360° and taking the intensity measurements. The theoretical total intensity signal is generated by using equation (120). Then, the theoretical curve is fit to the experimental one by changing the Fourier coefficient values and the normalization factor value. By changing these values, we can match the theoretical and the experimental curves. Finally, the Fourier coefficient values

found are used in equation (122) to calculate the retardance value of the wave plate analyzed for a specific wavelength.

Figure 20 shows the theoretical (line) and experimental (asterisk) curves for the three different wavelengths for the half-wave-plate. The quarter-wave plate theoretical and experimental curves are shown in figure 21 for the three wavelengths.

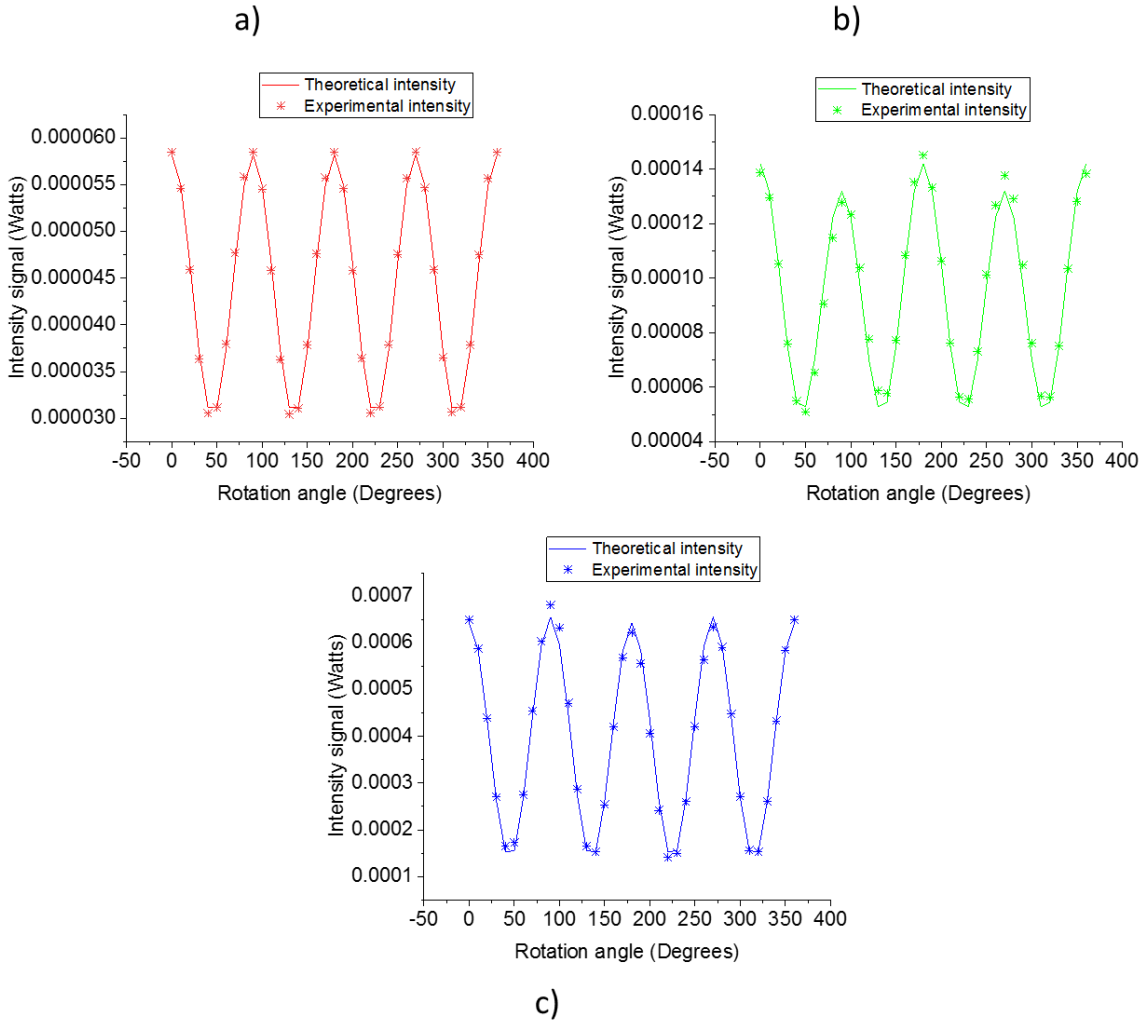

Figure 21 Theoretical (line) and experimental (asterisks) curves for the quarter-wave plate for a) 633 nm, b) 543 nm and c) 450 nm.

Table 3 shows the experimental values for the half-wave and quarter-wave plate retarders for the three wavelengths employed and the estimated average percentage error. These values are used for the known calibration samples for the corresponding colours in our calibration algorithm.

Table 3 shows the retardance values calculated for the half and quarter-wave plates for the three wavelengths.

Wavelength	Retardance (Degrees)			
	Half-wave plate	% Estimated error	Quarter-wave plate	% Estimated error
633	180	9.7	90	1.4
543	154.16	3.1	107.46	4
450	101.54	2.8	126.87	3.4

4.3 Stokes parameters measurement.

Considering 543 nm as the reference wavelength, the characteristic matrices for each color, for the case of 6 intensity measurements, calculated from equation (64), and from the data in Table 2, are given by:

$$\boldsymbol{M}_{C(GREEN)} = \begin{pmatrix} 0.5000 & 0.5000 & 0.0000 & 0.0000 \\ 0.5000 & -0.5000 & 0.0000 & 0.0000 \\ 0.5000 & 0.0000 & 0.5000 & 0.0000 \\ 0.5000 & 0.0000 & -0.5000 & 0.0000 \\ 0.5000 & 0.0000 & 0.0000 & 0.5000 \\ 0.5000 & 0.0000 & 0.0000 & -0.5000 \end{pmatrix} \tag{90}$$

$$\boldsymbol{M}_{C(BLUE)} = \begin{pmatrix} 0.5000 & 0.4981 & 0.0036 & -0.0438 \\ 0.5000 & -0.1364 & -0.0398 & 0.4794 \\ 0.5000 & -0.3030 & 0.3184 & 0.2384 \\ 0.5000 & -0.3030 & 0.0319 & -0.3964 \\ 0.5000 & -0.3030 & -0.3742 & 0.1346 \\ 0.5000 & -0.3030 & 0.0329 & -0.3963 \end{pmatrix} \tag{91}$$

$$\boldsymbol{M}_{C(RED)} = \begin{pmatrix} 0.5000 & 0.4996 & -0.0001 & -0.0192 \\ 0.5000 & -0.4236 & -0.0018 & -0.2656 \\ 0.5000 & 0.1486 & 0.4567 & -0.1391 \\ 0.5000 & 0.1486 & -0.2970 & 0.3738 \\ 0.5000 & 0.1486 & 0.2634 & 0.3982 \\ 0.5000 & 0.1486 & -0.0032 & -0.4774 \end{pmatrix} \tag{92}$$

The condition numbers for these matrices are 1.7322, 2.6196 and 2.3312, respectively for each color. We used the 6-intensity measurement case since here we can only have 1 optimized case, with green light, and the other two cases are not optimized. For the case of 4 intensity measurements, the non-optimized cases have very large condition numbers, which we found gives very large errors in the final Stokes parameters.

The required Stokes vector of the incident light is then calculated by using equation (72). To show the principle of operation of the polarimeter, results are presented for rotating known

components: a linear polarimeter, a half-wave plate and a quarter-wave plate. The reported total RMS error in each case is given by:

$$RMS = \sqrt{\sum_{\substack{rotation \\ angle}} \sum_{\substack{Stokes \\ parameter}} \frac{1}{4N} (S^{exp} - S^{teo})^2} \tag{93}$$

where S^{exp} is the experimental Stokes values, S^{teo} is the theoretical, expected Stokes values, and N is the number of rotation angles used.

4.4 Calibration method.

It is well-known that a precise polarization measurement requires a calibration and data extraction method to compensate the effect of experimental errors. In this work we use a recently developed fitting procedure [23]. Here we also compare the results of using four or six known polarization states as calibration samples: the four known samples are produced by:

- a linear polarizer with the transmission axis oriented at 130°
- a linear polarizer with the transmission axis oriented at 30°
- a horizontal linear polarizer followed by a half-wave plate with the fast axis oriented at 30°
- a horizontal linear polarizer followed by a quarter-wave plate with the fast axis oriented at 30°

For six known calibration samples we add the cases of:

- a horizontal polarizer followed by a half-wave plate with fast axes at 130°
- a horizontal polarizer followed by a quarter-wave plate with fast axes at 130°

Clearly, it is expected that the case of using 6 calibration polarization states should give better results than the case of 4 calibration states, since more data is being used to correct the experimental errors. However, this process will take more time with more data to be measured, which could be a disadvantage, and for this reason we tested both cases. The angles of 30° and 130° for the axes of the calibration samples were chosen to avoid problems with these axes being either parallel or perpendicular to the axes of the first polarizer on the left of Figure 18. Particularly, when polarizer axes are crossed there is no transmission.

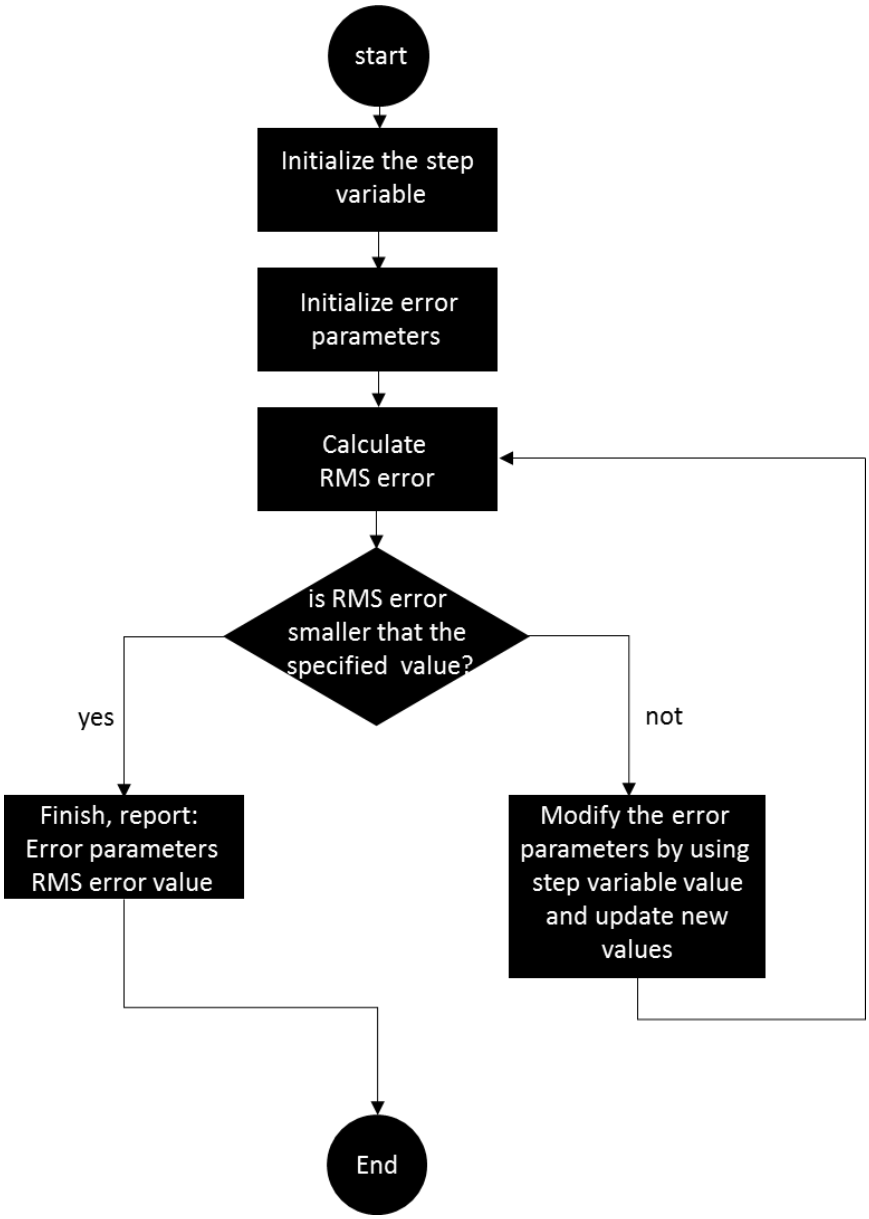

Figure 22 Flow diagram of the calibration method.

The intensity measurements obtained with these calibration samples in the polarimeter are different from the expected theoretical results, due to the experimental errors in the positions of the optical axes of the retarders, polarizers and LCVR's (a total of four error parameters) and errors in each of the different retardance values for the LCVR's and retarders used to generate the calibration beams. For the errors in the retardance values, it is important to take into account one error parameter for each different retardance value in the LCVR's (a total of 7 error parameters). All of these errors are taken as the fitting parameters to fit the theoretically expected values including the experimental errors, to the experimentally obtained intensity values [23]. Then in the data extraction step, these fitted parameters for

the experimental errors are taken as fixed and are used to give a better model for the polarimeter and a new fit is performed, fitting the theoretical signals for the unknown Stokes vectors to the experimental measurements to find the Stokes vector elements of the unknown beam [23]. This fitting procedure is performed independently for each of the wavelengths used in the experiment, although the measurements are performed simultaneously.

Figure 22 shows schematically the calibration method employed to fit experimental and theoretical curves through minimization of the RMS error parameter. This is a general scheme that can be applied for the cases reported in this thesis.

4.5 Results

Figures 23, 24 and 25 (left) show the uncalibrated Stokes parameters for rotating components of: a Glan-Thompson polarizer, a half-wave plate and a quarter-wave plate retarder, respectively. In all cases the expected theoretical data are represented by lines and experimental data are represented by geometrical shapes. In this case we take four calibration samples. Figures 26, 27 and 28 (left) show similar results, for the case of six calibration beams. Capital letters TR and ER refer to theoretical and experimental results, respectively.. The RMS error values are larger for the uncalibrated cases (left) than for the RMS error values for the calibrated cases (right). Also, for the 450 nm wavelength these values are larger than the other two wavelengths. This was expected since the condition number for this wavelength is the largest (section 4.3). For the 633 nm and 543 nm wavelengths the RMS error values are closer to each other. The polarimeter was optimized to the green colour, and the half-wave and quarter-wave plates are designed for the red colour (see Table 4).

When the calibration method is applied (figures 23, 24, 25, 26, 27 and 28, right), we can observe a better fit between experimental and theoretical results with respect to the original data (same figures, left). Figures 23, 24 and 25 (right) show the Stokes parameters for a rotating Glan-Thompsom polarizer, a half-wave plate and a quarter-wave plate retarder, respectively. Figures 26, 27 and 28 (right) show similar results, for the case of six calibration beams. Again, capital letters TR and ER refer to theoretical and experimental, respectively.

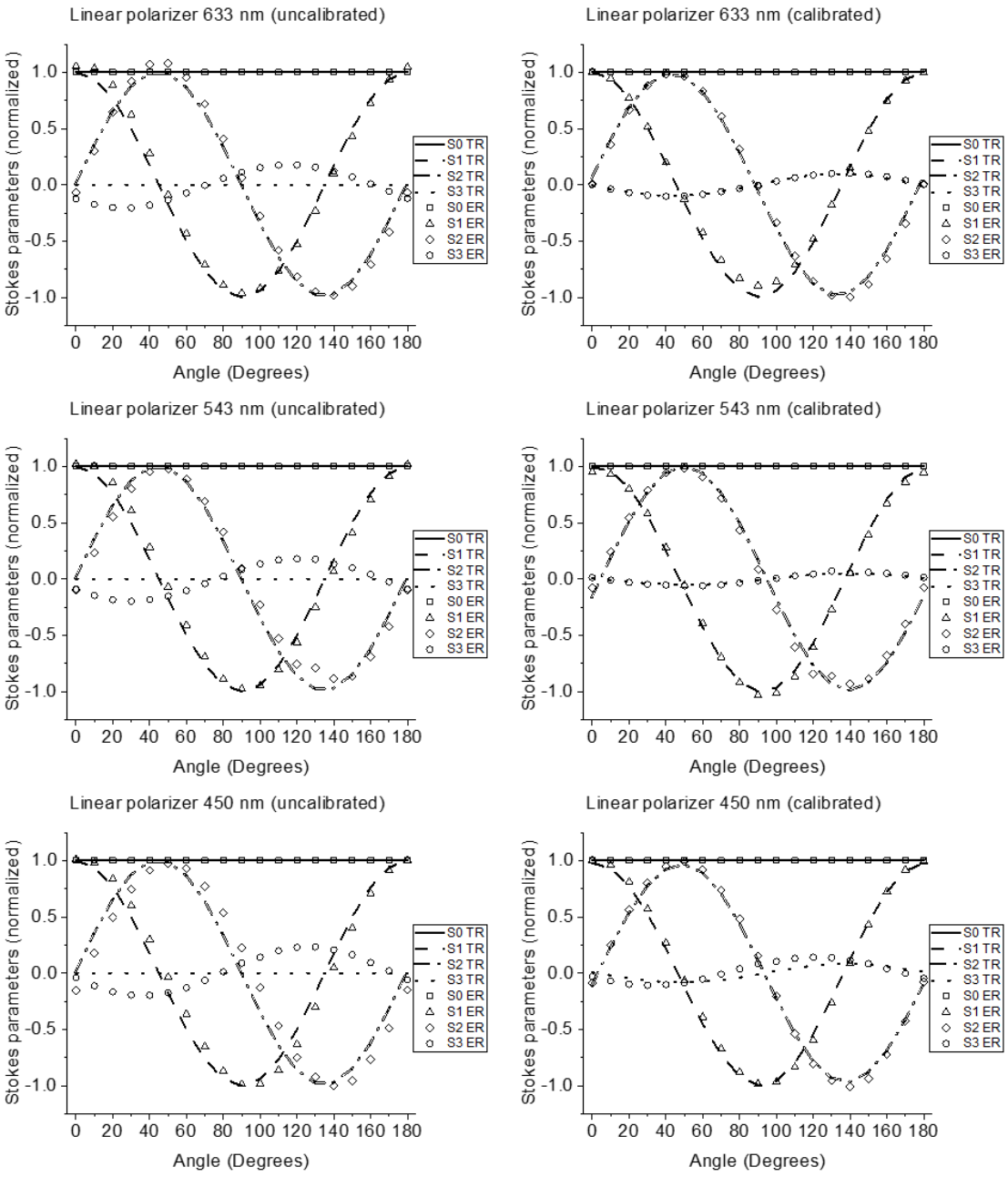

Figure 23 Stokes parameters for a Glan-Thompsom polarizer as a function of the angle for the three wavelengths. Uncalibrated (left) and calibrated (right).

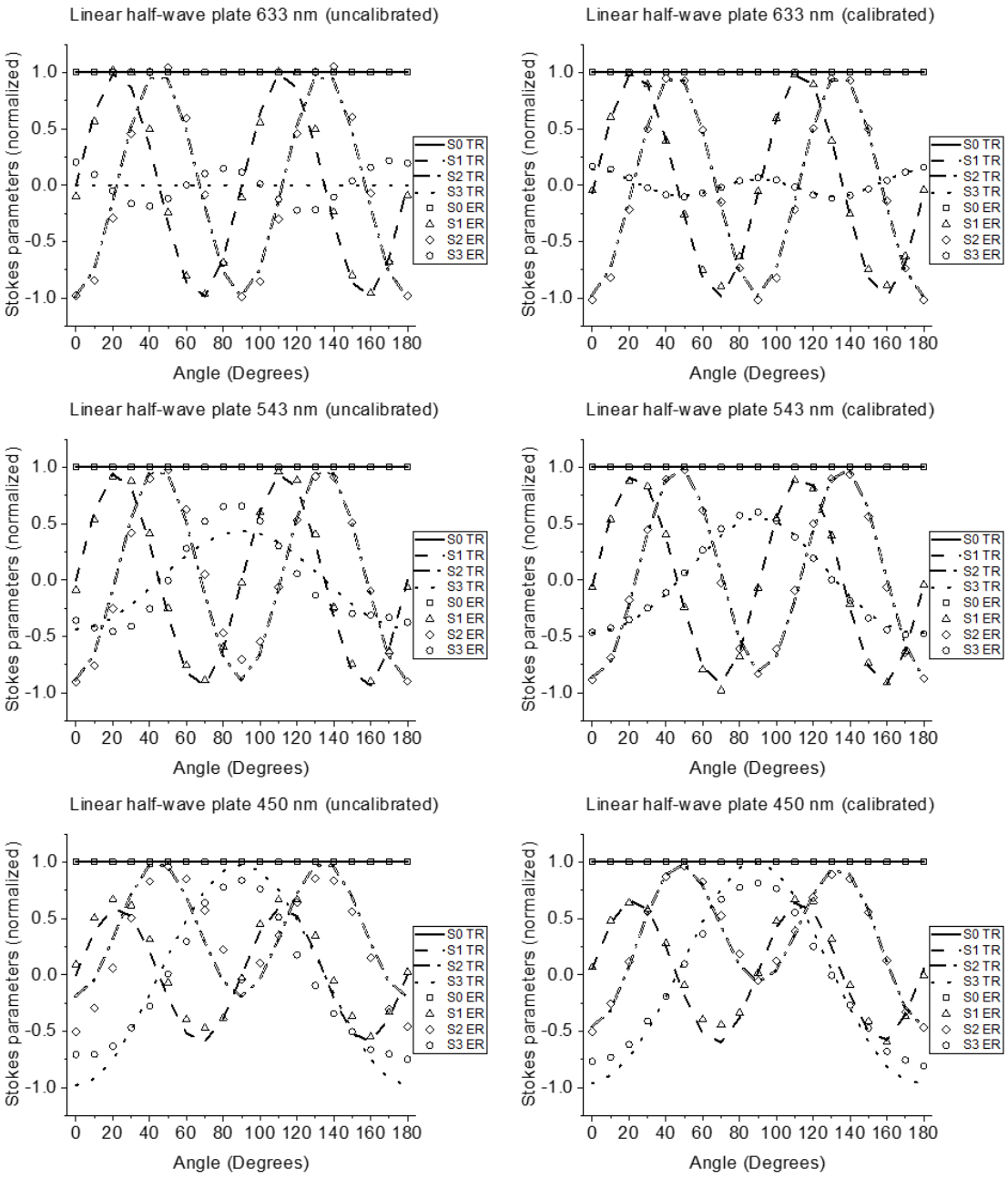

Figure 24 Stokes parameters for a half-wave plate as a function of the angle for the three wavelengths. Uncalibrated (left) and calibrated (right).

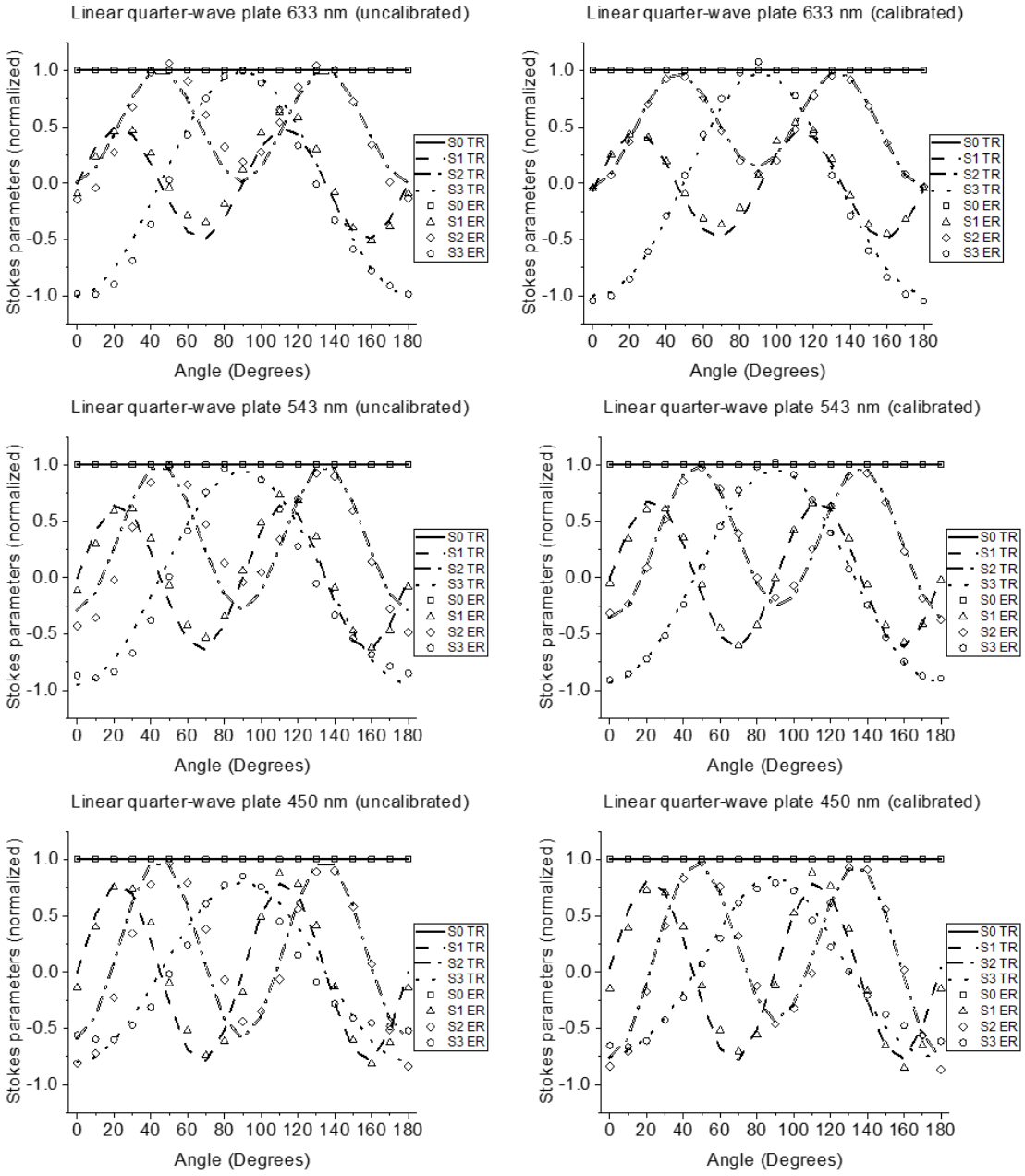

Figure 25 Stokes parameters for a quarter-wave plate as a function of the angle for the three wavelengths. Uncalibrated (left) and calibrated (right).

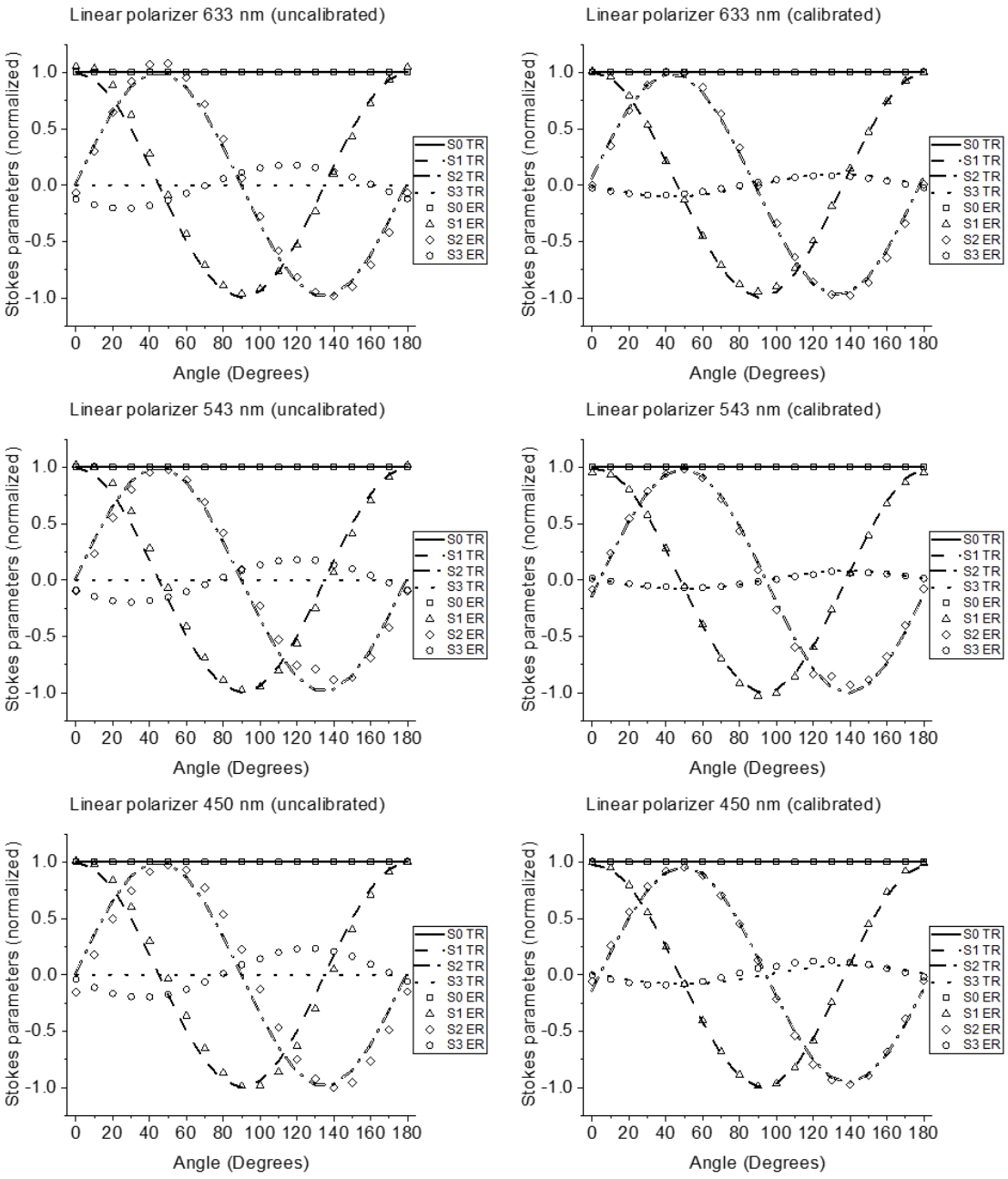

Figure 26 Stokes parameters for a Glan-Thompsom polarizer as a function of the angle for the three wavelengths. Uncalibrated (left) and calibrated (right).

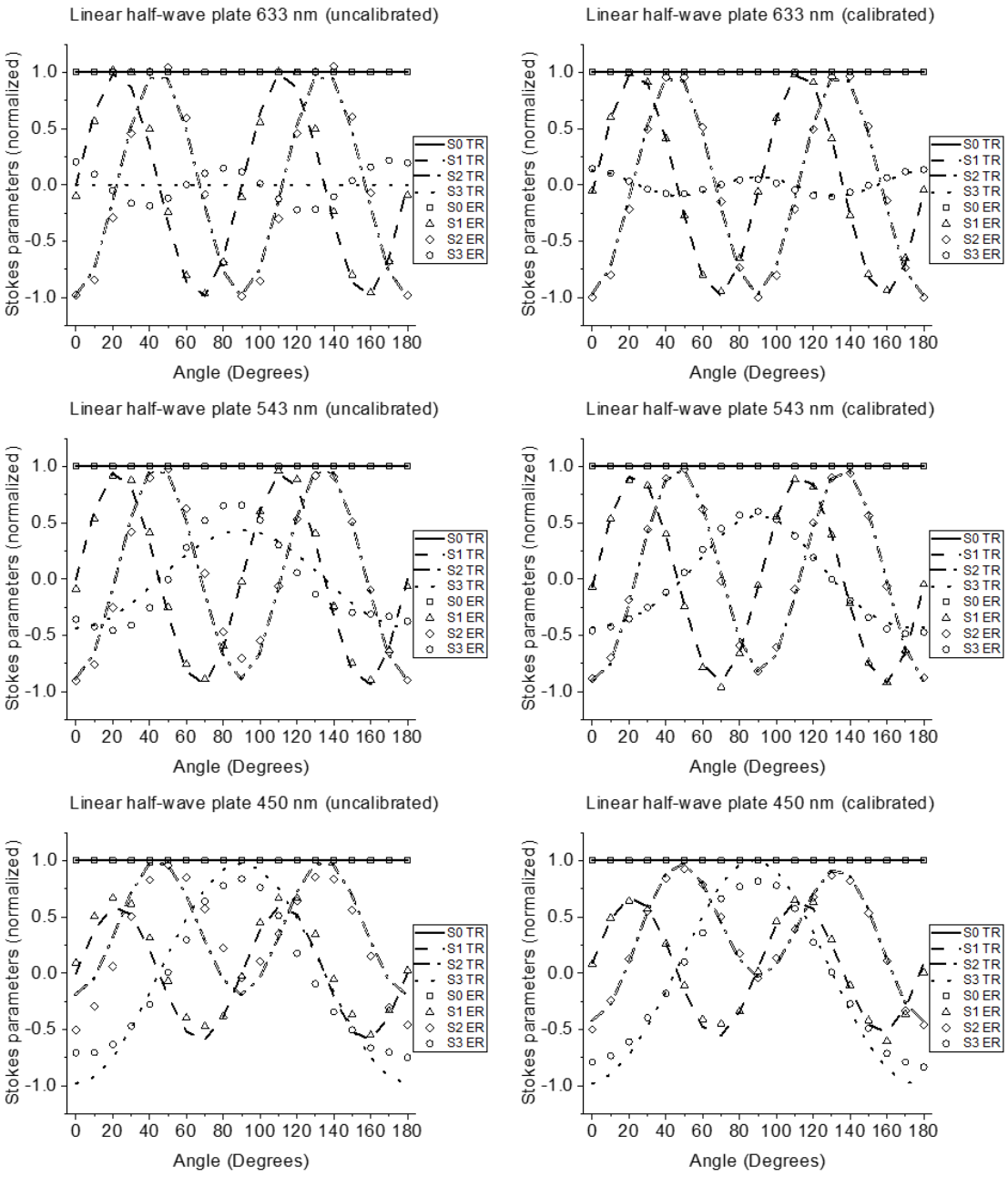

Figure 27 Stokes parameters for a half-wave plate as a function of the angle for the three wavelengths. Uncalibrated (left) and calibrated (right).

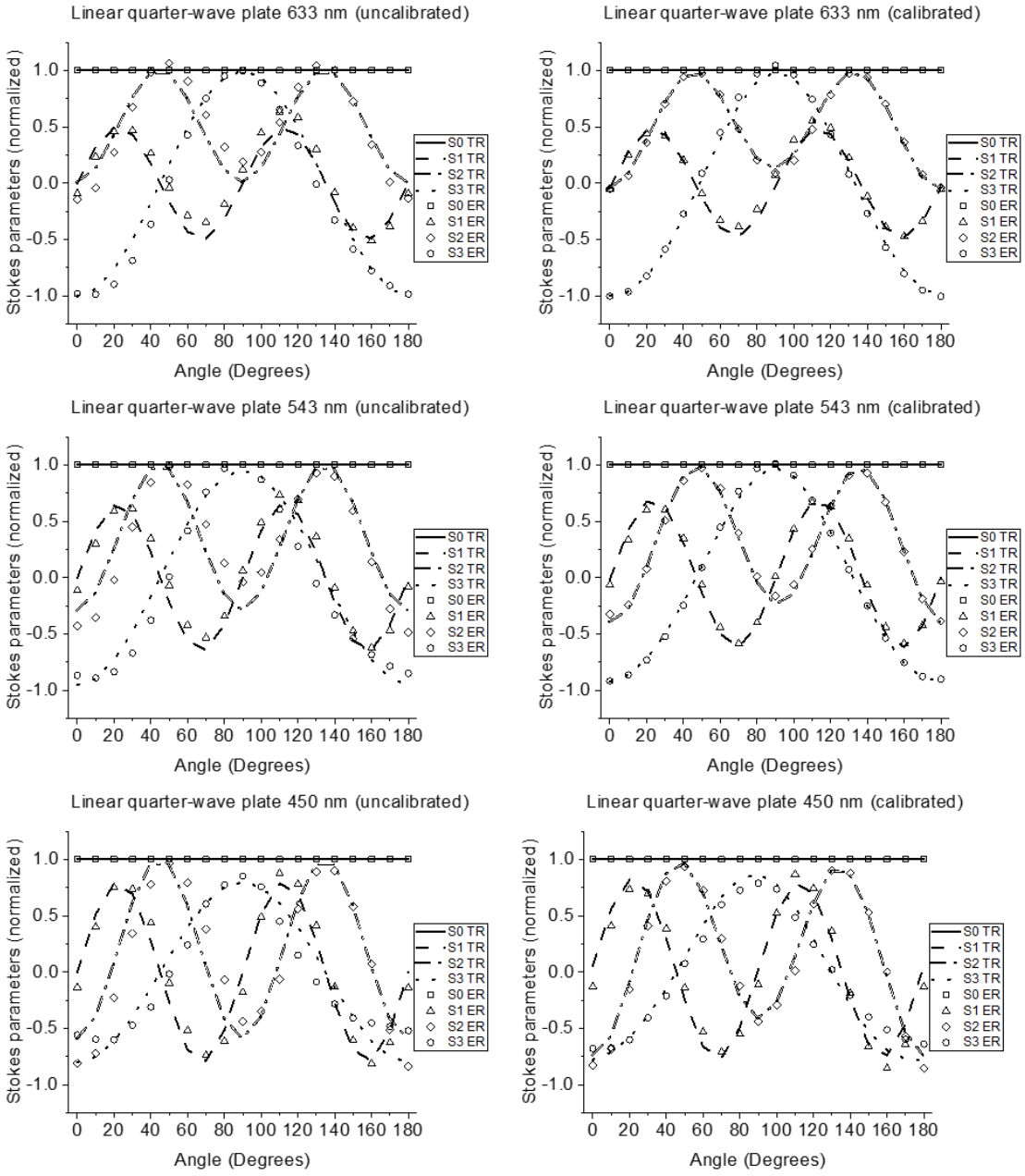

Figure 28 Stokes parameters for a quarter-wave plate as a function of the angle for the three wavelengths. Uncalibrated (left) and calibrated (right).

Figures 29, 30 and 31, show a reduction of the absolute error for the Stokes parameters between theoretical and experimental results after the calibration process. The absolute error was calculated for each Stokes parameter for the case of six calibration beams, where we have the smallest RMS error (see table 4).

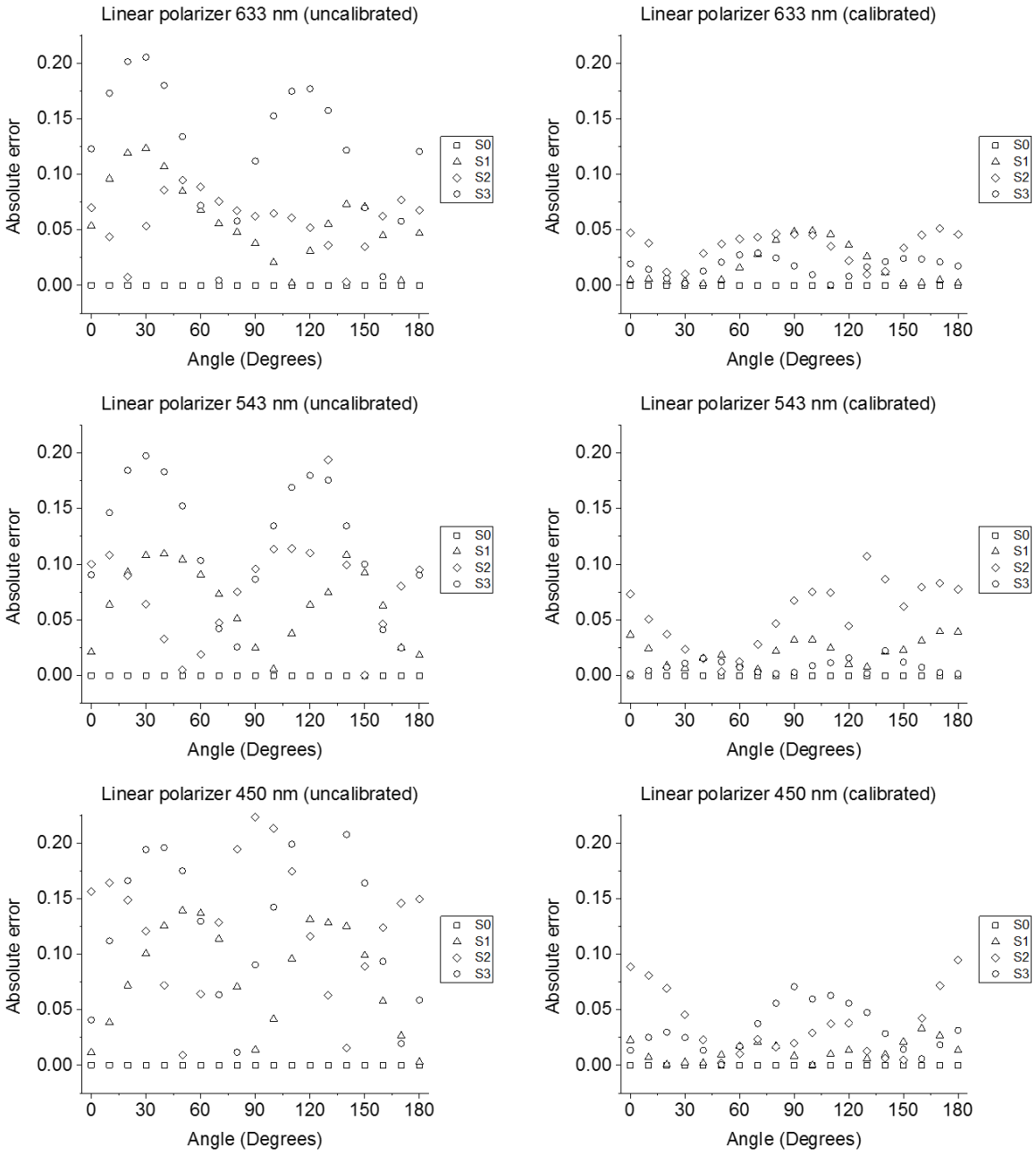

Figure 29 Absolute error for a Glan-Thompsom polarizer as a function of the angle for the three wavelengths. Uncalibrated (left) and calibrated (right).

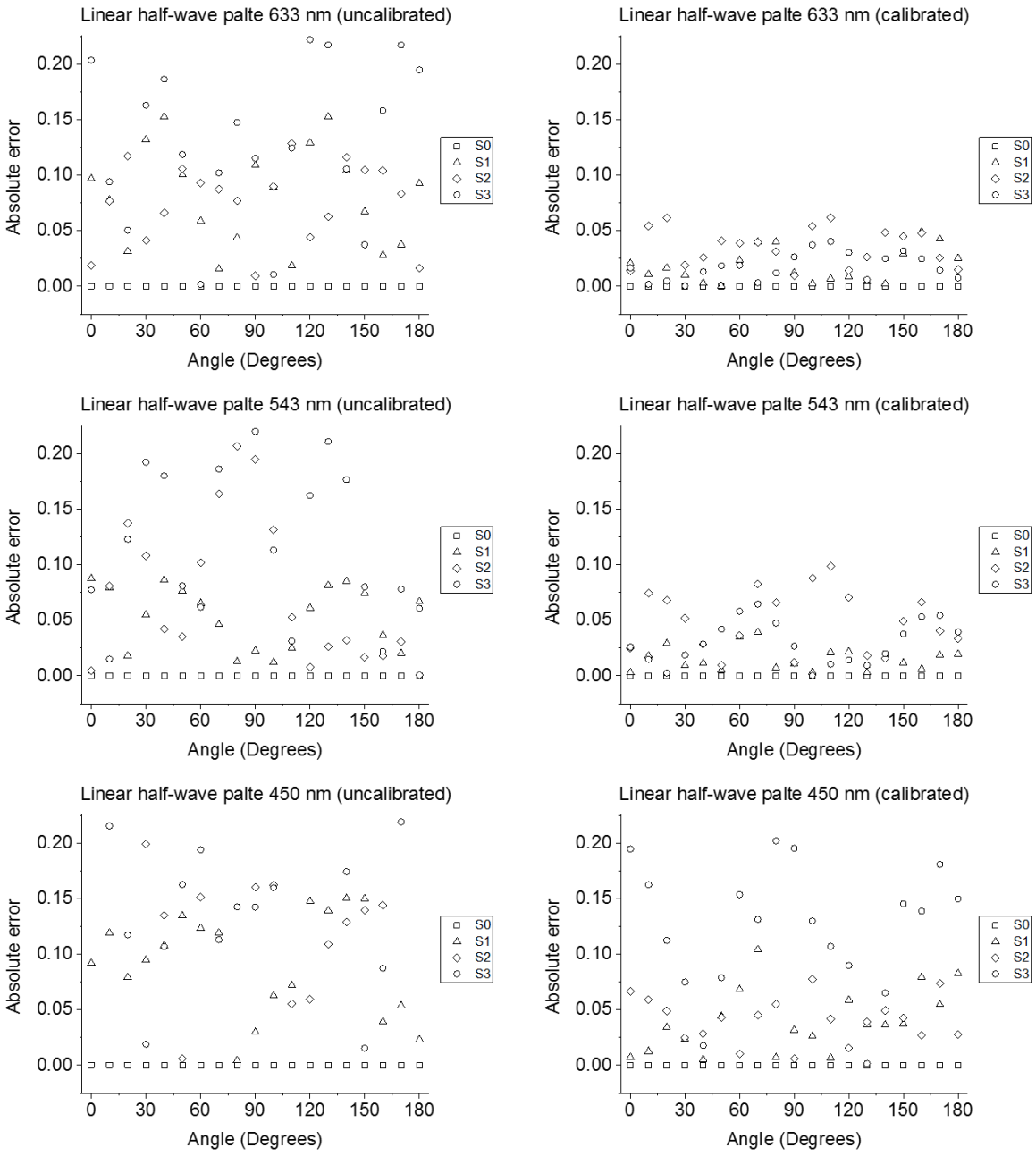

Figure 30 Absolute error for a half-wave plate as a function of the angle for the three wavelengths. Uncalibrated (left) and calibrated (right).

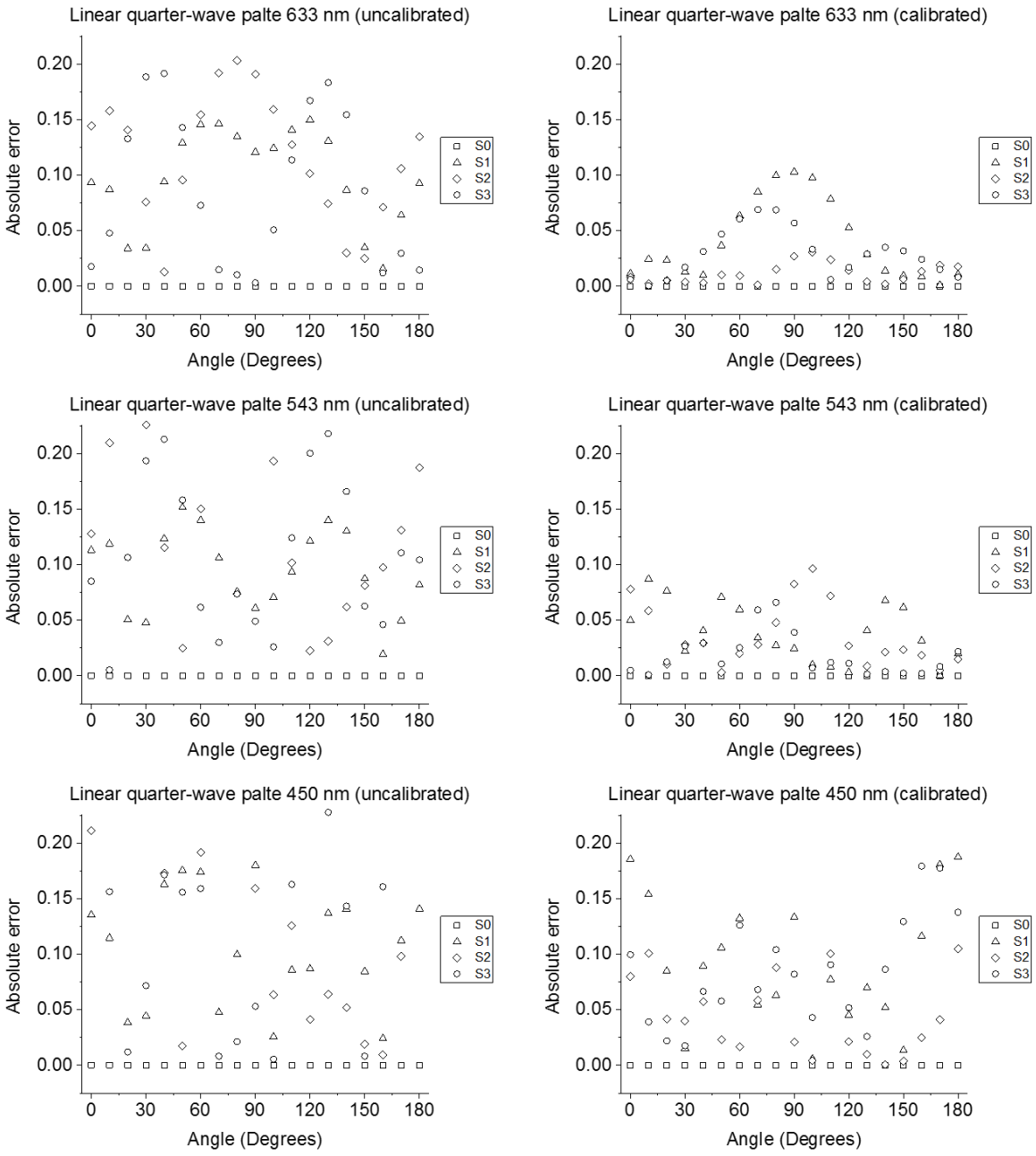

Figure 31 Absolute error for a quarter-wave plate as a function of the angle for the three wavelengths. Uncalibrated (left) and calibrated (right).

In general, we can see an important reduction of the absolute error for all cases after the calibration procedure. The absolute error values oscillate between 0 and 0.2 before calibration, and between 0 and 0.1 after that process. Although, for the half-wave plate and the quarter-wave plate to 450 nm this reduction is not very visible, it is noted that there is a flattening of most of the points in the graph.

Table 4 shows a comparison of the RMS error values for both cases studied in this section for each wavelength.

Table 4: RMS error values for each sample.

		Polarizer	Half-wave plate	Quarter-wave plate
RMS error values (without calibration)	633nm	0.0821	0.0960	0.0997
	543nm	0.0876	0.0905	0.1164
	450nm	0.1119	0.1427	0.1388
RMS error values (four calibration samples)	633nm	0.0298	0.0276	0.0454
	543nm	0.0408	0.0398	0.0414
	450nm	0.0366	0.0783	0.0798
RMS error values (six calibration samples)	633nm	0.0242	0.0252	0.0332
	543nm	0.0336	0.0344	0.0348
	450nm	0.0314	0.0751	0.0779

It is also interesting to note that the use of six calibration samples instead of four calibration samples gives a very small further reduction in the total RMS error, suggesting that for many cases the case of four calibration samples is adequate for many applications.

5. Optimized Stokes polarimeter with three simultaneous wavelengths

5.1 Experimental error propagation and the condition number of the characteristic matrix.

As described previously, the condition number is defined as the ratio between the largest and the smallest singular values in the characteristic matrix, κ. Also, the condition number measures how sensitive the inverse of a matrix is to perturbations in the input data and to roundoff errors made during the solution process. In this sense, an optimized Stokes polarimeter is defined as the optical system with a characteristic matrix which has a minimum error in the final Stokes vector result. In terms of the condition number, an optimized system must show the smallest value of κ. The minimum value reported by Tyo for an optimized characteristic matrix in a full-Stokes polarimeter is $\sqrt{3}$ (6). Experimentally, the condition number value of the characteristic matrix for a Stokes polarimeter can be modified by adjusting the individual retardance values to each retarder, and the relative positions of the principal axes to each polarizing element (retarders and polarizers).

The case reported in the previous chapter used the central green wavelength (543 nm) as reference to set the configuration of the applied voltages in order to reconstruct the Stokes parameters for the three wavelengths. In this case, the condition numbers for the three characteristic matrices of the wavelengths used were different from each other. In fact, the polarimeter is optimized for the 543 nm wavelength and therefore the condition number value for this wavelength was very close to $\sqrt{3}$, and the condition number values for the other two wavelengths were larger than this value, 2.6196 and 2.3312 for the blue and red cases, respectively

In this section the results obtained for an optimized case are presented. This is, the condition number values of all three characteristic matrices for the three wavelengths are set close to the minimum value by choosing the positions of the principal axes and the retardance values of the LCVR´s in the Stokes polarimeter to minimize the condition numbers of the three wavelengths simultaneously. Given that only one configuration of voltages is applied to the LCVR´s to vary the retardance values for the three wavelengths, if the applied voltage values are modified then the retardance values change for all three colors.

A MatLab program was written to search for optimized configurations for a 6 measurement Stokes polarimeter, varying the position of the principal axes and the applied voltage values of the LCVRs. The characterizations of the LCVRs in terms of the resulting retardance as a function of the applied voltage were used to calculate the retardances for each LCVR and for each wavelength, and then the characteristic matrices for each case were calculated. The

condition number values of the characteristic matrices for each wavelength were analyzed for each value of the polarimeter parameters. The cases of simultaneous minimum values of the condition number for the three characteristic matrices were stored as well as the corresponding LCVR axes angles and required voltage values. Given that almost all the optimized configurations published in the literature have the angle between the fast axes of the two LCVRs equal to 45°, this parameter was fixed in our search algorithm. The MatLab program used for this part of the project is presented in appendix D of this thesis.

5.2 Experimental results for the optimized case.

5.2.1 Determination of the configuration of retardances for the optimized case.

The results of the search algorithm described in the previous section were various different configurations of the Stokes polarimeter with slightly different condition numbers of the characteristic matrices for each wavelength. We chose one configuration with the three condition numbers nearly the same to better balance the error distribution between the three wavelengths. There were configurations where some of the condition numbers were smaller, but the corresponding condition numbers for the other wavelengths were larger, meaning that there would be a larger error in these cases.

Table 5 shows the retardances calculated from the characterization curves of Figure 17 for the optimized case.

Optimized case	Wavelength (nm)	LCVR 1		LCVR 2	
		Applied voltage (Volts)	Retardance (Degrees)	Applied voltage (Volts)	Retardance (Degrees)
Configuration 1	**633**	**2.883**	**120.986**	**5.742**	**2.059**
	543		**148.563**		**5.566**
	450		**206.116**		**9.120**
Configuration 2	**633**	**2.094**	**243.958**	**2.285**	**206.307**
	543		**301.598**		**256.491**
	450		**390.615**		**348.648**
Configuration 3	**633**	**4.14**	**35.289**	**3.006**	**102.133**
	543		**45.279**		**126.325**
	450		**64.853**		**178.780**
Configuration 4	**633**	**1.95**	**277.627**	**4.996**	**14.380**
	543		**345.328**		**20.053**
	450		**449.140**		**29.106**
Configuration 5	**633**	**2.952**	**108.495**	**3.053**	**97.853**
	543		**131.818**		**120.842**
	450		**185.494**		**170.123**
Configuration 6	**633**	**6.538**	**-8.726**	**2.604**	**148.299**
	543		**-8.350**		**187.272**
	450		**-7.425**		**252.332**

Table 5 presents the voltages used in the experimental configuration of the optimized polarimeter. As mentioned above, the positions of the fast axes of the LCVRs remain separated at 45° from one another, but the position of the fast axis of LCVR 1 is 21.96° with respect to the position of the polarizer in the Stokes polarimeter (defined as 0° with respect to the optical table).

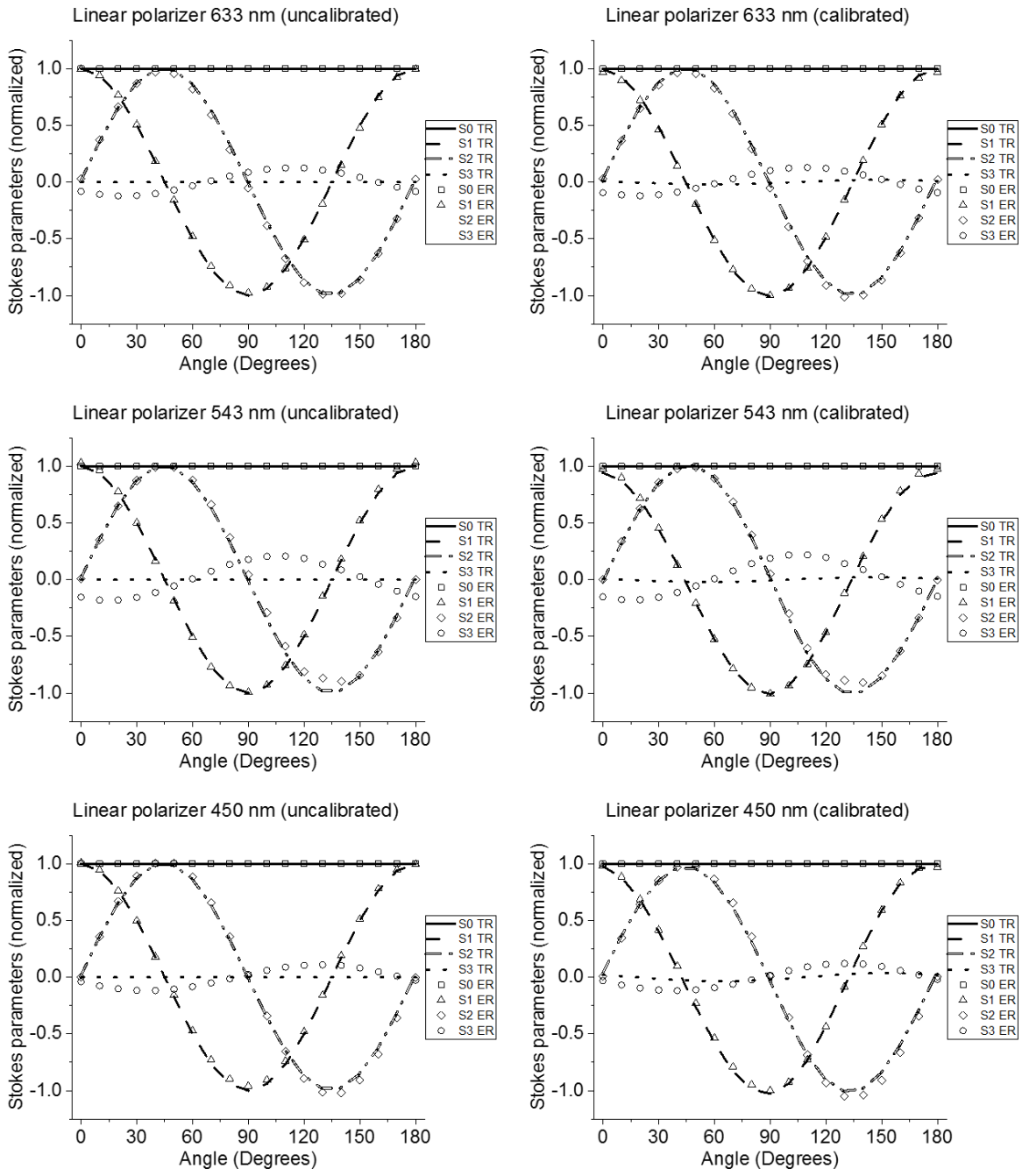

Figure 32 Stokes parameters for a Glan-Thompsom polarizer as a function of the angle for the three wavelengths. Uncalibrated (left) and calibrated (right).

5.2.2 Results for the optimized case.

From the retardance values shown in table 5, the three characteristic matrices can be calculated for the three wavelengths employed:

$$\boldsymbol{M}_{C(RED)} = \begin{pmatrix} 0.5000 & 0.1277 & 0.3863 & -0.2907 \\ 0.5000 & -0.4377 & -0.0110 & 0.2415 \\ 0.5000 & 0.0007 & -0.1099 & -0.4878 \\ 0.5000 & 0.3447 & 0.1450 & 0.3319 \\ 0.5000 & -0.3465 & 0.2888 & -0.2157 \\ 0.5000 & 0.0370 & -0.4802 & -0.1345 \end{pmatrix} \tag{94}$$

$$\boldsymbol{M}_{C(GREEN)} = \begin{pmatrix} 0.5000 & 0.0403 & 04749 & -0.1511 \\ 0.5000 & -0.1414 & 0.0256 & 0.4789 \\ 0.5000 & -0.1274 & -0.1753 & -0.4506 \\ 0.5000 & 0.4981 & -0.0295 & -0.0316 \\ 0.5000 & -0.4533 & 0.2045 & -0.0523 \\ 0.5000 & -0.0239 & -0.4902 & 0.0955 \end{pmatrix} \tag{95}$$

$$\boldsymbol{M}_{C(BLUE)} = \begin{pmatrix} 0.5000 & 0.0576 & 0.4529 & 0.2039 \\ 0.5000 & 0.4864 & 0.0039 & -0.1156 \\ 0.5000 & -0.1619 & -0.3509 & -0.3172 \\ 0.5000 & 0.1088 & 0.3407 & -0.3494 \\ 0.5000 & -0.4909 & -0.0017 & 0.0947 \\ 0.5000 & 0.1291 & -0.2916 & 0.3851 \end{pmatrix} \tag{96}$$

The condition number values for these cases are: 1.8855, 1.8974, and 1.9316 for the red, green and blue wavelengths, respectively. We could not find a different configuration with all three condition numbers smaller than these values. The average condition number in this case is 1.9048, which is better than the value for the nonoptimized case described in the previous chapter, for which the average is 2.2277.

Figures 32, 33 and 34 show the uncalibrated (left) and calibrated (right) Stokes parameters for rotating components of: a Glan-Thompsom polarizer, a half-wave plate retarder and a quarter-wave plate retarder, respectively, for this optimized case. In all cases the expected theoretical data are represented by lines and experimental data are represented by geometrical shapes. Here we take six calibration beams as known samples, as described in the previous section:

- a linear polarizer with the transmission axis oriented at 130°
- a linear polarizer with the transmission axis oriented at 30°
- a horizontal linear polarizer followed by a half-wave plate with the fast axis oriented at 30°

- a horizontal linear polarizer followed by a quarter-wave plate with the fast axis oriented at 30°
- a horizontal polarizer followed by a half-wave plate with fast axes at 130°
- a horizontal polarizer followed by a quarter-wave plate with fast axes at 130°.

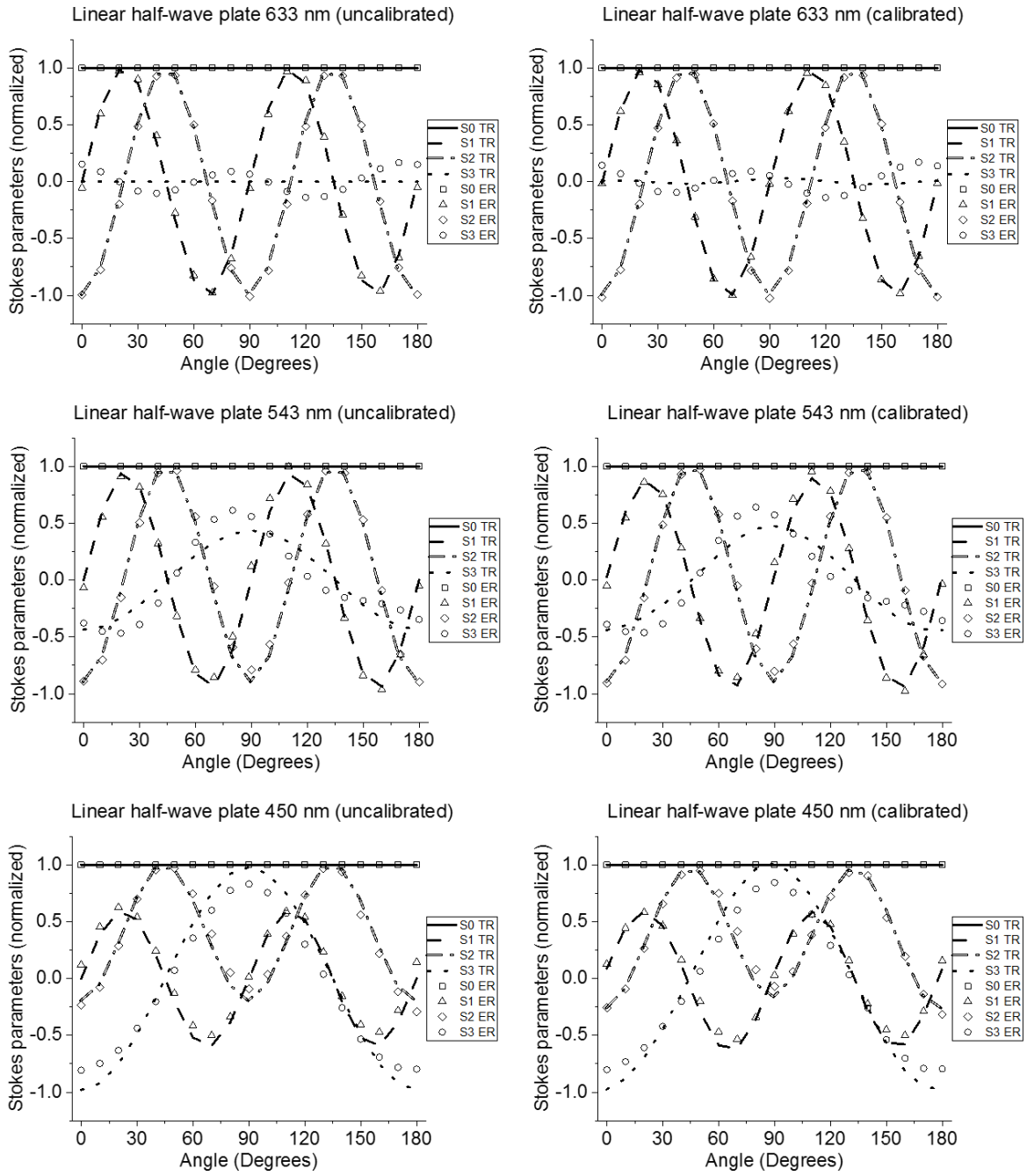

Figure 33 Stokes parameters for a half-wave plate as a function of the angle for the three wavelengths. Uncalibrated (left) and calibrated (right).

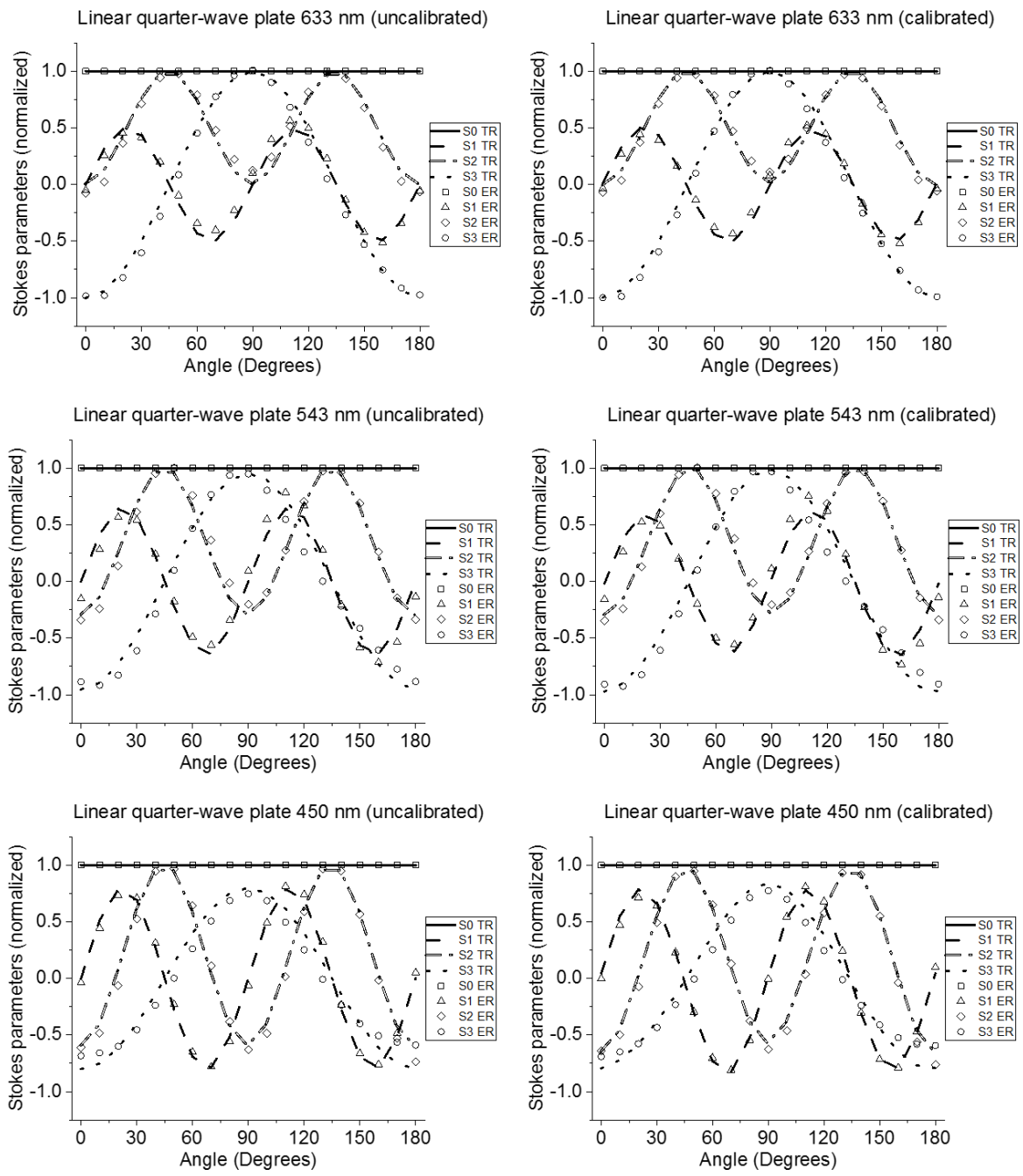

Figure 34 Stokes parameters for a quarter-wave plate as a function of the angle for the three wavelengths. Uncalibrated (left) and calibrated (right).

Table 6 shows a comparison of the RMS error values for each wavelength and optical element analyzed.

Table 6 RMS error values for each sample.

	Wavelength/Sample	Polarizer	Half-wave plate	Quarter-wave plate
RMS Error (without calibration)	633 nm	0.0471	0.0538	0.0596
	543 nm	0.0731	0.0751	0.0778
	450 nm	0.0429	0.0850	0.0696
RMS Error (six calibration samples)	633 nm	0.0465	0.0487	0.0475
	543 nm	0.0731	0.0728	0.0720
	450 nm	0.0391	0.0789	0.0627

Comparing these results with the results obtained in the previous chapter with a polarimeter optimized only for the central wavelength of 543 nm, it can be observed that the uncalibrated data for the optimized polarimeter described in this section has smaller errors than the uncalibrated data for the unoptimized polarimeter in the previous chapter. The largest reductions in rms errors, of around 50%, are for the cases of wavelengths 633 nm and 450 nm, which have reductions in the condition numbers of their characteristic matrices. Even the case of 543 nm, for which the condition number increases from the previous setup, has a small but noticeable reduction in the rms error for the uncalibrated cases. It can also be observed that the calibration process in this case shows less reduction in the rms error in the calibrated data. In fact, the calibrated rms errors in this case are either about the same as (for 450 nm), or larger than (for 633 nm and 543 nm) the calibrated values in the previous unoptimized cases. In the cases reported here for the optimized polarimeter the reduction of the RMS error values after the calibration method is applied for the quarter-wave plate is 20%, 7% and 10% for 633 nm, 543 nm and 450 nm, respectively. For the half wave-plate a small reduction of the RMS error values is observed (9%, 3% y 7% respectively). Finally, the reduction for the polarizer is smaller than the other polarizing elements (1%, 0% y 9% respectively).

The results presented here suggest that the method with one wavelength optimized and the other two wavelengths not optimized, with the calibration method used in this thesis gives better results than the method minimizing all three condition numbers of the characteristic matrices for the three wavelengths, as the final rms errors are smaller for the former case. One reason for this may be that it is not possible to minimize the three condition numbers more simultaneously, or at least we could not find a solution with smaller condition number. This means that none of the three wavelength systems are completely optimized (with condition number $\sqrt{3}$), whereas for the previous case one of the systems (for 543nm) was optimized, which may affect the obtained results.

Also, it is interesting that for the three wavelengths in the optimized case presented in this chapter, the uncalibrated rms errors are smaller than the unoptimized case. This suggests that the optimized polarimeter is closer to the ideal, expected configuration than the unoptimized case, which means that the experimental errors, in particular the alignment errors and errors in the retardance values required, are smaller in the optimized case. This in turn may mean that it is more difficult for the proposed calibration method to detect and correct these small errors. More work needs to be done to study these cases.

6. Conclusions and future work

6.1 Conclusions.

The operation principle for Stokes polarimeter working with three wavelengths simultaneously has been demonstrated. The Stokes polarimeter instrumented allows us to measure the Stokes vector of a light beam simultaneously for three different wavelengths. The measurement of the polarization intensities and calibration samples are simultaneous, with the calibration and data-extraction processes being performed by software, independently for each wavelength.

We have shown that a proposed fitting calibration method works correctly and improves the fit between the experimental and theoretical, or expected curves, when we use only four known calibration beams. The RMS error values show a reduction of about 50% in the total RMS values after calibration. It is interesting that for the case of six calibration samples, the results show only a slight improvement in the total RMS error values. This suggests that four calibration samples may be enough in many applications to achieve adequate results using the fitting calibration procedure used here.

We have compared results of measurements in a full Stokes LCVR polarimeter for the measurement of three wavelengths simultaneously, with two configurations. One, non-optimized, configuration has the CN for the central wavelength at the ideal value of $\sqrt{\mathbf{3}}$, and the other two wavelengths have high condition numbers, fixed by the voltages used in the configuration of the central wavelength. This configuration was presented in the paper published in the indexed journal Applied Optics [18]. The second, or optimized, configuration has all three wavelengths with approximately the same CN, and with a lower average value closer to the ideal. This second configuration has smaller errors in the measured Stokes parameters before calibration and generally worse errors than the first configuration after calibration.

The results presented here suggest that the method with one wavelength using an optimized condition number, with the other two wavelengths having an unoptimized condition number gives better results with the proposed calibration method. The method minimizing all three condition numbers of the characteristic matrices for the three wavelengths gives larger errors than the first case in the calibrated data. One reason for this may be that it is not possible to minimize the three condition numbers simultaneously closer to the ideal value of 1.732, or at least we could not find a solution with the three condition numbers with similar values less than the values obtained around 1.9. This means that none of the three wavelength systems are completely optimized (with condition number 1.732), whereas for the previous case one of the systems (for 543nm) was optimized to this value, and this may affect the obtained results. It is noticeable that the central wavelength of 543nm, which has an increase in the

condition number from the non-optimized to the optimized case, gives a calibrated RMS error of twice as much in the optimized case compared to the non-optimized case.

We have shown that the polarimeter configurations used in this work give average total RMS error values of 0.0601 for the optimized case, and 0.0411 for the non-optimized case, averaged over the three wavelengths and the three reference samples used. These values are comparable to values reported in the literature for one-wavelength polarimeters and is adequate for many applications. Another general conclusion from this work is that it is not clear how to choose the best configuration for this type of polarimeter, where the characteristic matrices are coupled, but the analysis of the measured data is independent for each case. In the example presented here the characteristic matrices are coupled through the voltages applied to the LCVRs, and the analysis was independent for each wavelength. Since the unknown Stokes vector to be measured is different for each wavelength, it is not possible to write a single characteristic matrix for all the cases at once, and so a single minimum condition number cannot de defined.

6.2 Future work.

Possible activities required as future work to continue with the project described in this thesis are:

- To develop a simulation of the Stokes polarimeter working with three different wave lengths to analyze the error propagation.
- According to the above result, the simulation developed can be extended to more wavelengths to demonstrate how flexible the Stokes polarimeter developed can be.
- To review the literature on other calibration methods and analyze the implementation to the optimized case.
- To implement at least two different calibration methods reviewed on the above point to the data acquired for the optimized case.
- To define a general method for optimization of polarimeters with multiple, coupled characteristic matrices.

7. Appendices

7.1 Appendix A: LabVIEW programs for LCVR characterization.

In this appendix we present both the front panel and block diagrams of the LabView program to obtain the experimental data used to calculate the characterization curves of the LCVR´s for each wavelength used. Data are taken simultaneously for the three colours. 142 voltage values were measured.

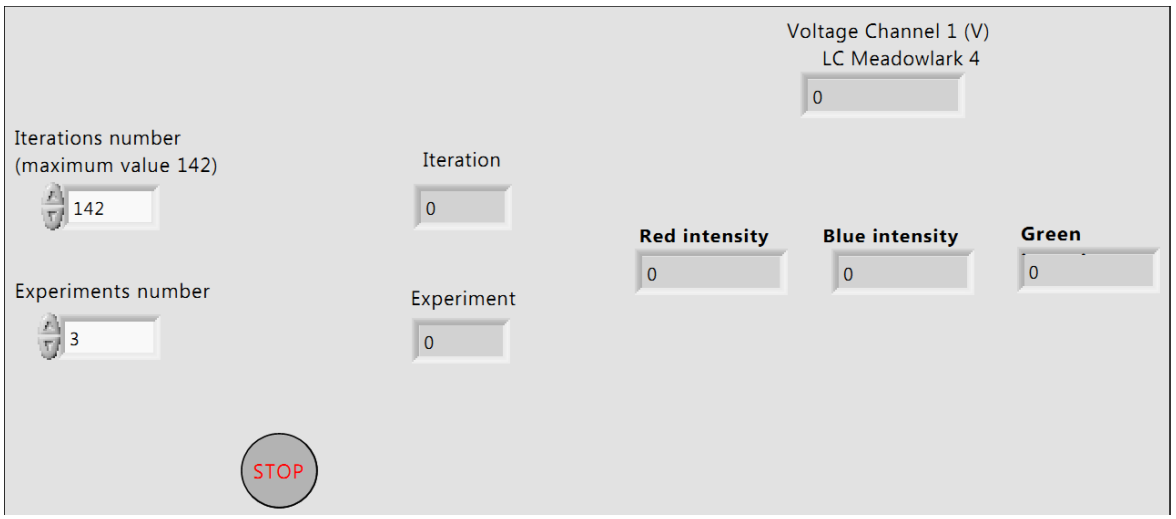

Figure A1: front panel of the LabView program. The inputs are the iteration and the experiment numbers. Outputs are the voltage applied on the LCVR, the intensity measured for the three wavelengths and the actual number of the iteration and the experiment.

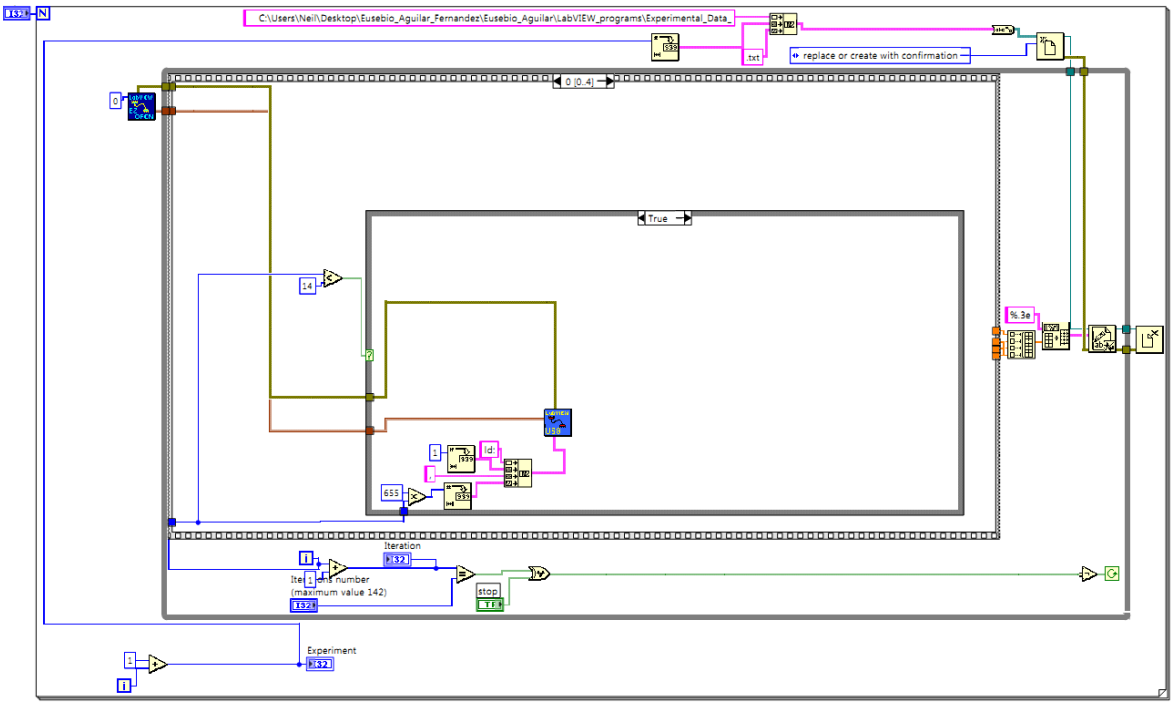

Figure A2: LabView block diagram for initializing the program to the first iteration and first experiment. Also, it allows us to setup the voltage values applied to generate the first section of the calibration curve, given that in the central curve it is necessary to use a smaller step than in the curve tails.

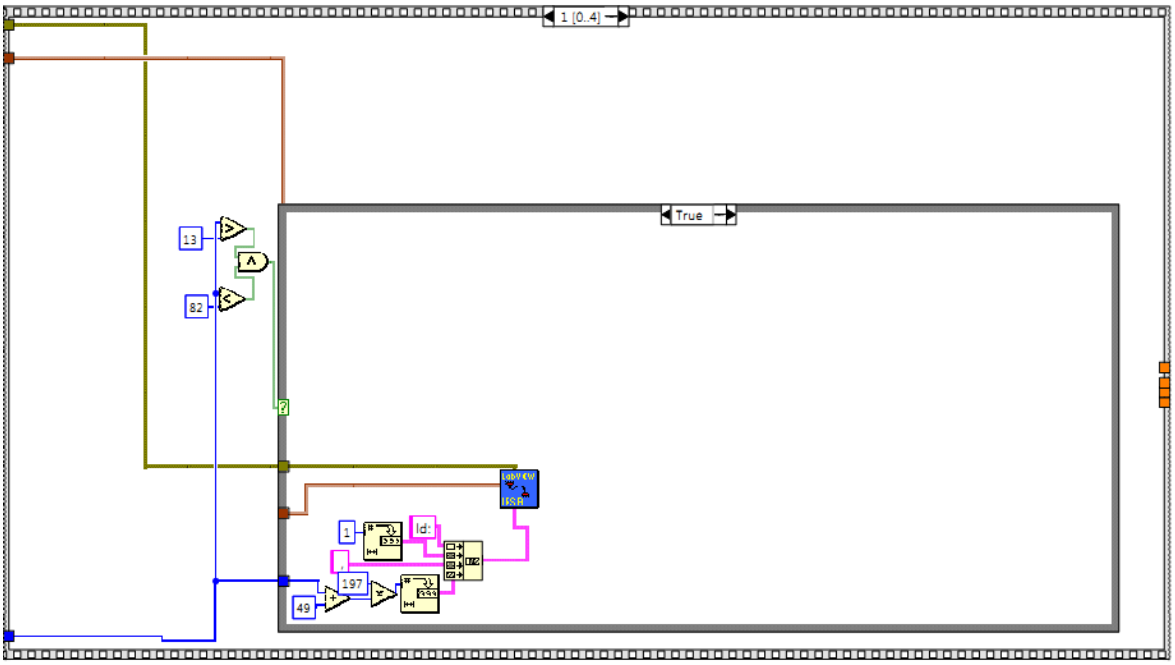

Figure A3: LabView block diagram to setup the voltage values for the central calibration curve with a smaller step than in the curve tails.

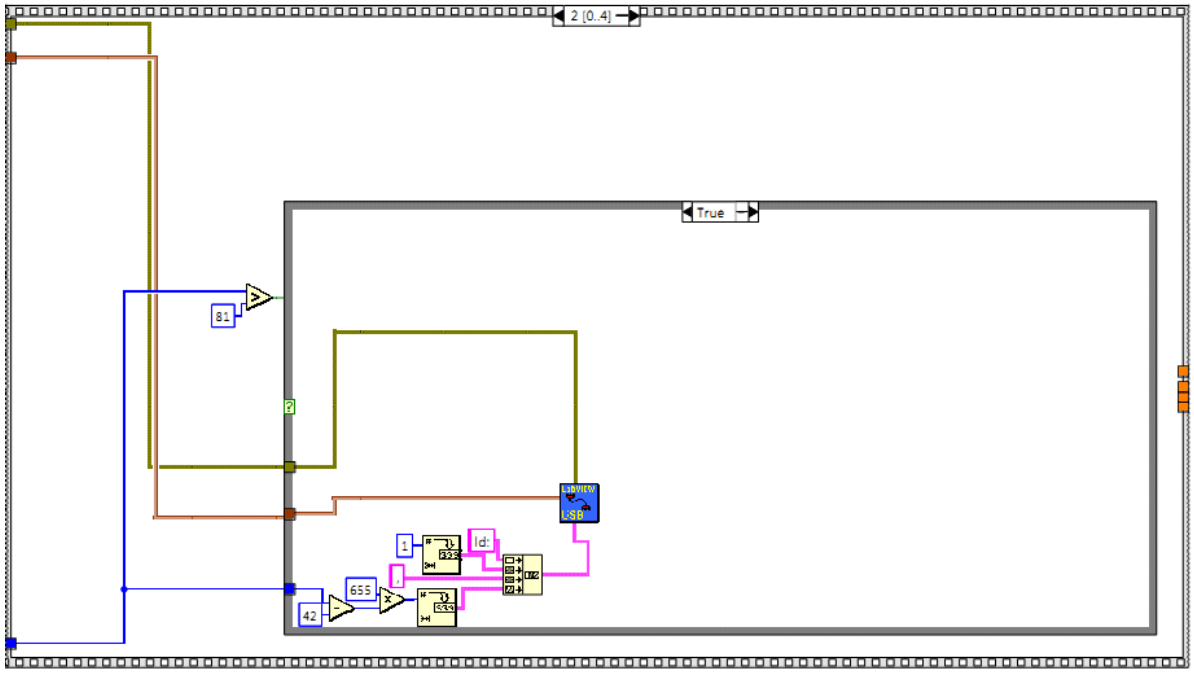

Figure A4: LabView block diagram to setup the voltage values to generate the last section of the calibration curve.

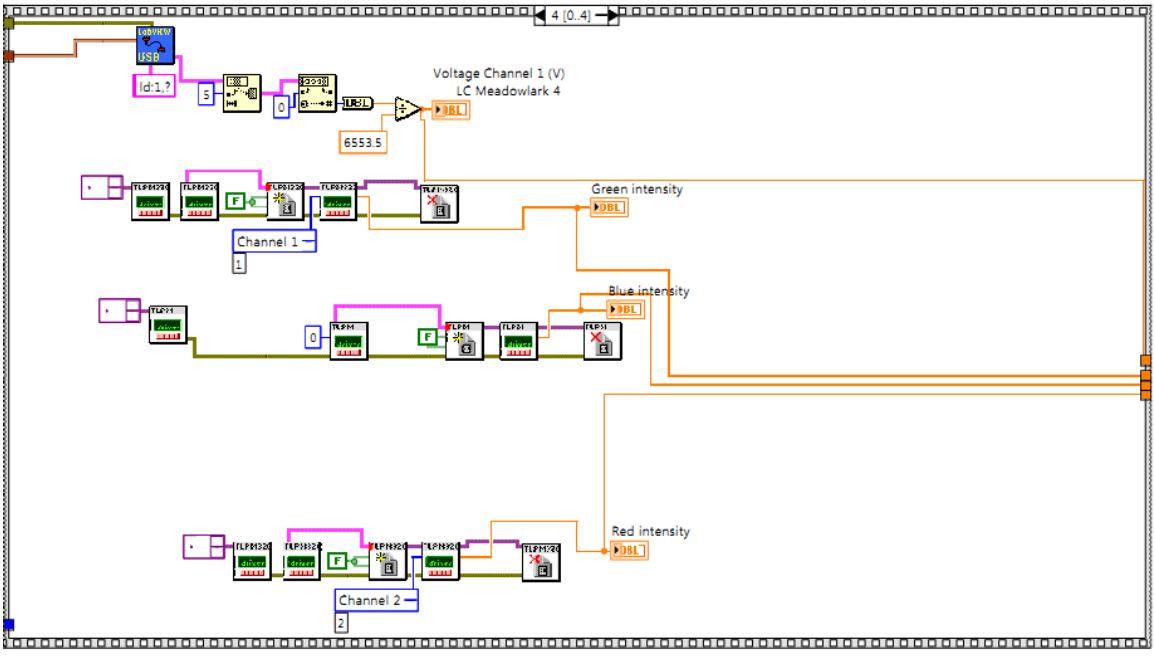

Figure A5: LabView block diagram for the overall data reading and storage for the three wavelengths. The intensity measured is showed in the front panel of the figure A1.

7.2 Appendix B: LabVIEW programs for the Chenault-Chipman method.

In this appendix we present the block diagram and front panel for the LabView program developed to take the experimental measurements for the calculation of the retardance values of the half-wave and quarter-wave plates using the Chenault-Chapman method.

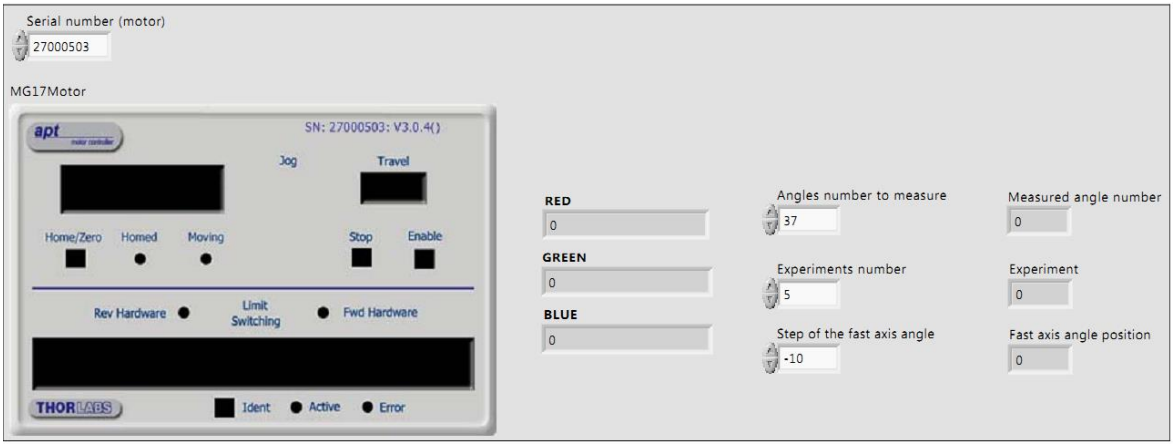

Figure B1: front panel for control of the Chenault-Chipman method. The inputs are the number of angles to measure, the number of experiments and the step to move the rotating mount. The outputs are the intensity values for the three wavelengths and the indicators of the angle, the experiment and the position of the fast axis for the analyzed retarder.

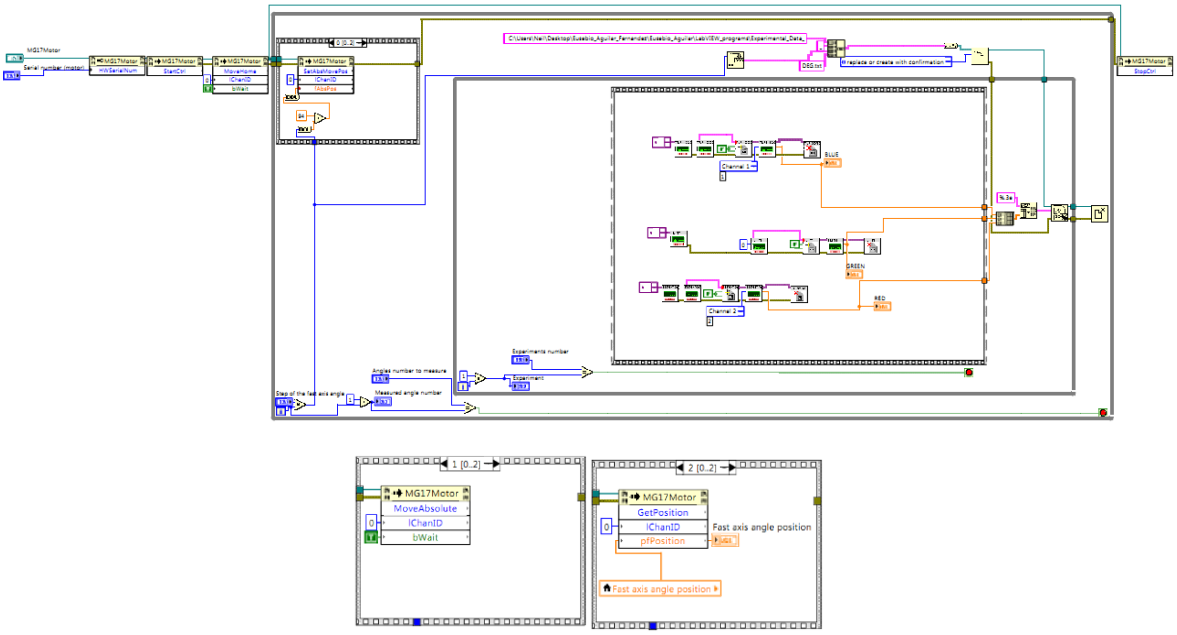

Figure B2: Block diagram of the program developed to obtain the data used to calculate the retardance values of the half-wave and quarter-wave plates using the Chenault-Chipman method. This program allows us to read and store the intensities measured for the three wavelengths to generate the characteristic curves for each wave plate. This information is shown in the front panel of figure B1.

7.3 Appendix C: LabVIEW programs for the Stokes polarimeter.

In this appendix we present the program developed to obtain the experimental data used to calculate the Stokes parameters for each sample analyzed.

Figure C1: front panel of the LabView program to control the Stokes polarimeter. The inputs are the number of voltages to set up for each channel, the configuration voltage values to apply, also, the angle and experiment numbers to analyze, and finally, the step to rotate the principal axis of the sample. In the output, the front panel shows the voltage applied to the current iteration, the angle and experiment numbers, the current position of the principal axis angle, and finally, the current intensity value measured for each wavelength.

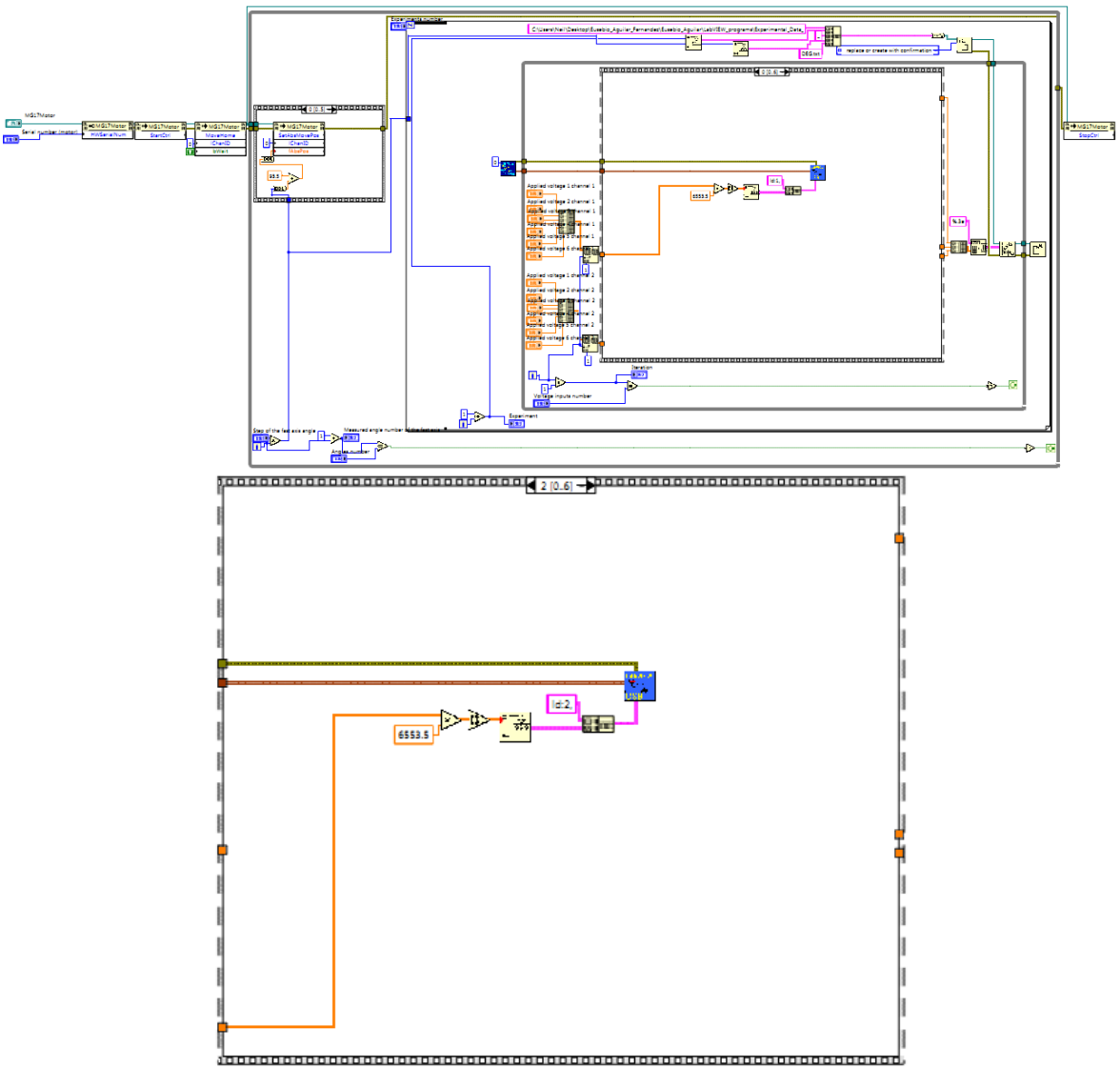

Figure C2: block diagram of the LabView program to setup the voltage on the LCVRs. The voltage values are set up from the front panel.

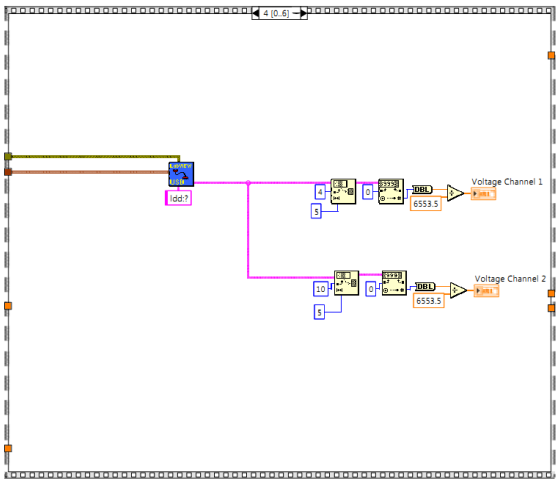

Figure C3: block diagram of the LabView program to read the voltage values applied to the LCVRs for a specific configuration of retardances. These values are shown on the front panel.

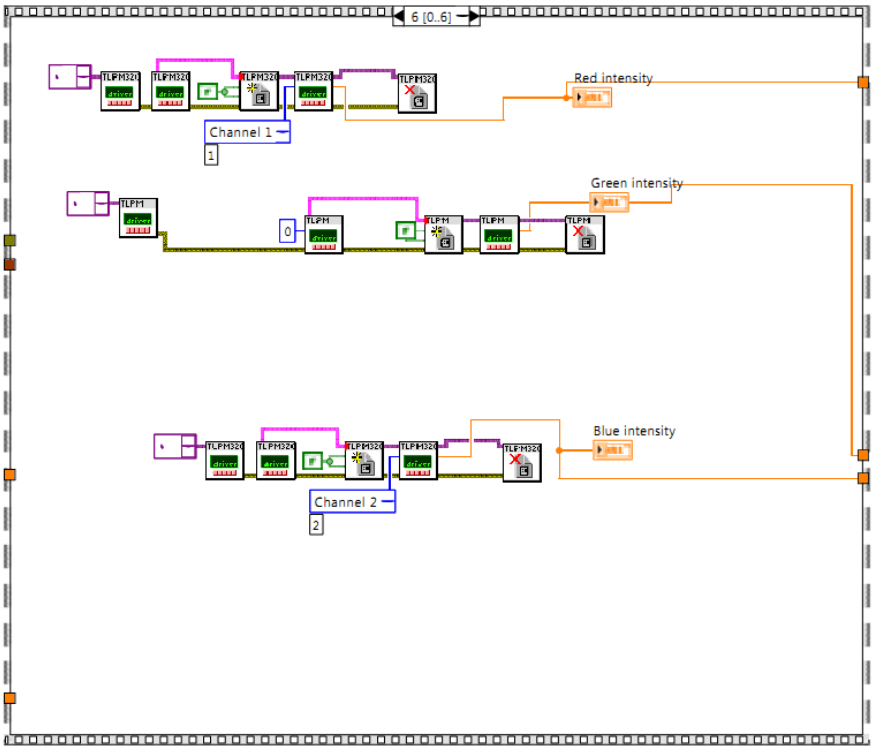

Figure C4: block diagram of the LabView program to read the intensity measurement for a specific configuration of retardances for the three wavelengths. This information is sent to be averaged later in a text document.

7.4 Appendix D: MatLab programs.

Appendix D1: MatLab program developed to generate the theoretical and experimental curves for the Stokes parameters for the three wavelengths. Also, it allows us to calculate the RMS error for both four and six calibration samples.

```
clear all
close all
clc

v=[5.697 3.286 2.142 2.555 5.797 2.585 3.325]; %v=[v1I v1III v1IV v1V v2I
v2II v2III] Configuration of voltage values applied to the LCVRs.

CCDa=importdata('Char_Cur_all_wavelengths.txt'); %Storage data of the
retardances values from the characteristic curves for three wavelengths.

CCR1=[CCDa(:,1) CCDa(:,2)]; %633 nm LCVR1
CCR2=[CCDa(:,4) CCDa(:,5)]; %633 nm LCVR2
CCG1=[CCDa(:,7) CCDa(:,8)]; %543 nm LCVR1
CCG2=[CCDa(:,10) CCDa(:,11)]; %543 nm LCVR2
CCB1=[CCDa(:,13) CCDa(:,14)]; %450 nm LCVR1
CCB2=[CCDa(:,16) CCDa(:,17)]; %450 nm LCVR2

%Position of the principal axes for the polarizing elements
ar1=0; %fast axis of the first LCVR
ar2=45; %fast axis of the second LCVR
ap=0; %transmission axis of the linear polarizer in the Stokes
polarimeter
ai=45; %transmission axis of the firts linear polarizer (it allows us to
be sure that the incident beams are linearly polarized)

%Retardance values for the three wavelengths
%the function RET allows us to find the retardance value for a specific
%voltage value in the characteristic curve previously storaged.
r1IR=RET(CCR1,length(CCR1),v(1)); %retardance value on the LCVR 1 for
case I and 633 nm (it is the same value for cases II and VI)
r1IIR=r1IR;
r1IIIR=RET(CCR1,length(CCR1),v(2)); %retardance value on the LCVR 1 for
case III and 633 nm
r1IVR=RET(CCR1,length(CCR1),v(3)); %retardance value on the LVR 1 for
case IV and 633 nm
r1VR=RET(CCR1,length(CCR1),v(4)); %retardance value on the LVR 1 for case
V and 633 nm
r1VIR=r1IR;

r2IR=RET(CCR2,length(CCR2),v(5)); %retardance value on the LCVR 2 for
case I and 633 nm
r2IIR=RET(CCR2,length(CCR2),v(6)); %retardance value on the LCVR 2 for
case II and 633 nm
r2IIIR=RET(CCR2,length(CCR2),v(7)); %retardance value on the LCVR 2 for
case III and 633 nm (it is the same value for cases IV, V nad VI)
r2IVR=r2IIIR;
r2VR=r2IIIR;
r2VIR=r2IIIR;
```

```
r1IG=RET(CCG1,length(CCG1),v(1)); %retardance value on the LCVR 1 for
case I and 543 nm (it is the same value for cases II and VI)
r1IIG=r1IG;
r1IIIG=RET(CCG1,length(CCG1),v(2)); %retardance value on the LCVR 1 for
case III and 543 nm
r1IVG=RET(CCG1,length(CCG1),v(3)); %retardance value on the LVR 1 for
case IV and 543 nm
r1VG=RET(CCG1,length(CCG1),v(4)); %retardance value on the LVR 1 for case
V and 543 nm
r1VIG=r1IG;

r2IG=RET(CCG2,length(CCG2),v(5)); %retardance value on the LCVR 2 for
case I and 543 nm
r2IIG=RET(CCG2,length(CCG2),v(6)); %retardance value on the LCVR 2 for
case II and 543 nm
r2IIIG=RET(CCG2,length(CCG2),v(7)); %retardance value on the LCVR 2 for
case III and 543 nm (it is the same value for cases IV, V nad VI)
r2IVG=r2IIIG;
r2VG=r2IIIG;
r2VIG=r2IIIG;

r1IB=RET(CCB1,length(CCB1),v(1)); %retardance value on the LCVR 1 for
case I and 450 nm (it is the same value for cases II and VI)
r1IIB=r1IB;
r1IIIB=RET(CCB1,length(CCB1),v(2)); %retardance value on the LCVR 1 for
case III and 450 nm
r1IVB=RET(CCB1,length(CCB1),v(3)); %retardance value on the LVR 1 for
case IV and 450 nm
r1VB=RET(CCB1,length(CCB1),v(4)); %retardance value on the LVR 1 for case
V and 450 nm
r1VIB=r1IB;

r2IB=RET(CCB2,length(CCB2),v(5)); %retardance value on the LCVR 2 for
case I and 450 nm
r2IIB=RET(CCB2,length(CCB2),v(6)); %retardance value on the LCVR 2 for
case II and 450 nm
r2IIIB=RET(CCB2,length(CCB2),v(7)); %retardance value on the LCVR 2 for
case III and 450 nm (it is the same value for cases IV, V nad VI)
r2IVB=r2IIIB;
r2VB=r2IIIB;
r2VIB=r2IIIB;

%Definition of the error parameters
eai=0;
ear1=0;
ear2=0;
eas=0;
er1I=0;
er1II=0;
er1III=0;
er1IV=0;
er1V=0;
er1VI=0;
er2I=0;
er2II=0;
```

```
er2III=0;
er2IV=0;
er2V=0;
er2VI=0;
erhb=0;
erhg=0;
erhr=0;
erqb=0;
erqg=0;
erqr=0;

for k=1:19
as=10*(k-1); %principal axis of the sample. It is rotating from 0° to
180°
Msp=0.5*[1 cos(2*deg2rad(as+eas)) sin(2*deg2rad(as+eas))
0;cos(2*deg2rad(as+eas)) (cos(2*deg2rad(as+eas)))^2
sin(2*deg2rad(as+eas))*cos(2*deg2rad(as+eas)) 0;sin(2*deg2rad(as+eas))
sin(2*deg2rad(as+eas))*cos(2*deg2rad(as+eas)) (sin(2*deg2rad(as+eas)))^2
0;0 0 0 0];
rh=180+erhr; %retardance of the half-wave plate for 633 nm.
Msh=[1 0 0 0;0
(cos(2*deg2rad(as+eas)))^2+cos(deg2rad(rh))*(sin(2*deg2rad(as+eas)))^2
(1-cos(deg2rad(rh)))*sin(2*deg2rad(as+eas))*cos(2*deg2rad(as+eas)) -
sin(deg2rad(rh))*sin(2*deg2rad(as+eas));0 (1-
cos(deg2rad(rh)))*sin(2*deg2rad(as+eas))*cos(2*deg2rad(as+eas))
(sin(2*deg2rad(as+eas)))^2+cos(deg2rad(rh))*(cos(2*deg2rad(as+eas)))^2
sin(deg2rad(rh))*cos(2*deg2rad(as+eas));0
sin(deg2rad(rh))*sin(2*deg2rad(as+eas)) -
sin(deg2rad(rh))*cos(2*deg2rad(as+eas)) cos(deg2rad(rh))];
rq=90+erqr; %retardance of the quarter-wave plate for 633 nm.
Msq=[1 0 0 0;0
(cos(2*deg2rad(as+eas)))^2+cos(deg2rad(rq))*(sin(2*deg2rad(as+eas)))^2
(1-cos(deg2rad(rq)))*sin(2*deg2rad(as+eas))*cos(2*deg2rad(as+eas)) -
sin(deg2rad(rq))*sin(2*deg2rad(as+eas));0 (1-
cos(deg2rad(rq)))*sin(2*deg2rad(as+eas))*cos(2*deg2rad(as+eas))
(sin(2*deg2rad(as+eas)))^2+cos(deg2rad(rq))*(cos(2*deg2rad(as+eas)))^2
sin(deg2rad(rq))*cos(2*deg2rad(as+eas));0
sin(deg2rad(rq))*sin(2*deg2rad(as+eas)) -
sin(deg2rad(rq))*cos(2*deg2rad(as+eas)) cos(deg2rad(rq))];
%StTheo is a function which allow us to obtain the theoretical intensity
%vector. The inputs are the principal axis position of the polarizing
elements, the configuration of retardance for the wavelength used, the
error parameter values calculated previously and the Mueller matrix of
the sample.
IPR{k}=StTheo(ar1,ar2,ap,ai,r1IR,r1IIR,r1IIIR,r1IVR,r1VR,r1VIR,r2IR,r2IIR
,r2IIIR,r2IVR,r2VR,r2VIR,ear1,ear2,eai,er1I,er1II,er1III,er1IV,er1V,er1VI
,er2I,er2II,er2III,er2IV,er2V,er2VI,Msp);
IHR{k}=StTheo(ar1,ar2,ap,ai,r1IR,r1IIR,r1IIIR,r1IVR,r1VR,r1VIR,r2IR,r2IIR
,r2IIIR,r2IVR,r2VR,r2VIR,ear1,ear2,eai,er1I,er1II,er1III,er1IV,er1V,er1VI
,er2I,er2II,er2III,er2IV,er2V,er2VI,Msh);
IQR{k}=StTheo(ar1,ar2,ap,ai,r1IR,r1IIR,r1IIIR,r1IVR,r1VR,r1VIR,r2IR,r2IIR
,r2IIIR,r2IVR,r2VR,r2VIR,ear1,ear2,eai,er1I,er1II,er1III,er1IV,er1V,er1VI
,er2I,er2II,er2III,er2IV,er2V,er2VI,Msq);
end

%PMC function is employed to calculate the characteristic matrix and its
pseudo-inverse
```

```
PMCR=PMC(r1IR,r1IIR,r1IIIR,r1IVR,r1VR,r1VIR,r2IR,r2IIR,r2IIIR,r2IVR,r2VR,
r2VIR,er1I,er1II,er1III,er1IV,er1V,er1VI,er2I,er2II,er2III,er2IV,er2V,er2
VI);

%StPar function is used to obtain the normalized Stokes parameters of the
%theorteical case. This function requires as input data the pseudo-
inverse
%of the characteristic matrix and the intensity vector which were
%calculated previously.
SPR=StPar(PMCR,IPR{1,1},IPR{1,2},IPR{1,3},IPR{1,4},IPR{1,5},IPR{1,6},IPR{
1,7},IPR{1,8},IPR{1,9},IPR{1,10},IPR{1,11},IPR{1,12},IPR{1,13},IPR{1,14},
IPR{1,15},IPR{1,16},IPR{1,17},IPR{1,18},IPR{1,19});
SHR=StPar(PMCR,IHR{1,1},IHR{1,2},IHR{1,3},IHR{1,4},IHR{1,5},IHR{1,6},IHR{
1,7},IHR{1,8},IHR{1,9},IHR{1,10},IHR{1,11},IHR{1,12},IHR{1,13},IHR{1,14},
IHR{1,15},IHR{1,16},IHR{1,17},IHR{1,18},IHR{1,19});
SQR=StPar(PMCR,IQR{1,1},IQR{1,2},IQR{1,3},IQR{1,4},IQR{1,5},IQR{1,6},IQR{
1,7},IQR{1,8},IQR{1,9},IQR{1,10},IQR{1,11},IQR{1,12},IQR{1,13},IQR{1,14},
IQR{1,15},IQR{1,16},IQR{1,17},IQR{1,18},IQR{1,19});

for k=1:19
as=10*(k-1);
Msp=0.5*[1 cos(2*deg2rad(as+eas)) sin(2*deg2rad(as+eas))
0;cos(2*deg2rad(as+eas)) (cos(2*deg2rad(as+eas)))^2
sin(2*deg2rad(as+eas))*cos(2*deg2rad(as+eas)) 0;sin(2*deg2rad(as+eas))
sin(2*deg2rad(as+eas))*cos(2*deg2rad(as+eas)) (sin(2*deg2rad(as+eas)))^2
0;0 0 0 0];
rh=154.158+erhg;
Msh=[1 0 0 0;0
(cos(2*deg2rad(as+eas)))^2+cos(deg2rad(rh))*(sin(2*deg2rad(as+eas)))^2
(1-cos(deg2rad(rh)))*sin(2*deg2rad(as+eas))*cos(2*deg2rad(as+eas)) -
sin(deg2rad(rh))*sin(2*deg2rad(as+eas));0 (1-
cos(deg2rad(rh)))*sin(2*deg2rad(as+eas))*cos(2*deg2rad(as+eas))
(sin(2*deg2rad(as+eas)))^2+cos(deg2rad(rh))*(cos(2*deg2rad(as+eas)))^2
sin(deg2rad(rh))*cos(2*deg2rad(as+eas));0
sin(deg2rad(rh))*sin(2*deg2rad(as+eas)) -
sin(deg2rad(rh))*cos(2*deg2rad(as+eas)) cos(deg2rad(rh))];
rq=107.46+erqg;
Msq=[1 0 0 0;0
(cos(2*deg2rad(as+eas)))^2+cos(deg2rad(rq))*(sin(2*deg2rad(as+eas)))^2
(1-cos(deg2rad(rq)))*sin(2*deg2rad(as+eas))*cos(2*deg2rad(as+eas)) -
sin(deg2rad(rq))*sin(2*deg2rad(as+eas));0 (1-
cos(deg2rad(rq)))*sin(2*deg2rad(as+eas))*cos(2*deg2rad(as+eas))
(sin(2*deg2rad(as+eas)))^2+cos(deg2rad(rq))*(cos(2*deg2rad(as+eas)))^2
sin(deg2rad(rq))*cos(2*deg2rad(as+eas));0
sin(deg2rad(rq))*sin(2*deg2rad(as+eas)) -
sin(deg2rad(rq))*cos(2*deg2rad(as+eas)) cos(deg2rad(rq))];
IPG{k}=StTheo(ar1,ar2,ap,ai,r1IG,r1IIG,r1IIIG,r1IVG,r1VG,r1VIG,r2IG,r2IIG
,r2IIIG,r2IVG,r2VG,r2VIG,ear1,ear2,eai,er1I,er1II,er1III,er1IV,er1V,er1VI
,er2I,er2II,er2III,er2IV,er2V,er2VI,Msp);
IHG{k}=StTheo(ar1,ar2,ap,ai,r1IG,r1IIG,r1IIIG,r1IVG,r1VG,r1VIG,r2IG,r2IIG
,r2IIIG,r2IVG,r2VG,r2VIG,ear1,ear2,eai,er1I,er1II,er1III,er1IV,er1V,er1VI
,er2I,er2II,er2III,er2IV,er2V,er2VI,Msh);
IQG{k}=StTheo(ar1,ar2,ap,ai,r1IG,r1IIG,r1IIIG,r1IVG,r1VG,r1VIG,r2IG,r2IIG
,r2IIIG,r2IVG,r2VG,r2VIG,ear1,ear2,eai,er1I,er1II,er1III,er1IV,er1V,er1VI
,er2I,er2II,er2III,er2IV,er2V,er2VI,Msq);
end
```

```
PMCG=PMC(r1IG,r1IIG,r1IIIG,r1IVG,r1VG,r1VIG,r2IG,r2IIG,r2IIIG,r2IVG,r2VG,
r2VIG,er1I,er1II,er1III,er1IV,er1V,er1VI,er2I,er2II,er2III,er2IV,er2V,er2
VI);

SPG=StPar(PMCG,IPG{1,1},IPG{1,2},IPG{1,3},IPG{1,4},IPG{1,5},IPG{1,6},IPG{
1,7},IPG{1,8},IPG{1,9},IPG{1,10},IPG{1,11},IPG{1,12},IPG{1,13},IPG{1,14},
IPG{1,15},IPG{1,16},IPG{1,17},IPG{1,18},IPG{1,19});
SHG=StPar(PMCG,IHG{1,1},IHG{1,2},IHG{1,3},IHG{1,4},IHG{1,5},IHG{1,6},IHG{
1,7},IHG{1,8},IHG{1,9},IHG{1,10},IHG{1,11},IHG{1,12},IHG{1,13},IHG{1,14},
IHG{1,15},IHG{1,16},IHG{1,17},IHG{1,18},IHG{1,19});
SQG=StPar(PMCG,IQG{1,1},IQG{1,2},IQG{1,3},IQG{1,4},IQG{1,5},IQG{1,6},IQG{
1,7},IQG{1,8},IQG{1,9},IQG{1,10},IQG{1,11},IQG{1,12},IQG{1,13},IQG{1,14},
IQG{1,15},IQG{1,16},IQG{1,17},IQG{1,18},IQG{1,19});

for k=1:19
as=10*(k-1);
Msp=0.5*[1 cos(2*deg2rad(as+eas)) sin(2*deg2rad(as+eas))
0;cos(2*deg2rad(as+eas)) (cos(2*deg2rad(as+eas)))^2
sin(2*deg2rad(as+eas))*cos(2*deg2rad(as+eas)) 0;sin(2*deg2rad(as+eas))
sin(2*deg2rad(as+eas))*cos(2*deg2rad(as+eas)) (sin(2*deg2rad(as+eas)))^2
0;0 0 0 0];
rh=101.537+erhb;
Msh=[1 0 0 0;0
(cos(2*deg2rad(as+eas)))^2+cos(deg2rad(rh))*(sin(2*deg2rad(as+eas)))^2
(1-cos(deg2rad(rh)))*sin(2*deg2rad(as+eas))*cos(2*deg2rad(as+eas)) -
sin(deg2rad(rh))*sin(2*deg2rad(as+eas));0 (1-
cos(deg2rad(rh)))*sin(2*deg2rad(as+eas))*cos(2*deg2rad(as+eas))
(sin(2*deg2rad(as+eas)))^2+cos(deg2rad(rh))*(cos(2*deg2rad(as+eas)))^2
sin(deg2rad(rh))*cos(2*deg2rad(as+eas));0
sin(deg2rad(rh))*sin(2*deg2rad(as+eas)) -
sin(deg2rad(rh))*cos(2*deg2rad(as+eas)) cos(deg2rad(rh))];
rq=126.87+erqb;
Msq=[1 0 0 0;0
(cos(2*deg2rad(as+eas)))^2+cos(deg2rad(rq))*(sin(2*deg2rad(as+eas)))^2
(1-cos(deg2rad(rq)))*sin(2*deg2rad(as+eas))*cos(2*deg2rad(as+eas)) -
sin(deg2rad(rq))*sin(2*deg2rad(as+eas));0 (1-
cos(deg2rad(rq)))*sin(2*deg2rad(as+eas))*cos(2*deg2rad(as+eas))
(sin(2*deg2rad(as+eas)))^2+cos(deg2rad(rq))*(cos(2*deg2rad(as+eas)))^2
sin(deg2rad(rq))*cos(2*deg2rad(as+eas));0
sin(deg2rad(rq))*sin(2*deg2rad(as+eas)) -
sin(deg2rad(rq))*cos(2*deg2rad(as+eas)) cos(deg2rad(rq))];
IPB{k}=StTheo(ar1,ar2,ap,ai,r1IB,r1IIB,r1IIIB,r1IVB,r1VB,r1VIB,r2IB,r2IIB
,r2IIIB,r2IVB,r2VB,r2VIB,ear1,ear2,eai,er1I,er1II,er1III,er1IV,er1V,er1VI
,er2I,er2II,er2III,er2IV,er2V,er2VI,Msp);
IHB{k}=StTheo(ar1,ar2,ap,ai,r1IB,r1IIB,r1IIIB,r1IVB,r1VB,r1VIB,r2IB,r2IIB
,r2IIIB,r2IVB,r2VB,r2VIB,ear1,ear2,eai,er1I,er1II,er1III,er1IV,er1V,er1VI
,er2I,er2II,er2III,er2IV,er2V,er2VI,Msh);
IQB{k}=StTheo(ar1,ar2,ap,ai,r1IB,r1IIB,r1IIIB,r1IVB,r1VB,r1VIB,r2IB,r2IIB
,r2IIIB,r2IVB,r2VB,r2VIB,ear1,ear2,eai,er1I,er1II,er1III,er1IV,er1V,er1VI
,er2I,er2II,er2III,er2IV,er2V,er2VI,Msq);
end

PMCB=PMC(r1IB,r1IIB,r1IIIB,r1IVB,r1VB,r1VIB,r2IB,r2IIB,r2IIIB,r2IVB,r2VB,
r2VIB,er1I,er1II,er1III,er1IV,er1V,er1VI,er2I,er2II,er2III,er2IV,er2V,er2
VI);
```

```
SPB=StPar(PMCB,IPB{1,1},IPB{1,2},IPB{1,3},IPB{1,4},IPB{1,5},IPB{1,6},IPB{
1,7},IPB{1,8},IPB{1,9},IPB{1,10},IPB{1,11},IPB{1,12},IPB{1,13},IPB{1,14},
IPB{1,15},IPB{1,16},IPB{1,17},IPB{1,18},IPB{1,19});
SHB=StPar(PMCB,IHB{1,1},IHB{1,2},IHB{1,3},IHB{1,4},IHB{1,5},IHB{1,6},IHB{
1,7},IHB{1,8},IHB{1,9},IHB{1,10},IHB{1,11},IHB{1,12},IHB{1,13},IHB{1,14},
IHB{1,15},IHB{1,16},IHB{1,17},IHB{1,18},IHB{1,19});
SQB=StPar(PMCB,IQB{1,1},IQB{1,2},IQB{1,3},IQB{1,4},IQB{1,5},IQB{1,6},IQB{
1,7},IQB{1,8},IQB{1,9},IQB{1,10},IQB{1,11},IQB{1,12},IQB{1,13},IQB{1,14},
IQB{1,15},IQB{1,16},IQB{1,17},IQB{1,18},IQB{1,19});

%STVEC function is used to obtain the normalized Stokes parameters of the
%experimental case. This function requires as input data the pseudo-
inverse
%of the characteristic matrix and the intensity values of experimental
measurements.
SVRP=STVEC('LP','RED',PMCR);
SVGP=STVEC('LP','GREEN',PMCG);
SVBP=STVEC('LP','BLUE',PMCB);

SVRH=STVEC('HWP','RED',PMCR);
SVGH=STVEC('HWP','GREEN',PMCG);
SVBH=STVEC('HWP','BLUE',PMCB);

SVRQ=STVEC('QWP','RED',PMCR);
SVGQ=STVEC('QWP','GREEN',PMCG);
SVBQ=STVEC('QWP','BLUE',PMCB);

%RMS Error for the three wavelengths and six calibration samples
SPGT30=SPG(4,:);
SPGE30=SVGP(4,:);
SPGT130=SPG(14,:);
SPGE130=SVGP(14,:);
SHGT30=SHG(4,:);
SHGE30=SVGH(4,:);
SHGT130=SHG(14,:);
SHGE130=SVGH(14,:);
SQGT30=SQG(4,:);
SQGE30=SVGQ(4,:);
SQGT130=SQG(14,:);
SQGE130=SVGQ(14,:);

RMSG=sqrt((1/24)*((SPGT30(1)-SPGE30(1))^2+(SPGT30(2)-
SPGE30(2))^2+(SPGT30(3)-SPGE30(3))^2+(SPGT30(4)-SPGE30(4))^2+(SPGT130(1)-
SPGE130(1))^2+(SPGT130(2)-SPGE130(2))^2+(SPGT130(3)-
SPGE130(3))^2+(SPGT130(4)-SPGE130(4))^2+(SHGT30(1)-
SHGE30(1))^2+(SHGT30(2)-SHGE30(2))^2+(SHGT30(3)-SHGE30(3))^2+(SHGT30(4)-
SHGE30(4))^2+(SHGT130(1)-SHGE130(1))^2+(SHGT130(2)-
SHGE130(2))^2+(SHGT130(3)-SHGE130(3))^2+(SHGT130(4)-
SHGE130(4))^2+(SQGT30(1)-SQGE30(1))^2+(SQGT30(2)-SQGE30(2))^2+(SQGT30(3)-
SQGE30(3))^2+(SQGT30(4)-SQGE30(4))^2+(SQGT130(1)-
SQGE130(1))^2+(SQGT130(2)-SQGE130(2))^2+(SQGT130(3)-
SQGE130(3))^2+(SQGT130(4)-SQGE130(4))^2));

SPRT30=SPR(4,:);
SPRE30=SVRP(4,:);
```

```
SPRT130=SPR(14,:);
SPRE130=SVRP(14,:);
SHRT30=SHR(4,:);
SHRE30=SVRH(4,:);
SHRT130=SHR(14,:);
SHRE130=SVRH(14,:);
SQRT30=SQR(4,:);
SQRE30=SVRQ(4,:);
SQRT130=SQR(14,:);
SQRE130=SVRQ(14,:);

RMSR=sqrt((1/24)*((SPRT30(1)-SPRE30(1))^2+(SPRT30(2)-
SPRE30(2))^2+(SPRT30(3)-SPRE30(3))^2+(SPRT30(4)-SPRE30(4))^2+(SPRT130(1)-
SPRE130(1))^2+(SPRT130(2)-SPRE130(2))^2+(SPRT130(3)-
SPRE130(3))^2+(SPRT130(4)-SPRE130(4))^2+(SHRT30(1)-
SHRE30(1))^2+(SHRT30(2)-SHRE30(2))^2+(SHRT30(3)-SHRE30(3))^2+(SHRT30(4)-
SHRE30(4))^2+(SHRT130(1)-SHRE130(1))^2+(SHRT130(2)-
SHRE130(2))^2+(SHRT130(3)-SHRE130(3))^2+(SHRT130(4)-
SHRE130(4))^2+(SQRT30(1)-SQRE30(1))^2+(SQRT30(2)-SQRE30(2))^2+(SQRT30(3)-
SQRE30(3))^2+(SQRT30(4)-SQRE30(4))^2+(SQRT130(1)-
SQRE130(1))^2+(SQRT130(2)-SQRE130(2))^2+(SQRT130(3)-
SQRE130(3))^2+(SQRT130(4)-SQRE130(4))^2));

SPBT30=SPB(4,:);
SPBE30=SVBP(4,:);
SPBT130=SPB(14,:);
SPBE130=SVBP(14,:);
SHBT30=SHB(4,:);
SHBE30=SVBH(4,:);
SHBT130=SHB(14,:);
SHBE130=SVBH(14,:);
SQBT30=SQB(4,:);
SQBE30=SVBQ(4,:);
SQBT130=SQB(14,:);
SQBE130=SVBQ(14,:);

RMSB=sqrt((1/24)*((SPBT30(1)-SPBE30(1))^2+(SPBT30(2)-
SPBE30(2))^2+(SPBT30(3)-SPBE30(3))^2+(SPBT30(4)-SPBE30(4))^2+(SPBT130(1)-
SPBE130(1))^2+(SPBT130(2)-SPBE130(2))^2+(SPBT130(3)-
SPBE130(3))^2+(SPBT130(4)-SPBE130(4))^2+(SHBT30(1)-
SHBE30(1))^2+(SHBT30(2)-SHBE30(2))^2+(SHBT30(3)-SHBE30(3))^2+(SHBT30(4)-
SHBE30(4))^2+(SHBT130(1)-SHBE130(1))^2+(SHBT130(2)-
SHBE130(2))^2+(SHBT130(3)-SHBE130(3))^2+(SHBT130(4)-
SHBE130(4))^2+(SQBT30(1)-SQBE30(1))^2+(SQBT30(2)-SQBE30(2))^2+(SQBT30(3)-
SQBE30(3))^2+(SQBT30(4)-SQBE30(4))^2+(SQBT130(1)-
SQBE130(1))^2+(SQBT130(2)-SQBE130(2))^2+(SQBT130(3)-
SQBE130(3))^2+(SQBT130(4)-SQBE130(4))^2));
```

In this part, the functions required for the above program are described.

StTheo function

StTheo is a function which allow us to obtain the theoretical intensity vector. The inputs are the principal axis position of the polarizing elements, the configuration of retardance for the

wavelength used, the error parameter values calculated previously and the Mueller matrix of the sample.

```
function
[I]=StTheo(ar1,ar2,ap,ai,r1I,r1II,r1III,r1IV,r1V,r1VI,r2I,r2II,r2III,r2IV
,r2V,r2VI,ear1,ear2,eai,er1I,er1II,er1III,er1IV,er1V,er1VI,er2I,er2II,er2
III,er2IV,er2V,er2VI,Ms)
%incident polarization state
Si=[1;0;0;0];

%Mueller matrices for the first polarizer Mi an the Polarizer in the
Stokes
%polarimeter Mp
Mi=0.5*[1 cos(2*deg2rad(ai+eai)) sin(2*deg2rad(ai+eai))
0;cos(2*deg2rad(ai+eai)) (cos(2*deg2rad(ai+eai)))^2
sin(2*deg2rad(ai+eai))*cos(2*deg2rad(ai+eai)) 0;sin(2*deg2rad(ai+eai))
sin(2*deg2rad(ai+eai))*cos(2*deg2rad(ai+eai)) (sin(2*deg2rad(ai+eai)))^2
0;0 0 0 0];
Mp=0.5*[1 cos(2*deg2rad(ap)) sin(2*deg2rad(ap)) 0;cos(2*deg2rad(ap))
(cos(2*deg2rad(ap)))^2 sin(2*deg2rad(ap))*cos(2*deg2rad(ap))
0;sin(2*deg2rad(ap)) sin(2*deg2rad(ap))*cos(2*deg2rad(ap))
(sin(2*deg2rad(ap)))^2 0;0 0 0 0];

%caso I
Mr1I=LCVRS(r1I,ar1,er1I,ear1); %LCVR function generates the Mueller
matrix for the LCVR for a specific retardance value and position of the
fast axis. Also, error parameters are considered.
Mr2I=LCVRS(r2I,ar2,er2I,ear2);

SoI=Mp*Mr2I*Mr1I*Ms*Mi*Si;
II=SoI(1); %Only the first parameter of the output Stokes vector is
obtained.

%caso II
Mr1II=LCVRS(r1II,ar1,er1II,ear1);
Mr2II=LCVRS(r2II,ar2,er2II,ear2);

SoII=Mp*Mr2II*Mr1II*Ms*Mi*Si;
III=SoII(1);

%caso III
Mr1III=LCVRS(r1III,ar1,er1III,ear1);
Mr2III=LCVRS(r2III,ar2,er2III,ear2);

SoIII=Mp*Mr2III*Mr1III*Ms*Mi*Si;
IIII=SoIII(1);

%caso IV
Mr1IV=LCVRS(r1IV,ar1,er1IV,ear1);
Mr2IV=LCVRS(r2IV,ar2,er2IV,ear2);

SoIV=Mp*Mr2IV*Mr1IV*Ms*Mi*Si;
IIV=SoIV(1);
```

```
%caso V
Mr1V=LCVRS(r1V,ar1,er1V,ear1);
Mr2V=LCVRS(r2V,ar2,er2V,ear2);

SoV=Mp*Mr2V*Mr1V*Ms*Mi*Si;
IV=SoV(1);

%caso VI
Mr1VI=LCVRS(r1VI,ar1,er1VI,ear1);
Mr2VI=LCVRS(r2VI,ar2,er2VI,ear2);

SoVI=Mp*Mr2VI*Mr1VI*Ms*Mi*Si;
IVI=SoVI(1);

%intensities
I=[II;III;IIII;IIV;IV;IVI];
end
```

LCVR function

LCVR function generates the Mueller matrix for the LCVR for a specific retardance value and position of the fast axis. Also, error parameters are considered.

```
function [Mr]=LCVRS(r,ar,er,ear)
Mr=[1 0 0 0;0
(cos(2*deg2rad(ar+ear)))^2+cos(deg2rad(r+er))*(sin(2*deg2rad(ar+ear)))^2
(1-cos(deg2rad(r+er)))*sin(2*deg2rad(ar+ear))*cos(2*deg2rad(ar+ear)) -
sin(deg2rad(r+er))*sin(2*deg2rad(ar+ear));0 (1-
cos(deg2rad(r+er)))*sin(2*deg2rad(ar+ear))*cos(2*deg2rad(ar+ear))
(sin(2*deg2rad(ar+ear)))^2+cos(deg2rad(r+er))*(cos(2*deg2rad(ar+ear)))^2
sin(deg2rad(r+er))*cos(2*deg2rad(ar+ear));0
sin(deg2rad(r+er))*sin(2*deg2rad(ar+ear)) -
sin(deg2rad(r+er))*cos(2*deg2rad(ar+ear)) cos(deg2rad(r+er))];
end
```

PMC function

PMC function is employed to calculate the characteristic matrix and its pseudo-inverse for the Stokes polarimeter. The inputs are the retardance configuration and the errors associated with this value.

```
%Functión to calculate the characteristic matrix and its pseudo-inverse

function
[PMC]=PMC(r1I,r1II,r1III,r1IV,r1V,r1VI,r2I,r2II,r2III,r2IV,r2V,r2VI,er1I,
er1II,er1III,er1IV,er1V,er1VI,er2I,er2II,er2III,er2IV,er2V,er2VI)
MC=0.5*[1 cos(deg2rad(r2I+er2I))
sin(deg2rad(r1I+er1I))*sin(deg2rad(r2I+er2I)) -
cos(deg2rad(r1I+er1I))*sin(deg2rad(r2I+er2I));1 cos(deg2rad(r2II+er2II))
sin(deg2rad(r1II+er1II))*sin(deg2rad(r2II+er2II)) -
cos(deg2rad(r1II+er1II))*sin(deg2rad(r2II+er2II));1
cos(deg2rad(r2III+er2III))
```

```
sin(deg2rad(r1III+er1III))*sin(deg2rad(r2III+er2III)) -
cos(deg2rad(r1III+er1III))*sin(deg2rad(r2III+er2III));1
cos(deg2rad(r2IV+er2IV))
sin(deg2rad(r1IV+er1IV))*sin(deg2rad(r2IV+er2IV)) -
cos(deg2rad(r1IV+er1IV))*sin(deg2rad(r2IV+er2IV));1
cos(deg2rad(r2V+er2V)) sin(deg2rad(r1V+er1V))*sin(deg2rad(r2V+er2V)) -
cos(deg2rad(r1V+er1V))*sin(deg2rad(r2V+er2V));1 cos(deg2rad(r2VI+er2VI))
sin(deg2rad(r1VI+er1VI))*sin(deg2rad(r2VI+er2VI)) -
cos(deg2rad(r1VI+er1VI))*sin(deg2rad(r2VI+er2VI))];

PMC=((MC.')*MC)\(MC.');
end
```

StPar function

StPar function is used to obtain the normalized Stokes parameters of the theoretical data. This function requires as input data the pseudo-inverse of the characteristic matrix and the intensity vector which were calculated previously.

```
function
[SPN]=StPar(PMC,IP1,IP2,IP3,IP4,IP5,IP6,IP7,IP8,IP9,IP10,IP11,IP12,IP13,I
P14,IP15,IP16,IP17,IP18,IP19)
S0P=PMC*IP1;
S0PN=[S0P(1)/S0P(1) S0P(2)/S0P(1) S0P(3)/S0P(1) S0P(4)/S0P(1)];

S10P=PMC*IP2;
S10PN=[S10P(1)/S10P(1) S10P(2)/S10P(1) S10P(3)/S10P(1) S10P(4)/S10P(1)];

S20P=PMC*IP3;
S20PN=[S20P(1)/S20P(1) S20P(2)/S20P(1) S20P(3)/S20P(1) S20P(4)/S20P(1)];

S30P=PMC*IP4;
S30PN=[S30P(1)/S30P(1) S30P(2)/S30P(1) S30P(3)/S30P(1) S30P(4)/S30P(1)];

S40P=PMC*IP5;
S40PN=[S40P(1)/S40P(1) S40P(2)/S40P(1) S40P(3)/S40P(1) S40P(4)/S40P(1)];

S50P=PMC*IP6;
S50PN=[S50P(1)/S50P(1) S50P(2)/S50P(1) S50P(3)/S50P(1) S50P(4)/S50P(1)];

S60P=PMC*IP7;
S60PN=[S60P(1)/S60P(1) S60P(2)/S60P(1) S60P(3)/S60P(1) S60P(4)/S60P(1)];

S70P=PMC*IP8;
S70PN=[S70P(1)/S70P(1) S70P(2)/S70P(1) S70P(3)/S70P(1) S70P(4)/S70P(1)];

S80P=PMC*IP9;
S80PN=[S80P(1)/S80P(1) S80P(2)/S80P(1) S80P(3)/S80P(1) S80P(4)/S80P(1)];

S90P=PMC*IP10;
S90PN=[S90P(1)/S90P(1) S90P(2)/S90P(1) S90P(3)/S90P(1) S90P(4)/S90P(1)];
```

```
S100P=PMC*IP11;
S100PN=[S100P(1)/S100P(1) S100P(2)/S100P(1) S100P(3)/S100P(1)
S100P(4)/S100P(1)];

S110P=PMC*IP12;
S110PN=[S110P(1)/S110P(1) S110P(2)/S110P(1) S110P(3)/S110P(1)
S110P(4)/S110P(1)];

S120P=PMC*IP13;
S120PN=[S120P(1)/S120P(1) S120P(2)/S120P(1) S120P(3)/S120P(1)
S120P(4)/S120P(1)];

S130P=PMC*IP14;
S130PN=[S130P(1)/S130P(1) S130P(2)/S130P(1) S130P(3)/S130P(1)
S130P(4)/S130P(1)];

S140P=PMC*IP15;
S140PN=[S140P(1)/S140P(1) S140P(2)/S140P(1) S140P(3)/S140P(1)
S140P(4)/S140P(1)];

S150P=PMC*IP16;
S150PN=[S150P(1)/S150P(1) S150P(2)/S150P(1) S150P(3)/S150P(1)
S150P(4)/S150P(1)];

S160P=PMC*IP17;
S160PN=[S160P(1)/S160P(1) S160P(2)/S160P(1) S160P(3)/S160P(1)
S160P(4)/S160P(1)];

S170P=PMC*IP18;
S170PN=[S170P(1)/S170P(1) S170P(2)/S170P(1) S170P(3)/S170P(1)
S170P(4)/S170P(1)];

S180P=PMC*IP19;
S180PN=[S180P(1)/S180P(1) S180P(2)/S180P(1) S180P(3)/S180P(1)
S180P(4)/S180P(1)];

SPN=[S0PN;S10PN;S20PN;S30PN;S40PN;S50PN;S60PN;S70PN;S80PN;S90PN;S100PN;S1
10PN;S120PN;S130PN;S140PN;S150PN;S160PN;S170PN;S180PN];
end
```

STEVEC function

This function is used to obtain the normalized Stokes parameters of the experimental case. This function requires as input data the pseudo-inverse of the characteristic matrix and the intensity values of experimental measurements.

```
function [StVe]=STVEC(sa,w,MPse)
for k=1:19
%Lect function allows us to storage the intensity vector obtained
experimentally.
I=Lect(sa,w,10*(k-1));
S=MPse*I';
SN{k}=[S(1)/S(1) S(2)/S(1) S(3)/S(1) S(4)/S(1)];
```

```
end

S0=SN{1,1};
S10=SN{1,2};
S20=SN{1,3};
S30=SN{1,4};
S40=SN{1,5};
S50=SN{1,6};
S60=SN{1,7};
S70=SN{1,8};
S80=SN{1,9};
S90=SN{1,10};
S100=SN{1,11};
S110=SN{1,12};
S120=SN{1,13};
S130=SN{1,14};
S140=SN{1,15};
S150=SN{1,16};
S160=SN{1,17};
S170=SN{1,18};
S180=SN{1,19};

StVe=[S0;S10;S20;S30;S40;S50;S60;S70;S80;S90;S100;S110;S120;S130;S140;S15
0;S160;S170;S180];
end
```

Lect function

Lect function allows us to store the intensity vector obtained experimentally.

```
function [I]=Lect(samp,wale,angle)
filename=sprintf('%s_%s_%d.txt',samp,wale,angle);
D=importdata(filename);
I=[mean(D(1,:)) mean(D(2,:)) mean(D(3,:)) mean(D(4,:)) mean(D(5,:))
mean(D(6,:))];
end
```

RET function

```
% Function to calculate the retardance values from the characterization
curves

function [ret]=RET(CC,l,v)
for i=1:l
   va=CC(i,1);
   if (v>=va)
       ret=((CC(i+1,2)-CC(i,2))/(CC(i+1,1)-CC(i,1)))*(v-CC(i,1))+CC(i,2);
   end
end
end
```

Appendix D2: MatLab program developed to calibrate the Stokes polarimeter. The error parameters are calculated by applying Powell´s method.

```
toclear all
close all
clc

step=0.5; %step fixed value

%Initializing error parameter values
eai=0;
ear1=0;
ear2=0;
eas=0;
er1I=0;
er1II=0;
er1III=0;
er1IV=0;
er1V=0;
er1VI=0;
er2I=0;
er2II=0;
er2III=0;
er2IV=0;
er2V=0;
er2VI=0;
erhb=0;
erhg=0;
erhr=0;
erqb=0;
erqg=0;
erqr=0;

%RMS error value for a specific wavelength. This is calculated for the
%initializing error parameter values defined above

%RMSError function is showed in appendix D1
RMSG=RMSError(eas,ear1,ear2,eai,er1I,er1II,er1III,er1IV,er1V,er1VI,er2I,e
r2II,er2III,er2IV,er2V,er2VI,erhr,erhg,erhb,erqr,erqg,erqb);

%Powell´s method is applied for the RMS  function that allows us to move
%along the first direction to its minimum (first error parameter), then
from here along the second direction to its minimum, and so on, cycling
through the whole set of directions as many times as necessary, until the
function stops decreasing or take a smaller than a fixed value.

while RMSG>0.026 %fixed limit of RMS error value
%Each function into the cycle allows us to vary the error parameters
%defined above by a step fixed. The RMSError value varies by variation of
the error parameter values.
Deas=RMSeas(step,eas,ear1,ear2,eai,er1I,er1II,er1III,er1IV,er1V,er1VI,er2
I,er2II,er2III,er2IV,er2V,er2VI,erhr,erhg,erhb,erqr,erqg,erqb,RMSG);
eas=Deas(1);
RMSG=Deas(2);
```

```
Dear1=RMSear1(step,eas,ear1,ear2,eai,er1I,er1II,er1III,er1IV,er1V,er1VI,e
r2I,er2II,er2III,er2IV,er2V,er2VI,erhr,erhg,erhb,erqr,erqg,erqb,RMSG);
ear1=Dear1(1);
RMSG=Dear1(2);
Dear2=RMSear2(step,eas,ear1,ear2,eai,er1I,er1II,er1III,er1IV,er1V,er1VI,e
r2I,er2II,er2III,er2IV,er2V,er2VI,erhr,erhg,erhb,erqr,erqg,erqb,RMSG);
ear2=Dear2(1);
RMSG=Dear2(2);
Deai=RMSeai(step,eas,ear1,ear2,eai,er1I,er1II,er1III,er1IV,er1V,er1VI,er2
I,er2II,er2III,er2IV,er2V,er2VI,erhr,erhg,erhb,erqr,erqg,erqb,RMSG);
eai=Deai(1);
RMSG=Deai(2);
Der1I=RMSer1I(step,eas,ear1,ear2,eai,er1I,er1II,er1III,er1IV,er1V,er1VI,e
r2I,er2II,er2III,er2IV,er2V,er2VI,erhr,erhg,erhb,erqr,erqg,erqb,RMSG);
er1I=Der1I(1);
RMSG=Der1I(2);
Der1II=RMSer1II(step,eas,ear1,ear2,eai,er1I,er1II,er1III,er1IV,er1V,er1VI
,er2I,er2II,er2III,er2IV,er2V,er2VI,erhr,erhg,erhb,erqr,erqg,erqb,RMSG);
er1II=Der1II(1);
RMSG=Der1II(2);
Der1III=RMSer1III(step,eas,ear1,ear2,eai,er1I,er1II,er1III,er1IV,er1V,er1
VI,er2I,er2II,er2III,er2IV,er2V,er2VI,erhr,erhg,erhb,erqr,erqg,erqb,RMSG)
;
er1III=Der1III(1);
RMSG=Der1III(2);
Der1IV=RMSer1IV(step,eas,ear1,ear2,eai,er1I,er1II,er1III,er1IV,er1V,er1VI
,er2I,er2II,er2III,er2IV,er2V,er2VI,erhr,erhg,erhb,erqr,erqg,erqb,RMSG);
er1IV=Der1IV(1);
RMSG=Der1IV(2);
Der1V=RMSer1V(step,eas,ear1,ear2,eai,er1I,er1II,er1III,er1IV,er1V,er1VI,e
r2I,er2II,er2III,er2IV,er2V,er2VI,erhr,erhg,erhb,erqr,erqg,erqb,RMSG);
er1V=Der1V(1);
RMSG=Der1V(2);
Der1VI=RMSer1VI(step,eas,ear1,ear2,eai,er1I,er1II,er1III,er1IV,er1V,er1VI
,er2I,er2II,er2III,er2IV,er2V,er2VI,erhr,erhg,erhb,erqr,erqg,erqb,RMSG);
er1VI=Der1VI(1);
RMSG=Der1VI(2);
Der2I=RMSer2I(step,eas,ear1,ear2,eai,er1I,er1II,er1III,er1IV,er1V,er1VI,e
r2I,er2II,er2III,er2IV,er2V,er2VI,erhr,erhg,erhb,erqr,erqg,erqb,RMSG);
er2I=Der2I(1);
RMSG=Der2I(2);
Der2II=RMSer2II(step,eas,ear1,ear2,eai,er1I,er1II,er1III,er1IV,er1V,er1VI
,er2I,er2II,er2III,er2IV,er2V,er2VI,erhr,erhg,erhb,erqr,erqg,erqb,RMSG);
er2II=Der2II(1);
RMSG=Der2II(2);
Der2III=RMSer2III(step,eas,ear1,ear2,eai,er1I,er1II,er1III,er1IV,er1V,er1
VI,er2I,er2II,er2III,er2IV,er2V,er2VI,erhr,erhg,erhb,erqr,erqg,erqb,RMSG)
;
er2III=Der2III(1);
RMSG=Der2III(2);
Der2IV=RMSer2IV(step,eas,ear1,ear2,eai,er1I,er1II,er1III,er1IV,er1V,er1VI
,er2I,er2II,er2III,er2IV,er2V,er2VI,erhr,erhg,erhb,erqr,erqg,erqb,RMSG);
er2IV=Der2IV(1);
RMSG=Der2IV(2);
Der2V=RMSer2V(step,eas,ear1,ear2,eai,er1I,er1II,er1III,er1IV,er1V,er1VI,e
r2I,er2II,er2III,er2IV,er2V,er2VI,erhr,erhg,erhb,erqr,erqg,erqb,RMSG);
er2V=Der2V(1);
```

```
RMSG=Der2V(2);
Der2VI=RMSer2VI(step,eas,ear1,ear2,eai,er1I,er1II,er1III,er1IV,er1V,er1VI
,er2I,er2II,er2III,er2IV,er2V,er2VI,erhr,erhg,erhb,erqr,erqg,erqb,RMSG);
er2VI=Der2VI(1);
RMSG=Der2VI(2);
Derhr=RMSerhr(step,eas,ear1,ear2,eai,er1I,er1II,er1III,er1IV,er1V,er1VI,e
r2I,er2II,er2III,er2IV,er2V,er2VI,erhr,erhg,erhb,erqr,erqg,erqb,RMSG);
erhr=Derhr(1);
RMSG=Derhr(2);
Derhg=RMSerhg(step,eas,ear1,ear2,eai,er1I,er1II,er1III,er1IV,er1V,er1VI,e
r2I,er2II,er2III,er2IV,er2V,er2VI,erhr,erhg,erhb,erqr,erqg,erqb,RMSG);
erhg=Derhg(1);
RMSG=Derhg(2);
Derhb=RMSerhb(step,eas,ear1,ear2,eai,er1I,er1II,er1III,er1IV,er1V,er1VI,e
r2I,er2II,er2III,er2IV,er2V,er2VI,erhr,erhg,erhb,erqr,erqg,erqb,RMSG);
erhb=Derhb(1);
RMSG=Derhb(2);
Derqr=RMSerqr(step,eas,ear1,ear2,eai,er1I,er1II,er1III,er1IV,er1V,er1VI,e
r2I,er2II,er2III,er2IV,er2V,er2VI,erhr,erhg,erhb,erqr,erqg,erqb,RMSG);
erqr=Derqr(1);
RMSG=Derqr(2);
Derqg=RMSerqg(step,eas,ear1,ear2,eai,er1I,er1II,er1III,er1IV,er1V,er1VI,e
r2I,er2II,er2III,er2IV,er2V,er2VI,erhr,erhg,erhb,erqr,erqg,erqb,RMSG);
erqg=Derqg(1);
RMSG=Derqg(2);
Derqb=RMSerqb(step,eas,ear1,ear2,eai,er1I,er1II,er1III,er1IV,er1V,er1VI,e
r2I,er2II,er2III,er2IV,er2V,er2VI,erhr,erhg,erhb,erqr,erqg,erqb,RMSG);
erqb=Derqb(1);
RMSG=Derqb(2);
end
```

Appendix D3: In this appendix we present the MatLab program which was used to find the optimum retardance values for the optimized case described in Chapter 5.

```
OptimizeCondNum3LambdaSearch.m

clear
clc

% program to read in the data of volts vs retardance for two LCVRs in a
% Stokes polarimeter, for 3 wavelengths. This data is then used to
optimize
% the polarimeter simultaneously for the 3 wavelengths.
% This program fixes the polarizer of the polarimeter at 0 degs, and
varies
% the axis angles of the 2 LCVRs between 0 and 90 degs with step
axis_step
% degs, with axis2 = axis1 + 45 degs, and the voltage of the 2 LCVRs
% between the minimum and the maximum given by the data read in.
% Note that there are num_meas intensity measurements for each
polarization
% measurement, and each intensity measurement must be included in the
% optimization.
% The first row of the Mueller matrix of each intensity measurement
```

```
% configuration gives the characteristic matrix of the polarimeter, and
the
% optimized polarimeter is given by the lowest condition number of the
% characteristic matrix. The lowest average condition number gives the
% optimized system for the 3 simultaneous wavelengths.

%%%%%%%%%%%%%%%%%%%%%%%%%%%%%%%%%%
% set parameters for the program %
%%%%%%%%%%%%%%%%%%%%%%%%%%%%%%%%%%

% number of intensity measurements
global num_meas;
num_meas = 4;

% fixed polarizer angle in the polarimeter
polangle = 0.0;

global mpol;
% Mueller matrix for the polarizer at this angle
mpol = mueller_polarizer(polangle);

%%%%%%%%%%%%%%%%%%%%%%%%%%%%%%%%%%%%
% read in volts vs retardance data %
%%%%%%%%%%%%%%%%%%%%%%%%%%%%%%%%%%%%

global lcvr1450;
global lcvr2450;
global lcvr1543;
global lcvr2543;
global lcvr1633;
global lcvr2633;

lcvr1450 = Lect('450_LCVR1');
lcvr2450 = Lect('450_LCVR2');

lcvr1543 = Lect('543_LCVR1');
lcvr2543 = Lect('543_LCVR2');

lcvr1633 = Lect('633_LCVR1');
lcvr2633 = Lect('633_LCVR2');

% vectors of sizes of data
szx = zeros(1,6);
szy = zeros(1,6);

[szx(1),szy(1)] = size(lcvr1450);
[szx(2),szy(2)] = size(lcvr2450);

[szx(3),szy(3)] = size(lcvr1543);
[szx(4),szy(4)] = size(lcvr2543);

[szx(5),szy(5)] = size(lcvr1633);
[szx(6),szy(6)] = size(lcvr2633);

% get the smallest size to search for the minimum condition number in
this
% range.
```

```
sx = min(szx);

%%%%%%%%%%%%%%%%%%%%%%%%%%%%%
% optimize condition number %
%%%%%%%%%%%%%%%%%%%%%%%%%%%%%

% number of parameters for optimization
N = 13;

% p is the matrix with the N polarimeter parameters
% (here first = nearest sample, second = further from sample)
%      p(1) = voltage of LCVR 1 for measurement 1
%      p(2) = voltage of LCVR 2 for measurement 1
%      p(3) = voltage of LCVR 1 for measurement 2
%      p(4) = voltage of LCVR 2 for measurement 2
%      p(5) = voltage of LCVR 1 for measurement 3
%      p(6) = voltage of LCVR 2 for measurement 3
%      p(7) = voltage of LCVR 1 for measurement 4
%      p(8) = voltage of LCVR 2 for measurement 4
%      p(9) = voltage of LCVR 1 for measurement 5
%      p(10) = voltage of LCVR 2 for measurement 5
%      p(11) = voltage of LCVR 1 for measurement 6
%      p(12) = voltage of LCVR 2 for measurement 6
%      p(13) = axis angle of LCVR1

p =
[3.28,5.797,3.28,2.585,3.28,3.31,2.15,3.31,2.55,3.31,5.697,3.31,50.0];
% p = [3.28,5.797,3.28,2.585,3.28,3.31,2.15,3.31,30.0];

% define optp as global to be able to read it in the sample optiimization
% this will be the optimized polarimeter configuration
global optp;

% parameter used to find the values of the signals after optimization
global done;
done = 0;

% call the optimization algorithm
options = optimset('MaxFunEvals',10000,'MaxIter',10000,'TolFun',1e-
6,'TolX',1e-6);
[optp,funval] = fminsearch(@StokesCondNum, p, options);

p = optp;
p(13) = 20.0;
[optp,funval] = fminsearch(@StokesCondNum, p, options);

% store the optimized values of the intensities to file
done = 1;
StokesCondNum(optp);
done = 0;

optp*180.0/pi
funval


StokesCondNum()
function cn = StokesCondNum(p)
```

```
% StokesCondNum calculates the average condition number of a Stokes
% polarimeter characterization matrix for 3 wavelengths.
% There are 13 parameters: 2 voltages for the 2 LCVRs in the system
% for each of the 6 measuerements, and the
% axis angle for the first LCVR. It is assumed that the second retarder
% axis angle is at 45 degs from the first retarder and that the polarizer
% in the polarimeter is at 0 degs.
% Returns the condition number of the polarimeter configuration

global num_meas;
% maximum index in parameter vector
max_ind = 2*num_meas+1;

global mpol;

global lcvr1450;
global lcvr2450;
global lcvr1543;
global lcvr2543;
global lcvr1633;
global lcvr2633;

global done;

cm450 = zeros(num_meas,4);
cm543 = zeros(num_meas,4);
cm633 = zeros(num_meas,4);

% generate the characteristic matrices for the 3 wavelengths
for i = 1:num_meas

    temp = interp1(lcvr1450(:,1),lcvr1450(:,2),p(2*1-1));

    % wavelength 450nm
    % calculate the characteristic matrix for each case
    mret1 = mueller_retarder(interp1(lcvr1450(:,1),lcvr1450(:,2),p(2*i-
1)), p(max_ind));
    mret2 = mueller_retarder(interp1(lcvr2450(:,1),lcvr2450(:,2),p(2*i)),
p(max_ind)+45);

    polar = mpol * mret2 * mret1;

    cm450(i,:) = polar(1,:);

    % wavelength 543nm
    % calculate the characteristic matrix for each case
    mret1 = mueller_retarder(interp1(lcvr1543(:,1),lcvr1543(:,2),p(2*i-
1)), p(max_ind));
    mret2 = mueller_retarder(interp1(lcvr2543(:,1),lcvr2543(:,2),p(2*i)),
p(max_ind)+45);

    polar = mpol * mret2 * mret1;

    cm543(i,:) = polar(1,:);

    % wavelength 633nm
    % calculate the characteristic matrix for each case
```

```
    mret1 = mueller_retarder(interp1(lcvr1633(:,1),lcvr1633(:,2),p(2*i-
1)), p(max_ind));
    mret2 = mueller_retarder(interp1(lcvr2633(:,1),lcvr2633(:,2),p(2*i)),
p(max_ind)+45);

    polar = mpol * mret2 * mret1;

    cm633(i,:) = polar(1,:);
end

% get the condition numbers
cn450 = cond(cm450);
cn543 = cond(cm543);
cn633 = cond(cm633);

% average condition number
cn = (cn450 + cn543 + cn633) / 3.0;

if (done == 1)

    fileID = fopen('volts.txt','w');
    fprintf(fileID,'LCVR1\tLCVR2\n');
    for i = 1:num_meas
        fprintf(fileID,'%4.4g\t%4.4g\n',p(2*i-1),p(2*i));
    end
    fprintf(fileID,'\nLCVR1 axis angle %4.4g %4s\n',p(max_ind),'degs');
    fclose(fileID);

    fileID = fopen('retardances450.txt','w');
    fprintf(fileID,'LCVR1\tLCVR2\n');
    for i = 1:num_meas


fprintf(fileID,'%4.4g\t%4.4g\n',interp1(lcvr1450(:,1),lcvr1450(:,2),p(2*i
-1)),interp1(lcvr1450(:,1),lcvr1450(:,2),p(2*i)));
    end
    fclose(fileID);

    fileID = fopen('retardances543.txt','w');
    fprintf(fileID,'LCVR1\tLCVR2\n');
    for i = 1:num_meas

fprintf(fileID,'%4.4g\t%4.4g\n',interp1(lcvr1543(:,1),lcvr1543(:,2),p(2*i
-1)),interp1(lcvr1543(:,1),lcvr1543(:,2),p(2*i)));
    end
    fclose(fileID);

    fileID = fopen('retardances633.txt','w');
    fprintf(fileID,'LCVR1\tLCVR2\n');
    for i = 1:num_meas

fprintf(fileID,'%4.4g\t%4.4g\n',interp1(lcvr1633(:,1),lcvr1633(:,2),p(2*i
-1)),interp1(lcvr1633(:,1),lcvr1633(:,2),p(2*i)));
    end
    fclose(fileID);

    fileID = fopen('cm450.txt','w');
```

```
    for i = 1:num_meas

fprintf(fileID,'%4.4g\t%4.4g\t%4.4g\t%4.4g\n',cm450(i,1),cm450(i,2),cm450
(i,3),cm450(i,4));
    end
    fclose(fileID);

    fileID = fopen('cm543.txt','w');
    for i = 1:num_meas

fprintf(fileID,'%4.4g\t%4.4g\t%4.4g\t%4.4g\n',cm543(i,1),cm543(i,2),cm543
(i,3),cm543(i,4));
    end
    fclose(fileID);

    fileID = fopen('cm633.txt','w');
    for i = 1:num_meas

fprintf(fileID,'%4.4g\t%4.4g\t%4.4g\t%4.4g\n',cm633(i,1),cm633(i,2),cm633
(i,3),cm633(i,4));
    end
    fclose(fileID);

    fileID = fopen('CondNum.txt','w');
    fprintf(fileID,'%8s %4.6g\n', 'cn450',cn450);
    fprintf(fileID,'%8s %4.6g\n', 'cn543',cn543);
    fprintf(fileID,'%8s %4.6g\n', 'cn633',cn633);
    fprintf(fileID,'\n%8s %4.6g\n', 'average',cn);
    fclose(fileID);
  end
end

mueller_polarizer()

function m = mueller_polarizer(theta)

% Calculate the Mueller matrix of a polarizer m
% input extinction values in x and y, px and py
% and the angle of the polarizer axis theta

a = 0.5;

m(1,1) = a;
m(1,2) = a * cosd(2 * theta);
m(1,3) = a * sind(2 * theta);
m(1,4) = 0;

m(2,1) = a * cosd(2 * theta);
m(2,2) = a * cosd(2 * theta) * cosd(2 * theta);
m(2,3) = a * sind(2 * theta) * cosd(2 * theta);
m(2,4) = 0;

m(3,1) = a * sind(2 * theta);
m(3,2) = a * sind(2 * theta) * cosd(2 * theta);
m(3,3) = a * sind(2 * theta) * sind(2 * theta);
m(3,4) = 0;
```

```
m(4,1) = 0;
m(4,2) = 0;
m(4,3) = 0;
m(4,4) = 0;


mueller_retarder()

function m = mueller_retarder(ret,thetar)

% Calculate the Mueller matrix of a retarder m
% input retardance ret and axis angle thetar

m(1,1) = 1;
m(1,2) = 0;
m(1,3) = 0;
m(1,4) = 0;

m(2,1) = 0;
m(2,2) = cosd(2 * thetar)*cosd(2 * thetar) + cosd(ret)* sind(2 *
thetar)*sind(2 * thetar);
m(2,3) = (1 - cosd(ret)) * cosd(2 * thetar) * sind(2 * thetar);
m(2,4) = sind(ret) * sind(2 * thetar);

m(3,1) = 0;
m(3,2) = (1 - cosd(ret)) * cosd(2 * thetar) * sind(2 * thetar);
m(3,3) = sind(2 * thetar)*sind(2 * thetar) + cosd(ret)* cosd(2 *
thetar)*cosd(2 * thetar);
m(3,4) = - sind(ret) * cosd(2 * thetar);

m(4,1) = 0;
m(4,2) = -sind(ret) * sind(2 * thetar);
m(4,3) = sind(ret) * cosd(2 * thetar);
m(4,4) = cosd(ret);
```

7.5 Appendix E: publications and presentations.

Appendix E1 shows the first article published on Applied Optics journal on June 2021.

Research Article Vol. 60, No. 17 / 10 June 2021 / Applied Optics 5153

applied optics

Calibration and data extraction in a Stokes polarimeter employing three wavelengths simultaneously

EUSEBIO AGUILAR-FERNÁNDEZ,[1] NEIL C. BRUCE,[1,*] OSCAR G. RODRÍGUEZ-HERRERA,[1] AND RAFAEL ESPINOSA-LUNA[2]

[1]Instituto de Ciencias Aplicadas y Tecnología, Universidad Nacional Autónoma de México, Circuito Exterior, Ciudad Universitaria, Ciudad de México 04510, Mexico
[2]Centro de Investigaciones en Óptica, A. C., Loma del Bosque 115, Col. Lomas del Campestre, León, Gto. 37150, Mexico
*Corresponding author: neil.bruce@icat.unam.mx

Received 4 May 2021; accepted 15 May 2021; posted 20 May 2021 (Doc. ID 430687); published 10 June 2021

We present a method for calibration and data extraction for a Stokes polarimeter working with three different wavelengths simultaneously. In the Stokes polarimeter considered in this work, we use two liquid crystal variable retarders (LCVRs) combined with a Glan–Thompson linear polarizer. A recently developed fitting calibration procedure is used. We use the same calibration samples and LCVR voltages for all three wavelengths, giving simultaneous measurement and calibration. We compare the performance of the polarimeter, after calibration, using four or six calibration samples in our experiment. To generate the four known calibration beams, we use a linear polarizer oriented at 130° and 30° with respect to the horizontal, a horizontal linear polarizer followed by a half-wave plate (at 632 nm) with its fast axis at 30°, and a horizontal linear polarizer followed by a quarter-wave plate (at 632 nm) with its fast axis at 30°. For calibration with six reference beams, we add two known calibration beams by setting the fast axis of the half- and quarter-wave plates at 130°. Experimental results show good agreement with the expected results, with the fitting calibration procedure giving an approximately 50% reduction in total RMS error with four calibration samples. There is a negligible reduction in the error when six calibration samples are used compared to the case with four samples.

https://doi.org/10.1364/AO.430687

1. INTRODUCTION

Polarimetry has attracted a great deal of interest recently, particularly for applications in medicine [1–5], remote sensing [1,6,7] and astronomy [1,8–16], among others. New calibration and data-extraction techniques, combined with electro-optic retarders, have permitted the development of polarimeters that are faster and more precise [17–27]. There also have been developments in large bandwidth polarimeters, particularly in channeled spectropolarimeters. However, there are still many applications that require measurement of polarization at only a few wavelengths, particularly in medicine, microscopy, and remote sensing for which dual-wavelength or RGB (red, green, blue) polarization images provide useful information [2,3,28]. There are methods that can reconstruct the full Stokes spectra, for example, channeled polarimetry. However, this method requires measurement of the complete spectrum to be able to reconstruct the variation of the Stokes parameters, so it will not work if you only have a few wavelengths available. In addition, the calibration process for other methods becomes complicated to correct for all the wavelengths [2], and the experimental setups also are more complicated [28]. The method presented here uses a simple calibration process, a standard Stokes polarimeter experimental setup, and can be extended easily to more wavelengths.

The main problem with this type of system is the calibration and data extraction for the different wavelengths, since the retardances of the polarimeter components vary with these wavelengths [2,3]. In this work, we propose a calibration and data-extraction method for the measurement of three wavelengths simultaneously, which uses only one configuration of retardances and one set of calibration samples. The method is shown to be fast, robust, and precise. The proposed method can be extended to more wavelengths if required. In this work, the proposed method is applied to a Stokes polarimeter using two liquid-crystal variable retarders (LCVRs). It is clear that the polarimeter cannot be optimized for three wavelengths simultaneously; therefore, we use a recently developed fitting procedure to reduce the errors in the measured Stokes vectors [24].

1559-128X/21/175153-08 Journal © 2021 Optical Society of America

2. THEORY

A. LCVR Characterization

The proposed method in this paper uses only one Stokes polarimeter with two LCVRs, and with only one configuration of retardance values. Because of the nonlinear relationship between retardance and applied voltage for LCVRs, it is important to characterize them for all the wavelengths used.

The characterization of an LCVR involves the experimental setup shown in Fig. 1 [29,30]. The LCVR is fixed at an angle of 45° and is placed between two crossed linear polarizers.

The Mueller matrix of the full system is given by

$$M_{LC} = \frac{1}{4}\begin{pmatrix} 1-\cos\delta_L & 1-\cos\delta_L & 0 & 0 \\ -1+\cos\delta_L & -1+\cos\delta_L & 0 & 0 \\ 0 & 0 & 0 & 0 \\ 0 & 0 & 0 & 0 \end{pmatrix}, \quad (1)$$

where δ_L denotes the retardance of the LCVR. If we consider an unpolarized light beam at the input of the system, the total intensity detected by the sensor (I) is denoted by the first term of the Stokes vector reaching the detector:

$$S_0 = I = A\,(1-\cos\delta_L)\,, \quad (2)$$

where A is a constant that depends only on fixed experimental parameters such as the polarizer absorption and laser intensity. Measuring the intensity as the voltage applied to the LCVR is varied, and so the LCVR retardance is changed, the detected intensity varies periodically according to Eq. (2). Analyzing this expression, the maximum intensity detected by the sensor ($I_{\max}$) occurs when $\cos\delta_L = -1$, and the constant $A = \frac{I_{\max}}{2}$.

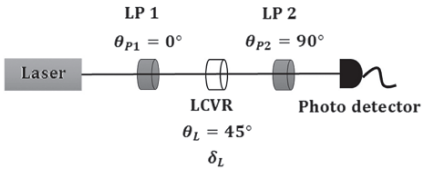

Fig. 1. Experimental setup required to characterize an LCVR [4].

Finally, the expression for the light intensity detected by the photodetector can be written as [29,30]

$$I = \frac{I_{\max}}{2}(1-\cos\delta_L)\,. \quad (3)$$

Hence, the retardance is given by

$$\delta = \cos^{-1}\left(1-\frac{2I}{I_{\max}}\right). \quad (4)$$

B. Polarimeter Theory

Equation (4) allows us to determine the retardance induced in an LCVR by measuring the intensity as the applied voltage is varying, so that applied voltage versus intensity can be plotted. However, Eq. (4) involves the $\cos^{-1}x$ function. It is well known that this is a periodic function in which period $T = \pi$. Therefore, to determine the retardance of the LCVR, it is necessary to unwrap the phase to obtain correct results [29,30].

Because the retardance induced by the LCVRs depends on the wavelength of the incident beam, the configurations of retardance at the polarimeter will be different for each wavelength for a chosen configuration of voltages. To choose the voltages to be used for the LCVRs, we take the Bickel and Bailey configuration [31] for the central wavelength, and calculate the retardances for the other wavelengths using their respective calibration curves.

Equation (5) is the Mueller matrix of the ideal Stokes polarimeter, which can be calculated as the product of the individual matrices of the optical elements. Any errors or deviations of the polarimeter from this ideal behavior is considered in the calibration process performed after the detection of the measured intensities. In this case, as shown in Fig. 2, $\theta_{L1} = 0°$ and δ_1 are the angle of the fast axis and the retardance, respectively, for LCVR 1. Similarly, for LCVR 2, $\theta_{L2} = 45°$ and δ_2 are the angles of the fast axis and the retardance, respectively, so

$$M_S = \frac{1}{2}\begin{pmatrix} 1 & \cos\delta_2 & \sin\delta_1\sin\delta_2 & -\cos\delta_1\sin\delta_2 \\ 1 & \cos\delta_2 & \sin\delta_1\sin\delta_2 & -\cos\delta_1\sin\delta_2 \\ 0 & 0 & 0 & 0 \\ 0 & 0 & 0 & 0 \end{pmatrix}. \quad (5)$$

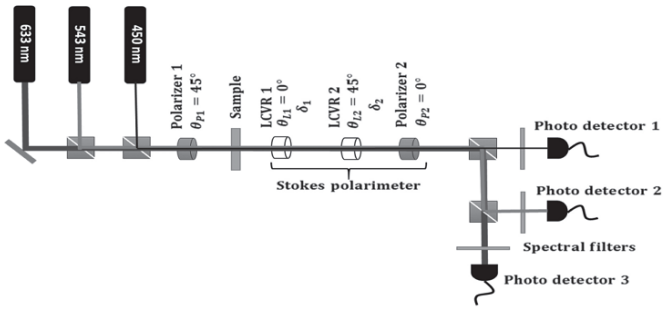

Fig. 2. Scheme of the Stokes polarimeter setup employed in this work. The angles associated with each component refer to the relative angle of the optical axis of that component with respect to the horizontal plane. Measurements are taken simultaneously. The wavelengths employed are 633 nm, 543 nm, and 450 nm.

Consider that the Stokes vector of the incident beam (the light beam coming from the laser) is given as $S_i = (S_{0i}\ S_{1i}\ S_{2i}\ S_{3i})^T$, where T is the transpose, and the total intensity, I, of the light beam at the photodetector is given by the first parameter of S (i.e., the Stokes vector at the output of the experimental system). By multiplying the Stokes vector S_i by the Mueller matrix M_S, we find that the first parameter of the Stokes vector S, denoted as S_0, is given by

$$S_0 = I = \frac{1}{2}\left(S_{0i} + S_{1i}\cos\delta_2 + S_{2i}\sin\delta_1\sin\delta_2 - S_{3i}\cos\delta_1\sin\delta_2\right). \tag{6}$$

According to the work of Bickel and Bailey [31], we can obtain the Stokes vector of a beam using

$$S = \begin{pmatrix} S_0 \\ S_1 \\ S_2 \\ S_3 \end{pmatrix} = \begin{pmatrix} I_H + I_V \\ I_H - I_V \\ I_{+45} - I_{-45} \\ I_R - I_L \end{pmatrix}, \tag{7}$$

where we require the detection of the linearly polarized components I_H, I_V, I_+, and I_-, (horizontal, vertical, +45, and −45 polarization, respectively), and the circularly polarized components, I_R and I_L, (circular right- and left-handed polarization, respectively). From Eqs. (6) and (7), it is clear that to detect the horizontal polarization component of the incident Stokes vector, there are two necessary conditions $\cos\delta_2 = 1$ and $\sin\delta_2 = 0$; (that is, $\delta_2 = 0, 2\pi, 4\pi, \ldots$). For those conditions, the intensity at the detector is described as

$$S_0 = I = \frac{1}{2}(S_{0i} + S_{1i}) = \frac{1}{2}((I_H + I_V) + (I_H - I_V)) = I_H. \tag{8}$$

In a similar way, it is possible to determine the other five configurations of retardance to detect the vertical, +45, −45, right-handed, and left-handed circular polarization components of the incident Stokes vector, and the results are shown in Table 1.

Table 1. Set of Combinations of Retardance (expressed in degrees) Used to Detect the Six Polarization States in a Light Beam with the Bickel and Bailey Method

Polarization State	LCVR1 Retardance (degrees)	LCVR2 Retardance (degrees)
Horizontal	0	0
Vertical	0	180
+45°	90	90
−45°	270	90
Right-handed circular	180	90
Left-handed circular	0	90

The required applied voltages are then found from the measured calibration curve for the central wavelength. It is important to note that this set of configurations can only be employed for the central wavelength. It is also important to point out that in many polarimeters of this type, a measuring scheme using only four modulations can be used; in fact, we tried to use a four modulation setup in our experiment. However, here, because we are using three wavelengths, we can ensure that we have an optimized polarimeter for only one wavelength and the other two wavelengths are not optimized. As a result, we found that with only four modulations, the errors in these other two wavelengths were very large, and our calibration method could not improve the results. With six modulations, as will be shown below, we found that, for the non-optimized cases, the measured Stokes parameters had smaller errors and our calibration scheme was able to improve the results. For this reason, we use six measurements. For the other wavelengths, we use Eq. (6), which represents the total intensity at the detector, where δ_1 and δ_2 are the retardances induced on the LCVRs at the other wavelengths. Now, the six measurements required for the Bickel and Bailey case for the central wavelength give six measurements of intensity for the other wavelengths, which we shall denote as cases I–VI. Using Eq. (6) for each of the six intensity measurements, we can write a matrix equation relating the detected intensities and the retardances of the LCVRs [17]:

$$\frac{1}{2}\begin{pmatrix} 1 & \cos\delta_{2I} & \sin\delta_{1I}\sin\delta_{2I} & \cos\delta_{1I}\sin\delta_{2I} \\ 1 & \cos\delta_{2II} & \sin\delta_{1II}\sin\delta_{2II} & \cos\delta_{1II}\sin\delta_{2II} \\ 1 & \cos\delta_{2III} & \sin\delta_{1III}\sin\delta_{2III} & \cos\delta_{1III}\sin\delta_{2III} \\ 1 & \cos\delta_{2IV} & \sin\delta_{1IV}\sin\delta_{2IV} & \cos\delta_{1IV}\sin\delta_{2IV} \\ 1 & \cos\delta_{2V} & \sin\delta_{1V}\sin\delta_{2V} & \cos\delta_{1V}\sin\delta_{2V} \\ 1 & \cos\delta_{2VI} & \sin\delta_{1VI}\sin\delta_{2VI} & \cos\delta_{1VI}\sin\delta_{2VI} \end{pmatrix}\begin{pmatrix} S_{0i} \\ S_{1i} \\ S_{2i} \\ S_{3i} \end{pmatrix} = \begin{pmatrix} I_I \\ I_{II} \\ I_{III} \\ I_{IV} \\ I_V \\ I_{VI} \end{pmatrix}, \tag{9}$$

which can be written as

$$M_C S_i = I, \tag{10}$$

where M_C is the characteristic matrix of the polarimeter for the configuration of retardances for the given wavelength, S_i is the Stokes vector of the incident beam, and I is the vector of the intensity measurements. From Eq. (10), it is possible to calculate the Stokes parameters of the incident beam by using the pseudo-inverse of the matrix M_C, denoted as $M_C^{\hat{}}$ [32], so

$$M_C^{\hat{}} = \left(M_C^T M_C\right)^{-1} M_C^T, \tag{11}$$

and the solution of Eq. (10) is given by

$$S_i = M_C^{\hat{}} I. \tag{12}$$

C. Calibration Procedure

It is also well-known that a precise polarization measurement requires a calibration and data extraction method. In this work, we use a recently developed fitting procedure [33]. Here, we also compare the results of using either four known polarization states or six known polarization states as calibration samples, since the case of six known polarization states has been found to improve the calibration results [33]. The four known polarization states are produced by: (i) a linear polarizer with the

transmission axis oriented at 130°, (ii) a linear polarizer with the transmission axis oriented at 30°, (iii) a system comprised of a horizontal linear polarizer followed by a half-wave plate (at 633 nm) with fast axes at 30°, and (iv) a system comprised of a horizontal linear polarizer followed by a quarter-wave plate (at 633 nm) with fast axes at 30°. For six known calibration samples, we add the cases of: (v) a system comprised of a horizontal polarizer followed by a half-wave plate (at 633 nm) with fast axes at 130°, and (vi) a system comprised of a horizontal polarizer followed by a quarter-wave plate (at 633 nm) with fast axes at 130°. Given that we used two wave plates to generate the calibration beams, and the retardance induced by these wave plates depends on the wavelength, we measured the retardance induced by the quarter-wave plate and the half-wave plate at the other two wavelengths using the technique described by Chenault and Chipman [34].

The intensity measurements obtained with the known, standard samples in the polarimeter are always different from the expected theoretical results due to the experimental errors in the positions of the optical axes of the retarders, polarizers, and LCVRs (a total of four error parameters), as well as errors in each of the different retardance values for the LCVRs and retarders used to generate the calibration beams. For the errors in the retardance values, it is important to take into account one parameter error for each different retardance value in the LCVRs (a total of seven error parameters). There are also errors due to the other components in the optical path, such as the beamsplitters and the color filters used. These other errors can be compensated to a large extent by the calibration process.

The axes and retardance errors are taken as the parameters in a fit of the experimentally obtained intensity values to the expected, or theoretical, intensity values taking into account the errors [33]. This step gives an estimation of the real, experimental, setup in the experiment, giving a better estimation of the real characteristic matrices of the system.

Then, these fitted parameters for the experimental setup are used in the data extraction step, through the corresponding characteristic matrices, to give a better model for the polarimeter, and a new fit is performed, this time using the Stokes vector elements of the unknown beam as the fitting parameters [33]. This fitting procedure is performed independently for each of the wavelengths used in the experiment, although the measurements are performed simultaneously.

3. EXPERIMENT

Figure 2 shows the experimental setup used in this work. Only one polarimeter is used to simultaneously analyze three wavelengths.

The laser sources used are two He–Ne polarized lasers (543 nm and 633 nm) and a polarized laser diode module (450 nm). One mirror and two beamsplitters are used to ensure co-propagating beams. At the input of the system there is a Glan–Thompson linear polarizer to ensure that all three input beams are linearly polarized in the same plane. Then, the sample is placed in the beam path, just before the components of the Stokes polarimeter, two Meadowlark compensated LCVRs and a Glan–Taylor linear polarizer, as described above. Finally, the light beam is split onto three photo sensors by using beamsplitters, and in front of each photo sensor there is a laser-line filter (bandwidth 10 nm) that selects only one of the three wavelengths to be analyzed. Note that the effect of the beamsplitters is also compensated by the calibration procedure. The experiment is controlled from the computer using LabVIEW. For the results presented below, the sample was rotated from 0° to 180° in steps of 10°. The LabVIEW software is used to configure the position of the rotation mount and the voltage values applied on the LCVRs.

4. RESULTS

Figure 3 shows the characterization curves for the two LCVRs used in this experiment for the three different wavelengths.

Table 2 presents the retardance values used in the experimental configuration of the polarimeter. The central wavelength, the green laser with a wavelength of 543 nm, was used as the reference wavelength, with the retardances for this color yielding the polarizations states required by the Bickel and Bailey method. Table 2 shows the retardances calculated from the characterization curves of Fig. 3, for the other two wavelengths using the same voltage values as for the central wavelength.

Considering 543 nm as the reference wavelength, the characteristic matrices and their pseudo-inverses for each color, calculated from Eqs. (9) and (11), and from the data in Table 2, are given by

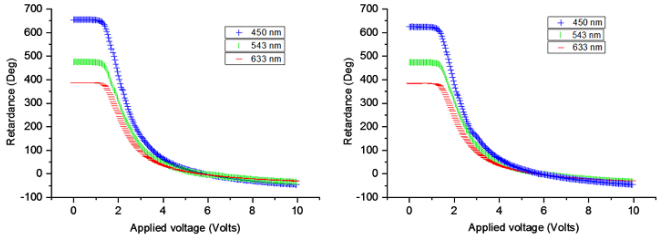

Fig. 3. LCVR1 (left) and LCVR2 (right) characterization curves for 450 nm, 543 nm, and 633 nm.

Table 2. Retardance Values at Each of the Wavelengths Used in the Polarimeter

Polarization at 543 nm	Wavelength	LCVR1 Retardance (degrees)	LCVR2 Retardance (degrees)
Horizontal	633 nm	−0.64	−1.47
	543 nm	0	0
	450 nm	5.12	4.01
Vertical	633 nm	−0.64	141.22
	543 nm	0	180
	450 nm	5.12	242.27
+45°	633 nm	74.21	73.67
	543 nm	90	90
	450 nm	128.59	128.21
−45°	633 nm	218.89	73.67
	543 nm	279	90
	450 nm	364.4	128.21
Right-handed circular	633 nm	149.74	73.67
	543 nm	180	90
	450 nm	254.76	128.21
Left-handed circular	633 nm	−0.64	73.67
	543 nm	0	90
	450 nm	5.12	128.21

$$M_{C(\mathrm{GREEN})} = \begin{pmatrix} 0.5000 & 0.5000 & 0.0000 & 0.0000 \\ 0.5000 & -0.5000 & 0.0000 & 0.0000 \\ 0.5000 & 0.0000 & 0.5000 & 0.0000 \\ 0.5000 & 0.0000 & -0.5000 & 0.0000 \\ 0.5000 & 0.0000 & 0.0000 & 0.5000 \\ 0.5000 & 0.0000 & 0.0000 & -0.5000 \end{pmatrix}, \tag{13}$$

$$M_{C(\mathrm{BLUE})} = \begin{pmatrix} 0.5000 & 0.4981 & 0.0036 & -0.0438 \\ 0.5000 & -0.1364 & -0.0398 & 0.4794 \\ 0.5000 & -0.3030 & 0.3184 & 0.2384 \\ 0.5000 & -0.3030 & 0.0319 & -0.3964 \\ 0.5000 & -0.3030 & -0.3742 & 0.1346 \\ 0.5000 & -0.3030 & 0.0329 & -0.3963 \end{pmatrix}, \tag{14}$$

$$M_{C(\mathrm{RED})} = \begin{pmatrix} 0.5000 & 0.4996 & -0.0001 & -0.0192 \\ 0.5000 & -.4236 & -0.0018 & -0.2656 \\ 0.5000 & 0.1486 & 0.4567 & -0.1391 \\ 0.5000 & 0.1486 & -0.2970 & 0.3738 \\ 0.5000 & 0.1486 & 0.2634 & 0.3982 \\ 0.5000 & 0.1486 & -0.0032 & -0.4774 \end{pmatrix}. \tag{15}$$

The condition number has been used as a metric for the noise immunity of the calculated Stokes parameters [19–22]. The condition number indicates how sensitive the inverse of a matrix is to small variations in the values of the elements of the matrix, and is calculated as the ratio of the largest singular value of the matrix to the smallest singular value. The optimum value of the condition number for a full Stokes polarimeter is $\sqrt{3}$ or 1.732. The condition number values for the matrices used here are 1.7322, 2.6196, and 2.3312, for green, blue, and red, respectively.

The required Stokes vector of the incident light is then calculated using Eq. (12). To show the principle of operation of the polarimeter, results are presented for rotating known components: a linear Glan–Thompson polarizer, a half-wave plate, and a quarter-wave plate. The reported total RMS error in each case is given by

$$\mathrm{RMS} = \sqrt{\sum_{\substack{\text{rotation}\\ \text{angle}}} \sum_{\substack{\text{Stokes}\\ \text{parameter}}} \frac{1}{4N}(S^{\mathrm{exp}} - S^{\mathrm{teo}})^2}, \tag{16}$$

where S^{exp} is the experimental Stokes values, S^{teo} is the theoretical, expected Stokes values, and N is the number of rotation angles used. Figures 4–6 show the Stokes parameters for a Glan–Thompson polarizer, a half-wave plate, and quarter-wave plate retarders, respectively. In all cases, the expected theoretical data are represented by lines and experimental data are represented by geometrical shapes. In this case, we take four calibration samples. Figures 7–9 show similar results for the case of six calibration samples. Capital letters TR and ER refer to the theoretical and experimental results, respectively.

Table 3 shows the total RMS errors given by Eq. (16), for the cases shown in Figs. 4–9. Figures 4–9 show that the calibration procedure used here significantly reduces the errors in the measured Stokes parameters. It is also interesting that Figs. 4–7 show a large error in the uncalibrated values of S_3, which are corrected in the calibrated graphs. In our experience with these types of polarimeters, the S_3 term tends to be more sensitive to small errors in the LCVR retardances and axes positions, which are the errors that we correct in our calibration process. From Table 3, it can be seen that the calibration process with four calibration samples reduces the total RMS error by at least 50% in all cases.

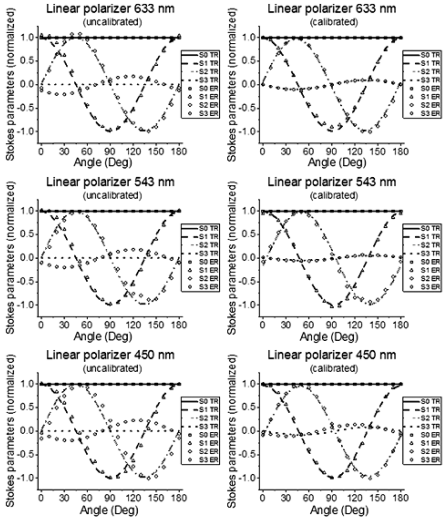

Fig. 4. Stokes parameters for a rotating Glan–Thompson polarizer as a function of the rotation angle for the four calibration polarization states. Uncalibrated (left) and calibrated (right). TR and ER refer to theoretical and experimental results, respectively.

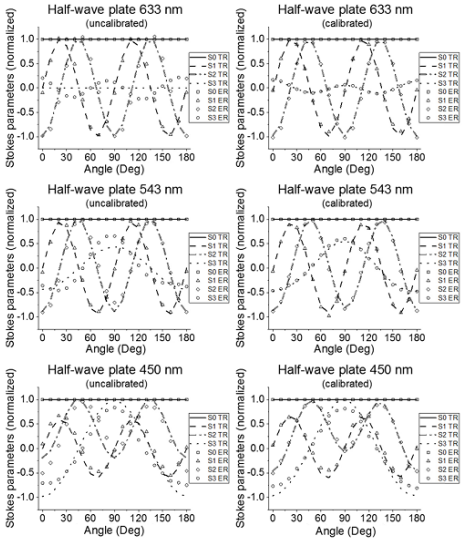

Fig. 5. As Fig. 4, but for a rotating half-wave plate (at 633 nm).

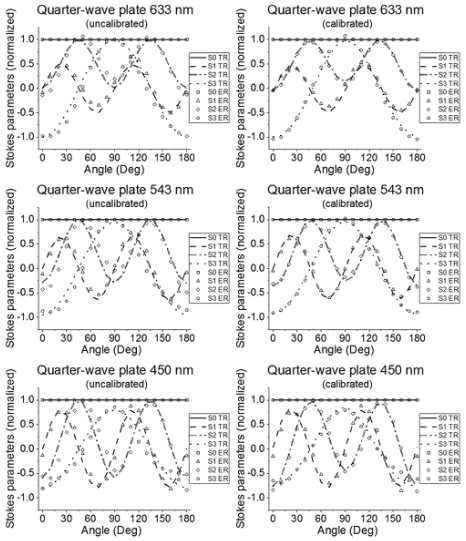

Fig. 6. As Fig. 4, but for a rotating quarter-wave plate (at 633 nm).

With six calibration samples, there is a further reduction in the total RMS errors, but the extra reduction is much smaller, around 25% or less. In all cases, measurement with 450 nm, the blue light, is the case with the largest errors.

It is also clear from Table 3 that the measurements without calibration are similar for all three wavelengths, with 450 nm having a slightly larger RMS, about 1.5 times the value for the other two wavelengths. Then, after the calibration process, the case of a rotating linear polarizer for 450 nm gives a smaller RMS very close to the values obtained for the other wavelengths.

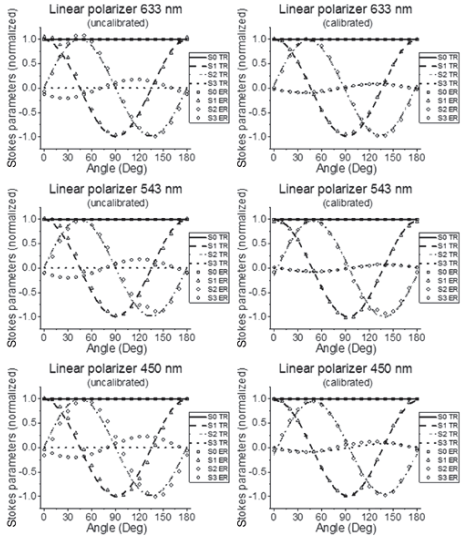

Fig. 7. As Fig. 4, but for the case using six calibration polarization states.

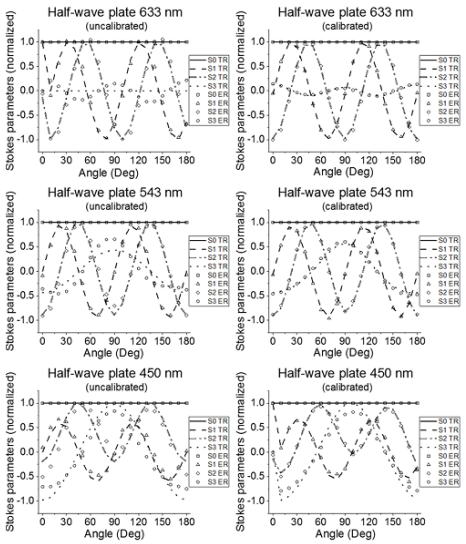

Fig. 8. As Fig. 4, but for the case of a rotating half-wave plate (at 633 nm) and using six calibration polarization states.

Table 3. RMS Error Values for Each Sample

	RMS Error (without calibration)			RMS Error (four calibration states)			RMS Error (six calibration states)		
Sample	**633 nm**	**543 nm**	**450 nm**	**633 nm**	**543 nm**	**450 nm**	**633 nm**	**543 nm**	**450 nm**
Polarizer	0.0821	0.0876	0.01119	0.0298	0.0408	0.0366	0.0242	0.0336	0.0314
Half-wave plate	0.0960	0.0905	0.1427	0.0276	0.0398	0.0783	0.0252	0.0344	0.0751
Quarter-wave plate	0.0997	0.1164	0.1388	0.0454	0.0414	0.0798	0.0332	0.0348	0.0779

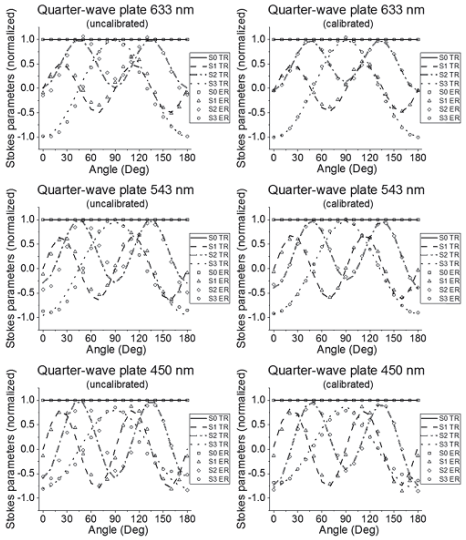

Fig. 9. As Fig. 4, but for the case of a rotating quarter-wave plate (at 633 nm) and using six calibration polarization states.

However, for the cases of the half-wave plate (at 633 nm) and the quarter-wave plate (at 633 nm), although the calibration process reduces the RMS for all the wavelengths, the case of 450 nm gives a value about two times the values for the other two cases. That is, the calibration process does not work as well for 450 nm as it does for the other two wavelengths, for the two fixed retarders, but works better for the linear polarizer. It is not clear to us why this happens, but we are using a nonlinear fitting process with multiple parameters in the calibration process, and so some variation for different cases should be expected.

5. CONCLUSIONS

The operation principle for a Stokes polarimeter working with three wavelengths simultaneously has been demonstrated. The Stokes polarimeter instrumented allows us to measure the Stokes vector of a light beam simultaneously for three different wavelengths. The measurement of the polarization intensities and calibration samples are simultaneous, with the calibration and data-extraction processes independently performed by software for each wavelength. We used the Bickel and Bailey [31] configuration for the central wavelength to define the retardance voltages used, but the configuration of retardances can be changed to different values. We are currently researching optimized cases with smaller characteristic matrix condition numbers for the three wavelengths.

We have shown that the calibration method works correctly and improves the fitting between experimental and theoretical results when we use four known calibration beams. The RMS error values in this case show a reduction of about 50% in the total RMS after calibration. It is interesting to note that, for the case of six calibration samples, compared to the case of four calibration samples, the results only show a slight improvement for the quarter-wave plate, no significant improvement for the half-wave plate, and a slight increase of the total RMS error for the Glan–Thompson polarizer. This suggests that four calibration samples are enough to achieve the best results from the fitting calibration procedure used here. We believe the calibration and data extraction method proposed here is valid for different experimental setups for the same measurements; for example, a spectrometer could be used to simultaneously measure the three wavelengths in place of the three individual detectors. We are currently working on different configurations of the polarimeter to find a smaller average condition number for the three wavelengths to further reduce the final RMS errors.

Funding. Dirección General de Asuntos del Personal Académico, Universidad Nacional Autónoma de México (PAPIIT IG100121, PAPIIT TA100219, PAPIIT TA101020).

Acknowledgment. Eusebio Aguilar-Fernández thanks the Consejo Nacional de Ciencia y Tecnología (CONACyT), México for a doctoral grant. This work was supported by Dirección General de Asuntos del Personal Académico (DGAPA) of the Universidad Nacional Autónoma de México (UNAM).

Disclosures. The authors declare no conflicts of interest.

Data Availability. Data underlying the results presented in this paper are not publicly available at this time but may be obtained from the authors upon reasonable request.

REFERENCES

1. F. Snik, J. Craven-Jones, M. Escuti, S. Fineschi, D. Harrington, A. D. Martino, D. Mawet, J. Riedi, and J. S. Tyo, "An overview of polarimetric sensing techniques and technology with applications to different research fields," Proc. SPIE **9099**, 90990B (2014).
2. X. Tan, X. Tu, K. Della Croce, G. Yao, H. Cai, N. Brock, S. Pau, and R. Liang, "Multi-wavelength quantitative polarization and phase microscopy," Biomed. Opt. Express **10**, 1638–1648 (2019).
3. B. H. Malik and G. L. Coté, "Characterizing dual wavelength polarimetry through the eye for monitoring glucose," Biomed. Opt. Express **1**, 1247–1258 (2010).

4. D. Ivanov, T. Genova-Hristova, E. Borisova, L. Nedelchev, and D. Nazarova, "Multiwavelength polarimetry of gastrointestinal ex vivo tissues for tumor diagnostic improvement," Proc. SPIE **11047**, 1104707 (2019).
5. M. Kupinski, M. Boffety, F. Goudail, R. Ossikovski, A. Pierangelo, J. Rehbinder, J. Vizet, and T. Novikova, "Polarimetric measurement utility for pre-cancer detection from uterine cervix specimens," Biomed. Opt. Express **9**, 5691–5702 (2018).
6. J. S. Tyo, D. L. Goldstein, D. B. Chenault, and J. A. Shaw, "Review of passive imaging polarimetry for remote sensing applications," Appl. Opt. **45**, 5453–5469 (2006).
7. W. Chen, S. Bai, D. Wang, H. Zhao, H. Sun, L. Yi, H. Zhao, D. Xie, J. Peltoniemi, and Z. Li, "Aerosol-induced changes in sky polarization pattern: potential hint on applications in polarimetric remote sensing," Int. J. Remote Sens. **41**, 4963–4980 (2020).
8. D. M. Arnold, I. A. Steele, S. D. Bates, C. J. Mottram, and R. J. Smith, "RINGO3: a multicolour fast response polarimeter," Proc. SPIE **8446**, 84462J (2012).
9. H. Jermak, I. A. Steele, and R. J. Smith, "MOPTOP: multicolour optimised optical polarimeter," Proc. IAU Symp. **12**, 357–358 (2016).
10. A. Alvarez-Herrero, N. Uribe-Patarroyo, P. G. Parejo, J. Vargas, R. L. Heredero, R. Restrepo, V. Martínez-Pillet, J. C. del Toro Iniesta, A. López, S. Fineschi, G. Capobianco, M. Georges, M. López, G. Boer, and I. Manolis, "Imaging polarimeters based on liquid crystal variable retarders: an emergent technology for space instrumentation," Proc. SPIE **8160**, 81600Y (2011).
11. L. J. November, "Liquid crystal polarimeter: a solid state imager for solar vector magnetic fields," Opt. Eng. **34**, 1659 (1995).
12. V. M. Pillet, M. Collados, J. S. Almeida, V. González, A. Cruz-Lopez, A. Manescau, E. Joven, E. Paez, J. Diaz, O. Feeney, V. Sánchez, G. Scharmer, and D. Soltau, "LPSP & TIP: full stokes polarimeters for the Canary Islands observatories," ASP Conf. Ser. **183**, 264–271 (1999).
13. T. Horn and A. Hofmann, "Liquid crystal imaging Stokes polarimeter," ASP Conf. Ser. **184**, 33–37 (1999).
14. V. Martínez Pillet, J. C. del Toro Iniesta, and A. Álvarez-Herrero et al., "The imaging magnetograph eXperiment (IMaX) for the Sunrise balloon-borne solar observatory," Solar Phys.**268**, 57–102 (2011).
15. S. K. Solanki, J. C. Iniesta del Toro, and J. Woch, et al., "The polarimetric and helioseismic imager on solar orbiter," Astron. Astrophys. **642**, A11 (2020).
16. J. C. del Toro Iniesta and M. Collados, "Optimum modulation and demodulation matrices for solar polarimetry," Appl. Opt. **39**, 1637–1642 (2000).
17. R. A. Chipman, "Polarimetry," in *Handbook of Optics*, M. Bass, ed. (McGraw-Hill, 1995), Chap. 22.
18. D. Goldstein, *Polarized Light*, 2nd ed. (CRC press, 2003).
19. J. S. Tyo, "Design of optimal polarimeters: maximization of signal to noise ratio and minimization of systematic errors," Appl. Opt. **41**, 619–630 (2002).
20. E. Compain, S. Poirier, and B. Drevillon, "General and self-consistent method for the calibration of polarization modulators, polarimeters and Mueller-matrix ellipsometers," Appl. Opt. **38**, 3490–3502 (1999).
21. A. de Martino, Y.-K. Kim, E. García-Caurel, B. Laude, and B. Drévillon, "Optimized Mueller polarimeter with liquid crystals," Opt. Lett. **28**, 616–618 (2003).
22. C. Macias-Romero and P. Török, "Eigenvalue calibration methods for polarimetry," J. Eur. Opt. Soc. Rapid Publ. **7**, 12004 (2012).
23. M. H. Smith, "Optimization of a dual-rotating-retarder Mueller matrix polarimeter," Appl. Opt. **41**, 2488–2493 (2002).
24. O. Rodríguez-Nuñez, J. M. López-Téllez, O. G. Rodríguez-Herrera, and N. C. Bruce, "Calibration and data extraction in non-optimized Mueller matrix polarimeters," Appl. Opt. **56**, 4398–4405 (2017).
25. A. Campos-Jara, P. GarciaParejo, and A. Álvarez-Herrero, "Optimization of the response time measuring method for liquid crystal variable retarders," J. Vac. Sci. Technol. B **37**, 062930 (2019).
26. P. G. Parejo, A. Campos-Jara, E. García-Caurel, O. Arteaga, and A. Álvarez-Herrero, "Nonideal optical response of liquid crystal variable retarders and its impact on their performance as polarization modulators," J. Vac. Sci. Technol. B **38**, 014009 (2019).
27. A. Álvarez-Herrero, P. G. Parejo, and M. Silva-López, "Fine tuning method for optimization of liquid crystal based polarimeters," Opt. Express **26**, 12038–12048 (2018).
28. X. Tu, S. McEldowney, Y. Zou, M. Smith, C. Guido, N. Brock, S. Miller, L. Jiang, and S. Pau, "Division of focal plane red-green-blue full-Stokes imaging polarimeter," Appl. Opt. **59**, 933–940 (2020).
29. J. M. López-Téllez, N. C. Bruce, and O. G. Rodríguez-Herrera, "Characterization of optical polarization properties for liquid crystal-based retarders," Appl. Opt. **55**, 6025–6033 (2016).
30. J. M. López-Téllez, N. C. Bruce, J. Delgado-Aguillón, J. Garduño-Mejía, and M. Avendaño-Alejo, "Experimental method to characterize the retardance function of optical variable retarders," Am. J. Phys. **83**, 143–149 (2015).
31. W. S. Bickel and W. M. Bailey, "Stokes vector, Mueller matrices, and polarized scattered light," Am. J. Phys. **53**, 468–478 (1985).
32. C. R. Rao and S. K. Mitra, "Generalized inverse of a matrix and its applications," in *6th Berkeley Symposium on Mathematical Statistics and Probability, Volume 1: Theory of Statistics* (The Regents of the University of California, 1972).
33. I. Montes-González, N. C. Bruce, O. G. Rodríguez-Herrera, and O. Rodríguez-Nuñez, "Method to calibrate a full-Stokes polarimeter based on variable retarders," Appl. Opt. **58**, 5952–5957 (2019).
34. D. B. Chenault and R. A. Chipman, "Measurements of linear diattenuation and linear retardance spectra with a rotating sample spectropolarimeter," Appl. Opt. **32**, 3513–3519 (1993).

Appendix E2: Proof of the participation in the virtual conference Roberto Ortega in the Instituto de Ciencias Aplicadas y Tecnología at the UNAM.

Universidad Nacional Autónoma de México
Instituto de Ciencias Aplicadas y Tecnología
Departamento de Óptica, Microondas y Acústica

otorgan la presente

CONSTANCIA

al: M. en C. Eusebio Aguilar Fernández

Por su participación en el Seminario ***Roberto Ortega***, modalidad virtual, con la plática titulada:

Desarrollo de un polarímetro de Stokes midiendo tres longitudes de onda simultáneamente.

"POR MI RAZA HABLARÁ EL ESPÍRITU"
Ciudad Universitaria, CDMX, a 4 de marzo de 2022.

Dr. Rodolfo Zanella Specia
Director del ICAT-UNAM

Dr. José Rufino Díaz Uribe
Jefe Depto. de Óptica, Microondas y Acústica

References

1. F. Snik, J. Craven-Jones, M. Escuti, S. Fineschi, D. Harrington, A. D. Martino, D. Mawet, J. Riedi, and J. S. Tyo, ," Proceedings SPIE 9099, (2014), 90990B
2. X. Tan, X. Tu, K. Della Croce, G. Yao, H. Cai, N. Brock, S.Pau and R. Liang, Multi-wavelength quantitative polarization and phase microscopy, Biomedical Optics Express, 10(4), (2019), 1638-1648
3. B.H. Malik, G.L. Coté, Characterizing dual wavelength polarimetry through the eye for monitoring glucose, Biomedical Optics Express, 1(5), (2010), 1247-1258
4. D. Ivanov, T. Genova-Hristova, E. Borisova, L. Nedelchev, and D. Nazarova, Multiwavelength polarimetry of gastrointestinal exvivo tissues for tumor diagnostic improvement, Proceedings SPIE 11047, (2019), 1104707
5. M. Kupinski, M. Boffety, F. Goudail, R. Ossikovski, A. Pierangelo, J. Rehbinder, J. Vizet and T. Novikova, Polarimetric measurement utility for pre-cancer detection from uterine cervix specimens, Biomedical Optics Express, 9(11), (2018), 5691-5702
6. J.S. Tyo, D.L. Goldstein, D.B. Chenault, J.A. Shaw, Review of passive imaging polarimetry for remote sensing applications, Applied Optics, 45(22), (2006), 5453-5469
7. W. Chen, S. Bai, D. Wang, H. Zhao, H. Sun, L.Yi, H. Zhao, D. Xie, J. Peltoniemi, Z Li, Aerosol-induced changes in sky polarization pattern: potential hint on applications in polarimetric remote sensing, International Journal of Remote Sensing, 41(13), (2020), 4963-4980
8. D.M. Arnold, I.A. Steele, S.D. Bates, C.J. Mottram, R,J, Smith, RINGO3: a multicolour fast response polarimeter, Proceedings SPIE 8446, (2012), 84462J
9. H. Jermak, I.A. Steele, R.J. Smith, MOPTOP: Multicolour optimised optical polarimeter, Proceedings IAU Symposium, 324, (2016), 357-358
10. Alvarez-Herrero, N. Uribe-Patarroyo, P. García Parejo, J. Vargas, R. L. Heredero, R. Restrepo, V. Martínez-Pillet, J. C. del Toro Iniesta, A. López, S. Fineschi, G. Capobianco, M. Georges, M. López, G. Boer, and I. Manolis, "Imaging polarimeters based on liquid crystal variable retarders: an emergent technology for space instrumentation," in Proc. SPIE(2011), Vol. 8160, p. 81600Y.
11. L. J. November, "Liquid crystal polarimeter: a solid state imager for solar vector magnetic fields," Opt. Eng. 34, 1659 (1995).
12. V. Mártinez Pillet, M. Collados, J. Sánchez Almeida, V. González, A. Cruz-Lopez, A. Manescau, E. Joven, E. Paez, J. Diaz, O. Feeney, V. Sánchez, G. Scharmer, and D. Soltau, "LPSP & TIP: Full Stokes Polarimeters for the Canary Islands Observatories,", ASP Conference Series, 183, (1999), p. 264.
13. T. Horn and A. Hofmann, "Liquid Crystal Imaging Stokes Polarimeter," , ASP Conference Series, 184, (1999), pp. 33–37.
14. V. MartínezPillet, J. C. del T. Iniesta, A. Álvarez-Herrero, V. Domingo, J. A. Bonet, L. GonzálezFernández, A. LópezJiménez, C. Pastor, J. L. GasentBlesa, P. Mellado, J. Piqueras,B. Aparicio, M. Balaguer, E. Ballesteros, T. Belenguer, L. R. BellotRubio, T. Berkefeld, M. Collados, W. Deutsch, A. Feller, F. Girela, B. Grauf, R. L. Heredero,

M. Herranz, J. M. Jerónimo, H. Laguna, R. Meller, M. Menéndez, R. Morales, D. OrozcoSuárez,G. Ramos, M. Reina, J. L. Ramos, P. Rodríguez, A. Sánchez, N. Uribe-Patarroyo, P. Barthol, A. Gandorfer, M. Knoelker, W. Schmidt, S. K. Solanki, and S. VargasDomínguez, "The Imaging Magnetograph eXperiment (IMaX) for the Sunrise Balloon-Borne Solar Observatory," Solar Physics, 268, 57–102 (2010).

15. S. K. Solanki, J. C. del T. Iniesta, J. Woch, A. Gandorfer, J. Hirzberger, A. Alvarez-Herrero, T. Appourchaux, V. M. Pillet, I. Pérez-Grande, E. S. Kilders, W. Schmidt, J. M. G. Cama, H. Michalik, W. Deutsch, G. Fernandez-Rico, B. Grauf, L. Gizon, K. Heerlein, M. Kolleck, A. Lagg, R. Meller, R. Müller, U. Schühle, J. Staub, K. Albert, M. A. Copano, U. Beckmann, J. Bischoff, D. Busse, R. Enge, S. Frahm, D. Germerott, L. Guerrero, B. Löptien, T. Meierdierks, D. Oberdorfer, I. Papagiannaki, S. Ramanath, J. Schou, S. Werner, D. Yang, A. Zerr, M. Bergmann, J. Bochmann, J. Heinrichs, S. Meyer, M. Monecke, M.-F. Müller, M. Sperling, D. Á. García, B. Aparicio, M. B. Jiménez, L. R. B. Rubio, J. P. C. Carracosa, F. Girela, D. H. Expósito, M. Herranz, P. Labrousse, A. L. Jiménez, D. O. Suárez, J. L. Ramos, J. Barandiarán, L. Bastide, C. Campuzano, M. Cebollero, B. Dávila, A. Fernández-Medina, P. G. Parejo, D. Garranzo-García, H. Laguna, J. A. Martín, R. Navarro, A. N. Peral, M. Royo, A. Sánchez, M. Silva-López, I. Vera, J. Villanueva, J.-J. Fourmond, C. R. de Galarreta, M. Bouzit, V. Hervier, J. C. L. Clec'h, N. Szwec, M. Chaigneau, V. Buttice, C. Dominguez-Tagle, A. Philippon, P. Boumier, R. L. Cocguen, G. Baranjuk, A. Bell, T. Berkefeld, J. Baumgartner, F. Heidecke, T. Maue, E. Nakai, T. Scheiffelen, M. Sigwarth, D. Soltau, R. Volkmer, J. B. Rodríguez, V. Domingo, A. F. Sabater, J. L. G. Blesa, P. R. Martínez, D. O. Caudel, J. Bosch, A. Casas, M. Carmona, A. Herms, D. Roma, G. Alonso, A. Gómez-Sanjuan, J. Piqueras, I. Torralbo, B. Fiethe, Y. Guan, T. Lange, H. Michel, J. A. Bonet, S. Fahmy, D. Müller, and I. Zouganelis, "The Polarimetric and Helioseismic Imager on Solar Orbiter," Astronomy and Astrophysics, 642, A11 (2020).
16. J. C. del Toro Iniesta and M. Collados, "Optimum Modulation and Demodulation Matrices for Solar Polarimetry," Applied Optics, 39, 1637–1642 (2000).
17. R.A. Chipman, Polarimetry, in Handbook of Optics, M. Bass editor, McGraw-Hill, Columbus, (1995), Chapter 22
18. D. Goldstein, Polarized Light, Second Edition, CRC Press, Boca Raton, (2003)
19. W. S. Bickel, W. M. Bailey, "Stokes vector, Mueller matrices, and polarized scattered light", Am. J. Phys. 53, (1985).
20. J.S. Tyo, Design of optimal polarimeters: maximization of signal to noise ratio and minimization of systematic errors, Applied Optics, 41(4), (2002), 619-630
21. E. Compain, S. Poirier and B. Drevillon, General and self-consistent method for the calibration of polarization modulators, polarimeters and Mueller-matrix ellipsometers, Applied Optics, 38(16), (1999), 3490-3502
22. A. de Martino, Y-K- Kim, E. García-Caurel, B. Laude and B. Drévillon, Optimized Mueller polarimeter with liquid crystals, Optics Letters, 28(8), (2003), 616-618
23. C. Macias-Romero and P. Török, "Eigenvalue calibration methods for polarimetry," Journal of the European Optical Society: Rapid publications, 7, (2012), 12004.
24. M.H. Smith, Optimization of a dual-rotating-retarder Mueller matrix polarimeter, Applied Optics, 41(13), (2002), 2488-2493

25. Omar Rodríguez-Nuñez, Juan Manuel López-Téllez, Oscar G. Rodríguez -Herrera, Neil C. Bruce, "Calibration and data extraction in non-optimized Mueller matrix polarimeters", Applied Optics, 56(15) (2017), 4398-4405
26. A. Campos-Jara, P. GarcíaParejo, and A. Álvarez-Herrero, "Optimization of the response time measuring method for liquid crystal variable retarders," Journal of Vacuum Science & Technology B 37, 062930 (2019).
27. P. García Parejo, A. Campos-Jara, E. García-Caurel, O. Arteaga, and A. Álvarez-Herrero, "Nonideal optical response of liquid crystal variable retarders and its impact on their performance as polarization modulators," Journal of Vacuum Science & Technology B 38, 014009 (2019).
28. A. Álvarez-Herrero, P. G. Parejo, and M. Silva-López, "Fine tuning method for optimization of liquid crystal based polarimeters," Optics Express, 26, 12038–12048 (2018).
29. X. Tu, S. McEldowney, Y. Zou, M. Smith, C. Guido, N. Brock, S. Miller, L. Jiang, S. Pau, Division of focal plane red-green-blue full-Stokes imaging polarimeter, Applied Optics, 59(22), (2020), 933-940
30. J. M. López-Téllez, N. C. Bruce, and O. G. Rodríguez-Herrera, "Characterization of optical polarization properties for liquid crystal-based retarders", Appl. Opt. 55, 6025–6033 (2016).
31. López-Téllez, Juan M., Bruce, Neil C., Delgado-Aguillón, Jesús, Garduño-Mejía, Jesús, & Avendaño-Alejo, Maximino, "Experimental method to characterize the retardance function of optical variable retarders", Am. J. Phys., 83, 143 (2015).
32. Rao, C. Radhakrishna, and Sujit Kumar Mitra. "Generalized inverse of a matrix and its applications." Proceedings of the Sixth Berkeley Symposium on Mathematical Statistics and Probability, Volume 1: Theory of Statistics. The Regents of the University of California, 1972.
33. I. Montes-González, N.C. Bruce, O.G. Rodríguez-Herrera, O. Rodríguez-Nuñez, Method to calibrate a full-Stokes polarimeter based on variable retarders, Applied Optics, 58(22), (2019), 5952-5957
34. David B. Chenault, Russel A. Chipman, "Measurements of linear diattenuation and linear retardance spectra with a rotating sample spectropolarimeter", Appl. Opt. 32, (1993).
35. Azzam, R. M. A., Elminyawi, I. M., & El-Saba, A. M. (1988). General analysis and optimization of the four-detector photopolarimeter. JOSA A, 5(5), 681-689.
36. Azzam, R. M. A. (1982). Division-of-amplitude photopolarimeter (DOAP) for the simultaneous measurement of all four Stokes parameters of light. Optica Acta: International Journal of Optics, 29(5), 685-689.
37. Mu, T., Zhang, C., & Liang, R. (2015). Demonstration of a snapshot full-Stokes division-of-aperture imaging polarimeter using Wollaston prism array. Journal of Optics, 17(12), 125708.
38. Mu, T., Zhang, C., Li, Q., & Liang, R. (2015). Error analysis of single-snapshot full-Stokes division-of-aperture imaging polarimeters. Optics express, 23(8), 10822-10835.